GEMS & GEMOLOGY

"Green Amber"

Modeling the Tavernier Blue

*"Fluorescence Cage" to
Identify HPHT Treatment*

Ammolite Update

OUR EDUCATION.
YOUR WORLD OF OPPORTUNITY.

SEOUL 8:00 PM
GIA alumni network at cultured pearl seminar.

LONDON
NOON
GIA-trained jeweler advises client on 5 carat solitaire.

NEW YORK
7:00 AM
Diamonds Graduate negotiates purchase of rough parcel.

TOKYO 8:00 PM
Student completes gem ID project.

MUMBAI 4:30 PM
Sales associate explains 4Cs to customer.

CARLSBAD
4:00 AM
Core gem curriculum updated to reflect new research.

HONG KONG 7:00 PM
Manufacturing exec expands business skills online.

BANGKOK 6:00 PM
Graduate Gemologist spots treated emeralds in bulk order.

Almost anywhere you go, someone is using education acquired from GIA. Our international campuses, traveling classes, corporate seminars and online courses help individuals define and refine vital skills. And GIA supports that learning with credentials valued throughout the gem and jewelry world.

WWW.GIA.EDU

GIA
GEMOLOGICAL INSTITUTE OF AMERICA®

CARLSBAD   NEW YORK   LONDON   ANTWERP   FLORENCE   GABORONE   JOHANNESBURG
MOSCOW   MUMBAI   BANGKOK   HONG KONG   BEIJING   TAIPEI   SEOUL   OSAKA   TOKYO

GMSGG

SUBSCRIPTIONS

Copies of the current issue may be purchased for **$19.00** in the U.S., **$22.00** elsewhere. Online subscriptions, and print subscriptions sent to addresses in the U.S., are $74.95 for one year (4 issues), $194.95 for three years (12 issues). Print subscriptions sent elsewhere are $85.00 for one year, $225.00 for three years. Combination print/online subscriptions are $99.95 in the U.S. and $110.00 elsewhere for one year, and $269.95 in the U.S. and $300.00 elsewhere for three years. Canadian subscribers should add GST. Discounts are available for group subscriptions, renewals, GIA alumni, and current GIA students.

To purchase subscriptions and single print issues, visit www.gia.edu/gandg or contact the Circulation Coordinator.

Electronic (PDF) versions of all articles and sections from Spring 1981 forward can be purchased at **gia.metapress.com** for $10 each. Full issue access can be purchased for $20.

To obtain a Japanese translation of *Gems & Gemology*, contact GIA Japan at info@giajpn.gr.jp. Our Canadian goods and service registration number is 126142892RT.

DATABASE COVERAGE

Gems & Gemology's impact factor is 1.172 (ranking 12th out of the 26 journals in the Mineralogy category), according to the Thomson Reuters 2008 Journal Citation Reports (issued July 2009). *Gems & Gemology* is abstracted in Thomson Reuters products (*Current Contents: Physical, Chemical & Earth Sciences* and Science Citation Index—Expanded, including the Web of Knowledge) and other databases. For a complete list, see www.gia.edu/gandg.

MANUSCRIPT SUBMISSIONS

Gems & Gemology welcomes the submission of articles on all aspects of the field. Please see the Guidelines for Authors on our Website, or contact the Managing Editor. Letters on articles published in *Gems & Gemology* are also welcome.

ABOUT THE COVER

A bright yellowish green to green material called "green amber" has recently appeared in the market. It is produced by treating natural amber or copal with heat and pressure. In the lead article in this issue, Dr. Ahmadjan Abduriyim and coauthors report the results of infrared and nuclear magnetic resonance spectroscopy to characterize this new gem material. The emerald cut shown here weighs 8.7 ct and the necklace contains 62.5 total carats of "green amber." Courtesy of Treasure Green Amber Ltd.; photo by Robert Weldon.
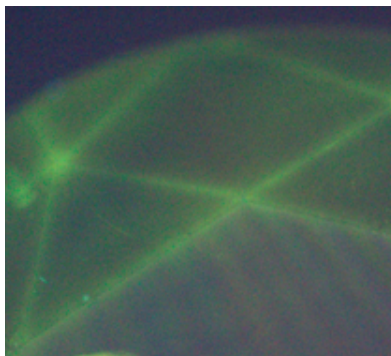
Color separations for Gems & Gemology *are by Pacific Plus, Carlsbad, California.*
Printing is by Allen Press, Lawrence, Kansas.

pg. 159

pg. 188

pg. 218

New Technologies Face Off with New Realities

It's no secret that gem treatments are becoming far more sophisticated and challenging to identify. Look no further than diamonds processed by high pressure and high temperature (HPHT), corundum diffused with beryllium, and topaz and other gems subjected to ultra-thin coatings. When some of these treatments were introduced, we did not know if the testing methods then available to gemologists and gemological labs could characterize them reliably. Fortunately, just as advances in technology have led to more sophisticated treatments, they have also hastened the development of powerful analytical techniques. Many of these techniques are now common in fields such as chemistry, physics, and materials science, and enterprising researchers are learning to adapt them to problems of gem identification.

Raman spectrometer

We have seen this over the years in *G&G* with, for example, the harnessing of the Raman spectrometer, first to identify inclusions in gem materials (and the materials themselves) and later to record photoluminescence spectra that help characterize HPHT-treated diamonds. Virtually unknown in gemology a decade ago, laser ablation–inductively coupled plasma–mass spectrometry (LA-ICP-MS) is now routinely used to identify Be-diffused ruby and sapphire. As featured in the Winter 2007 *G&G,* GIA and other gem laboratories are investigating the application of fluorescence spectroscopy to detect synthetic and treated colored diamonds. In the Summer 2008 issue, scientists at D. Swarovski & Co. showed us how X-ray photoemission spectroscopy can reveal characteristics of surface-coated vs. diffused topaz.

This issue of *G&G* introduces gemological applications for two additional instruments that have been used successfully in other fields. In the lead article on "green amber," Ahmadjan Abduriyim and coauthors identified a diagnostic signal with nuclear magnetic resonance (NMR) spectroscopy that proves whether a natural resin (amber or copal) was treated with a new two-stage heating process. Although NMR requires that a portion of the sample be destructively analyzed, the study offers valuable insights into how the treatment can artificially "age" copal so that it resembles amber (with a distinctive yellowish green color in some cases). In their article on the "fluorescence cage," Inga Dobrinets and Alexander Zaitsev employ fluorescence microscopy—a technique widely used in the life sciences—to identify type I diamonds that have been subjected to HPHT treatment. This could provide a rapid screening technique for gem laboratories.

While the application of new analytical techniques to gemology is not always immediately apparent, an awareness of them is critical as new treatments and synthetics reach the marketplace. We urge every gemologist to stay alert to developments in other fields that might have potential in gemology. In the meantime, escalating technologies provide a fascinating arena for face-offs between new synthetics and treatments and the means of accurately and efficiently identifying them.

◆ ◆ ◆ ◆ ◆

And while we're on the subject of new technologies, in early October *G&G* introduced a monthly e-newsletter, the *G&G eBrief.* This publication reports breaking developments in gemology—new materials seen in the GIA Laboratory, the latest treatments, emerging localities, and other must-have-now information for the practicing gemologist. If we have your email address on file, you should have received it. If you did not, please email us at gandg@gia.edu. Free to all in 2009, it will be delivered exclusively to the journal's subscribers starting in January. Prices for the print version of *G&G* will be going up in 2010 to offset higher printing and mailing costs, but we believe that the value of the journal—and of the new *G&G eBrief,* as well as additional benefits soon to be announced—will make your subscription to *G&G* more indispensable than ever.

Brendan M. Laurs • Editor • blaurs@gia.edu

CHARACTERIZATION OF "GREEN AMBER" WITH INFRARED AND NUCLEAR MAGNETIC RESONANCE SPECTROSCOPY

Ahmadjan Abduriyim, Hideaki Kimura, Yukihiro Yokoyama, Hiroyuki Nakazono, Masao Wakatsuki,
Tadashi Shimizu, Masataka Tansho, and Shinobu Ohki

A peridot-like bright greenish yellow to green gem material called "green amber" has recently appeared in the gem market. It is produced by treating natural resin (amber or copal) with heat and pressure in two stages in an autoclave. Differences in molecular structure between untreated amber and copal as compared to treated "green amber" were studied by FTIR and ^{13}C NMR spectroscopy, using powdered samples. Regardless of the starting material, the FTIR spectrum of "green amber" showed an amber pattern but with a characteristic small absorption feature at 820 cm^{-1}. Solid-state ^{13}C NMR spectroscopy of the treated material indicated a significantly lower volatile component than in the untreated natural resin, evidence that the treatment can actually "artificially age" copal. A new absorption observed near 179 ppm in the NMR spectra of all the treated samples also separated them from their natural-color counterparts.

I t has been known for quite some time that amber and copal may be treated with heat and pressure in an autoclave—or treated at high temperature with linseed oil—to improve their brownish yellow color, transparency, or hardness (e.g., O'Donoghue, 2006). These treatments have focused on amber from the Baltic Sea region (which includes localities in Poland, Scandinavia, Russia, the Baltic Republics [Estonia, Latvia, and Lithuania], and Germany), and also young amber and subfossilized copal mined in Latin America. In recent years, it appears that such treatments have been refined to produce a new product.

In May 2006, a gem material called "green amber" (figure 1) debuted at the Hong Kong Jewellery & Watch Fair, where it was offered by Treasure Green Amber Ltd., Hong Kong. Dealers from Poland (Amber Gallery Export-Import, Amber Line) and Lithuania (Amber Trip Lithuania) presented this material at the International Jewellery Tokyo (IJT) show in January 2008. It also appeared at the Tucson gem shows in February 2008, where it was sold by amber dealers and distributors under names such as "natural green Caribbean amber" or "very rare Baltic amber" (Pedersen, 2008). This material, which has a peridot-like bright greenish yellow to green color, displays a distinctive deeper green component than previously seen in amber, even in the rare green material from Mexico.

Author AA visited Treasure Green Amber Ltd. in June 2007 and was provided with information on the material by general manager Hung Chi and sales manager Steven Wai. They stated that their "green amber" is obtained from natural amber—allegedly of Brazilian, Baltic, or other origin—that has been treated by a two-stage procedure involving long time intervals under controlled heat, pressure, and atmosphere, in an autoclave developed in Germany for heat treatment. The green color of the treated
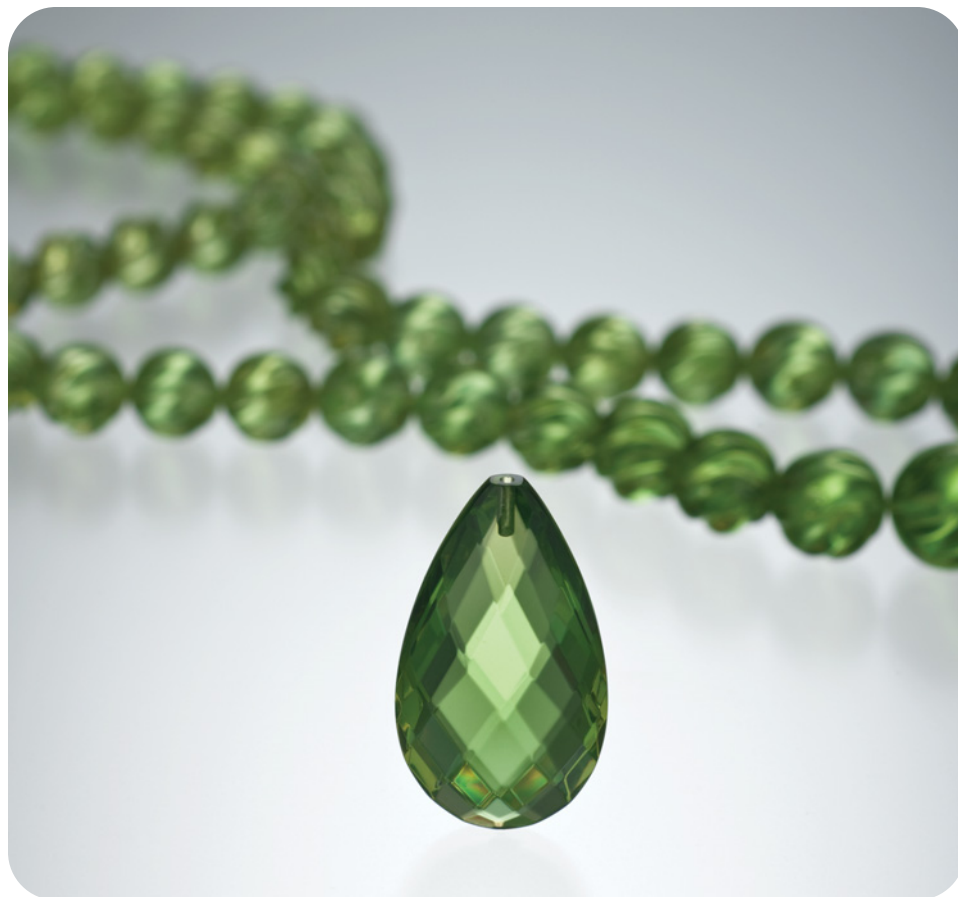
Figure 1. The 9.0 ct briolette and carved beads shown here are examples of "green amber" from Treasure Green Amber Ltd. Photo by Robert Weldon.

material reportedly becomes deeper as the number of heating stages increases. During treatment, volatile components are evidently emitted from the material, causing it to become harder and more stable. They further explained that the treatment process was derived from a traditional enhancement technique frequently used to improve the color, transparency, or hardness of amber in Germany, Russia, Poland, and Lithuania. This process was refined by Hans Werner Mueller of Facett Art in Idar-Oberstein, Germany, to produce "green amber." Treasure Green Amber Ltd. purchased the technique and installed more than a dozen autoclaves at its factory in Guangzhou, China. It subsequently improved the heating process to achieve a higher yield of fine green color.

Dr. Lore Kiefert of the former AGTA-GTC laboratory visited Facett Art in 2007 and reported that this company mainly treated amber from Ukraine to alter the color to green. She concluded that no synthetic resin such as plastic was detectable in the material (Kiefert, 2008).

At the 2008 IJT show, there was considerable discussion among amber dealers from Poland and Lithuania around the contention by some that the starting material for "green amber" also came from Poland, and that all the "green amber" for sale had been produced from copal. As a result, many laboratories and amber dealers in Japan became suspicious of "green amber" because of the possibility that amber was not used as the starting material.

Amber and copal can usually be separated with basic gemological testing because of differences in their physical properties (e.g., hardness and resistance to acid; O'Donoghue, 2006) and their infrared spectra (Brody et al., 2001; Guiliano et al., 2007). It appeared possible, however, that the "green amber" treatment could change the structure of the original starting material so identification was not as straightforward. Hence, we collected samples of amber and copal from various localities and performed heat-treatment experiments with the assistance of Treasure Green Amber Ltd. Using Fourier-transform infrared (FTIR) spectral analysis and high-resolution solid-state ^{13}C nuclear magnetic resonance (NMR) spectroscopy (box A), we studied the differences in molecular structure among "green amber," untreated amber, and untreated copal, as

BOX A: NUCLEAR MAGNETIC RESONANCE (NMR) SPECTROSCOPY

NMR spectroscopy is one of the most advanced techniques for structural studies of liquids and solid-state analysis of organic compounds. This instrumentation (figure A-1) gives detailed information about atomic environments based on the interactions of nuclear magnetic "moments" with electromagnetic radiation.

NMR spectroscopy is appropriate only for atomic nuclei that have an odd number of protons and/or neutrons and a nuclear magnetic moment. The nuclear spin takes two orientations that have different energy levels when a magnetic nucleus such as ^1H, ^{13}C, ^{15}N, or ^{31}P is placed in the magnetic field. Solid-state NMR spectroscopy is performed by placing the sample in a magnetic field and observing its response to pulses of energy in the radio frequency (RF) portion of the spectrum. The technique requires samples to be ground to a fine powder and loaded into a small capsule, called a rotor. The rotor is then placed into a probe, which is loaded into a large apparatus housing a very strong magnet. Depending on the quality of data desired, a technique called magic-angle spinning (MAS) may be employed. This technique involves rapidly spinning a sample within the magnetic field at an angle of 54.7°, which averages out orientation-dependent magnetic effects that blur spectra. The sample is then exposed to pulses of RF energy, and the frequencies it re-emits are collected by a spectrometer.

During an NMR experiment, the energy emitted in response to the RF energy is measured as a function of time, producing a time-domain spectrum. A Fourier-transform function is applied to the spectrum, producing a frequency-domain spectrum where relative intensity is shown along the Y axis and energy is shown along the X axis. The energies are measured relative to a standard material in which the bonding environment of a nuclide and the RF energy it emits are known. Because the energy difference between the standard material and the sample is very small, X-axis values are typically reported in parts per million (ppm), or chemical shift, with 0 ppm representing the characteristic energy of the standard. Peaks in these spectra correspond to various atomic environments, and in the case of ^{13}C NMR spectroscopy, their position depends on the carbon bonding site energy in the sample relative to that of the reference standard.

NMR spectroscopy has important applications in organic chemistry, and it may also find potential
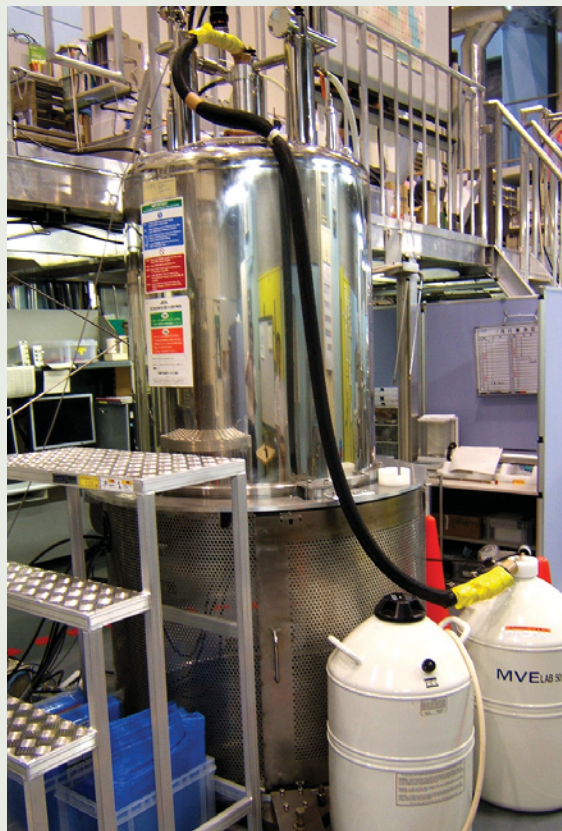
Figure A-1. This JEOL ECA-500 spectrometer is the NMR instrument used at the National Institute for Materials Science (NIMS) in Tsukuba, Japan, for this study. Photo by A. Abduriyim.

new uses in gemology. Unlike FTIR spectroscopy, NMR identifies unique atomic sites in organic molecular units or in the crystal lattice of a material. With further research, this technique may prove useful, in certain situations, for determining the relative age and the geographic origin of organic gems. NMR can be applied with minimal damage (i.e., it uses a small sample size, and chemical dissolution is not necessary). However, due to the high cost of the instrumentation (ranging from $355,000 to more than $5 million) and the potentially destructive nature of the method, it will likely see only limited application to gemology.

NEED TO KNOW

- Both copal and amber have been treated to produce "green amber."

- A two-stage heating process, in an autoclave, is used.

- The treatment "ages" copal so that its gemological properties resemble amber.

- Analysis of "green amber" with FTIR and ^{13}C NMR spectroscopy revealed diagnostic features at 820 cm^{-1} and near 179 ppm, respectively.

- The presence of "Baltic shoulder" features in the FTIR spectrum of a treated sample indicates that the starting material was amber; their absence cannot be used to identify the starting material.

- The green color appears to result from light scattering from fine clouds of inclusions.

Figure 2. Millions of years are required for tree resin to become amber. It first hardens to become copal, such as this sample from Madagascar (21.53 ct). Photo by Hideaki Fukushima.

well as the structural changes that occurred as the result of heat treatment. Following a discussion of the results of these studies, this article also covers the nomenclature for describing this material on laboratory reports.

BACKGROUND

Amber is fossilized tree resin. Resin is a semisolid amorphous organic hydrocarbon secreted by all plants. Amber forms when resin from certain trees hardens and fossilizes gradually over time (Schlee, 1984; Grimaldi, 1996; Lambert, 1997). The resin first hardens by losing volatile components such as alcohol and grease to become copal (figure 2), which then undergoes further devolatilization during burial in sediments to become amber.

Not all tree resin can become amber. In general, resins that fossilize to amber are secreted by trees in the families Araucariaceae (figure 3) and Fabaceae (the latter is commonly known as the legume family). In contrast, trees belonging to the family Pinaceae (i.e., the pine family) typically do not produce resin that fossilizes to amber (Kimura et al., 2006a). To become amber, the resin must contain a macromolecule called a diterpene, which is a type of hydrocarbon that is part of natural resin (Anderson and Winans, 1991; Anderson et al., 1992). Ozic acid, a diterpenoid, is a major component of resins produced by plants belonging to the family Fabaceae. Copal from Colombia, Tanzania, and Madagascar, as well as amber from the Dominican Republic, originates from trees that belong to this family. In contrast, communic acid is a major component of resin from trees in the

family Araucariaceae, which may produce Baltic and Ukrainian amber.

Polymerization of organic hydrocarbon molecules (each of which has a similar "skeleton" of carbon atoms) changes the resin to copal, and a cross-linkage reaction between chains of these hydrocarbons produces amber (Clifford and Hatcher, 1995; see appendix A). In nature, this cross-linkage reaction proceeds very slowly at elevated temperature and pressure during sedimentation and burial of organic sediments; in fact, it takes about 17 million years to reach the halfway point (Kimura et al., 2006a). This means that copal requires tens of millions of years to change into amber. However, these reactions can be significantly accelerated by exposing copal to an alternative set of pressure and temperature parameters in the laboratory.

Methods that can be used to study the molecular

Figure 3. Baltic amber, such as these samples (11.20 and 14.77 ct), formed from the resin derived from trees of the family Araucariaceae. The darker color of the sample on the right is due to natural oxidation in the ground. Photo by A. Abduriyim.

structure of amber and related materials include FTIR spectroscopy, NMR spectroscopy, and pyrolytic gas chromatographic (Py-GC) mass analysis. However, all these techniques require destructive experimental procedures (including FTIR, when applied to amber and copal).

MATERIALS AND METHODS

A total of 44 samples were used in this study, with a weight range of 0.81–67.20 ct (table 1). The samples included 14 pieces of treated "green amber" provided by Treasure Green Amber Ltd. (originally from Brazil), Facett Art (from Ukraine), and Amber Gallery Export-Import (locality unknown); a representative piece of untreated copal from each of four sources (Colombia, Brazil, Madagascar, and Tanzania); and a representative piece of untreated amber from each of five sources (Kuji in Japan, the Baltic Sea region, Ukraine, the Dominican Republic, and

Mexico). All the untreated samples were examined first in their untreated state and then after heat treatment (see below). The amber samples from the Baltic Sea region, the Dominican Republic, and Mexico were not sliced prior to heat treatment, while the other samples (both copal and amber) were cut into two portions so that one piece could be used for heat treatment and the other portion retained in its untreated state. In addition, for further heat-treatment experiments, the untreated portion of the Colombian copal was cut into several additional pieces (one more slice and 14 beads).

Heating Experiments. With the cooperation of Treasure Green Amber Ltd., heating experiments were performed in the same autoclave (figure 4) and under the same conditions used previously by this company to produce "green amber" (Hung Chi, pers. comm., 2007). All the untreated amber and copal samples, except for Col-03–17, were placed on trays

TABLE 1. Properties of untreated and heated amber and copal samples.

Material	Location	Sample no.	No. of samples	Treatment	Weight (ct)	Color	UV fluorescence		RI	SG	Age
							Long-wave	Short-wave			
Amber	Kuji, Japan	Kuj-01	1	Untreated[a]	1.29	Brown	Dark green	Dark green	1.55	1.05	83–89 Ma (Kimura et al., 2006b)
		Kuj-02	1	Treated	0.81	Dark brown	Whitish blue	Dark green	1.55	1.06	
Amber	Baltic Sea region	Bal-01	1	Untreated	14.79	Brown-yellow	Bluish green	Dark green	1.54	1.06	35–55 Ma (Kimura et al., 2006b)
		Bal-01H		Treated	14.35	Yellowish green	Whitish blue	Dark green	1.54	1.06	
Amber	Ukraine	Uk-01	1	Untreated	25.05	Yellowish brown	Dark green	Dark green	1.54	1.08	30–38 Ma (Perkovsky et al., 2003)
		Uk-02	1	Treated	15.50	Green	Whitish blue	Dark green	1.54	1.06	
Amber	Dominican Republic	Dom-01	1	Untreated	6.46	"Honey" yellow	Dark green	Dark green	1.54	1.05	15–45 Ma (Rikkinen and Poinar, 2001)
		Dom-01H		Treated	5.73	Yellowish green	Whitish blue	Dark green	1.54	1.05	
Amber	Mexico	Mex-01	1	Untreated	8.34	Greenish yellow	Whitish blue	Dark green	1.54	1.04	22–26 Ma (Cattaneo, 2008)
		Mex-01H		Treated	8.09	Yellowish green	Whitish blue	Dark green	1.54	1.04	
Copal	Colombia	Col-01	1	Untreated	67.20	"Lemon" yellow	Dark green	Dark green	1.55	1.06	400–600 years (Kimura et al., 2006b)
		Col-02	1	Treated	12.28	Green	Whitish blue	Dark green	1.54	1.05	
		Col-03	1	Treated	10.42	Brown	Dark green	Dark green	1.55	1.06	
		Col-04-17	14	Treated	1.03–1.05	Yellowish brown	Dark green	Dark green	1.54	1.05	
Copal	Madagascar	Mad-01	1	Untreated	19.47	Pale yellow	Dark green	Dark green	1.52	1.05	50–60 years (Kimura et al., 2006b)
		Mad-02	1	Treated	12.07	"Golden" yellow	Whitish blue	Dark green	1.53	1.03	
Copal	Tanzania	Tan-01	1	Untreated	2.53	Pale yellow	Dark green	Dark green	1.53	1.05	Unknown
		Tan-02	1	Treated	1.42	Brownish yellow	Whitish blue	Dark green	1.53	1.05	
Copal	Brazil	Bra-01	1	Untreated	8.33	"Honey" yellow	Dark green	Dark green	1.54	1.06	Unknown
		Bra-02	1	Treated	8.46	Green	Whitish blue	Dark green	1.54	1.05	
Amber	Brazil[b]	TR-001-005	5	Treated	1.20–5.49	Green	Whitish blue	Dark green	1.55	1.06	Unknown
Amber	Unknown	BR-001	1	Treated	14.49	Green	Whitish blue	Dark green	1.54	1.05	Unknown
Amber	Unknown	BR-002-003	2	Treated	6.88, 9.46	Yellowish green	Whitish blue	Dark green	1.54	1.05	Unknown
Amber	Unknown	BR-004	1	Treated	40.98	Greenish yellow	Whitish blue	Dark green	1.54	1.05	Unknown
Amber	Ukraine[c]	FA-001-004	4	Treated	1.40–4.69	Yellowish green	Whitish blue	Dark green	1.55	1.06	Unknown
Amber	Ukraine[c]	FA-005	1	Treated	3.92	Greenish yellow	Whitish blue	Dark green	1.55	1.06	Unknown

[a] The presence of sun spangle–like inclusions suggests that this "untreated" sample may have been exposed to a previous heating process.
[b] Origin of untreated starting material, as reported by Treasure Green Amber Ltd.
[c] Origin of untreated starting material, as reported by Facett Art.

with chalk powder on their surfaces to prevent adhesion if melting occurred during heat treatment. A vacuum atmosphere was created in the sample chamber of the autoclave and then a small amount of nitrogen gas was introduced. The temperature was raised to 150°C, and the pressure was gradually increased to ~14 bars. This pressurization prevented the samples from liquefying. After the samples were heated for 30 hours in this environment, the temperature and pressure were slowly reduced to ambient conditions. The sample chamber of the autoclave was kept closed and the process was repeated, but during the second run the temperature was raised to 200°C and the pressure was ~22 bars, with a heating period of 20 hours. The temperature and pressure were again slowly lowered and the samples were left in the chamber until ambient conditions were restored.

We used the same autoclave to conduct another set of experimental heating experiments on Colombian copal samples Col-03–17, in which we lowered the maximum temperature (since the 200°C used above is close to the melting point of copal under pressure). We tested two variations: (1) Col-04–17 underwent a two-stage heating process at 180°C and 20 bars for 20 hours at each stage, and (2) Col-03 was subjected to a one-stage heating process at 180°C and 20 bars for one hour. The latter treatment process has also been used routinely by Treasure Green Amber Ltd. to induce a yellowish brown color in amber and copal.

Gemological Testing. Standard gemological methods were used to document the samples' color, hardness (by the fingernail scratch test), refractive indices (the spot method was used on curved surfaces), specific gravity (by hydrostatic weighing), fluorescence to long- and short-wave ultraviolet radiation, and inclusions (examination with a gemological microscope). In addition, we performed: (1) an alcohol test, by placing a drop of ethanol on the surface of the sample and noting any reaction after it had evaporated; (2) a brine test, in which the sample was placed in a saturated salt solution (SG of 1.1) made by adding 4–5 teaspoons of salt to 200 ml water; (3) a hot point test, by positioning a heated needle near the surface of the sample; and (4) a static electricity test, by briskly rubbing the samples with a cloth and then seeing if they attracted small pieces of paper. We conducted all tests on all the commercial "green amber" and on all the amber and copal samples before and after the heating experiments. To determine the depth of the green color, we sliced three pieces of the commercially treated "green amber"
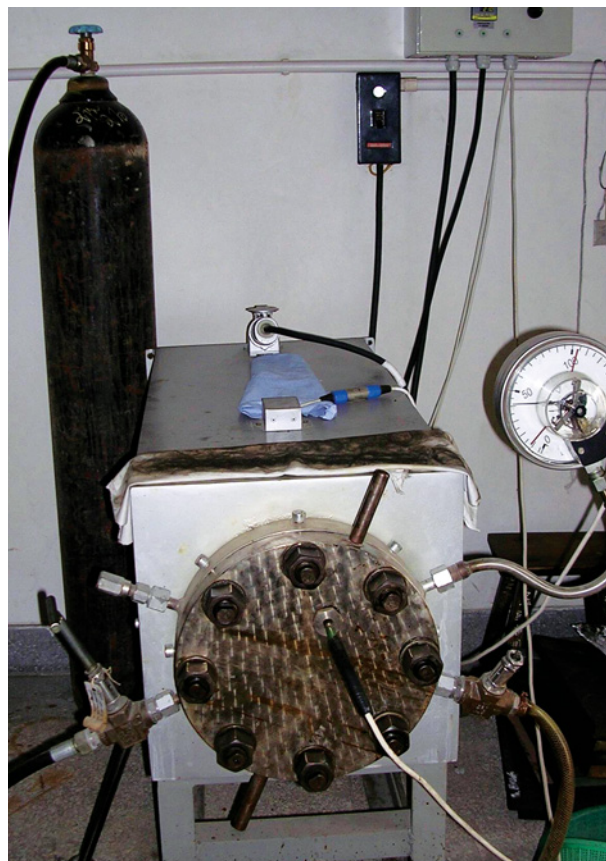
Figure 4. This autoclave was used for the treatment experiments in cooperation with Treasure Green Amber Ltd. It is equipped with a gas input system, and the temperature, pressure, and heating-time parameters can be carefully controlled. Photo by Hung Chi.

(TR-001–003) into thin sections. To check for color instability, we observed the coloration of all the commercially treated "green amber" samples after storing them in the dark for several months.

FTIR Spectroscopy. Infrared spectral analysis was performed on all samples with a Shimazu IR Prestige-21 FTIR spectrometer with a KBr beam splitter and DLATGS detector in the range 5000–400 cm^{-1}, with a resolution of 4.0 cm^{-1} and 100 scans. KBr tablets were prepared for each sample by evenly powdering several milligrams from each. The infrared beam was focused on the powdered sample holder in diffuse reflectance mode. All the spectra were normalized for differences in path length. It was necessary to use powdered samples because the FTIR absorption bands due to stretching and deformational vibrations in the various molecules of amber and copal cannot be resolved in spectra obtained using nondestructive transmittance or diffuse reflectance modes.

Figure 5. Representative amber and copal samples from various localities were used for the standard two-stage heating experiments. For each pair, the untreated samples are shown on the left, and those after heating are shown at the right. Colombian (Col-02) and Brazilian (Bra-02) copal turned bright green. Pale yellow copal from Madagascar (Mad-02) and Tanzania (Tan-02) turned intense yellow with a slight green hue. Kuji amber (Kuj-02) turned dark brown. Amber samples from the Baltic Sea region (Bal-01H) as well as from Ukraine (Uk-02), the Dominican Republic (Dom-01H), and Mexico (Mex-01H) generally turned green, although the color of the Dominican and Mexican material was not highly saturated. Photos by Masaaki Kobayashi.

NMR Spectroscopy. Thirty-three samples, including one representative sample of commercial "green amber" from each company and all amber and copal samples before and after the heat treatment experiments, were measured with solid-state ^{13}C CP-MAS (cross polarization–magic angle spinning) NMR spectroscopy (again, see box A). Analyses of the commercial "green amber" and other known amber samples were performed using a Bruker Avance DRX-600 spectrometer at Tsukuba University. NMR spectra of the copal samples were obtained with a JEOL ECA-500 spectrometer at the National Institute for Materials Science (NIMS) in Tsukuba City. Powdered samples weighing ~280 mg were analyzed. A description of the experimental parameters can be found in the *G&G* Data Depository at www.gia.edu/gandg.

Figure 6. A yellowish brown color resulted from treating 14 beads of "lemon" yellow Colombian copal (1.03–1.05 ct) with an experimental two-stage heating process (180°C and 20 bars, at 20 hours for each stage). Photo by A. Abduriyim.

RESULTS

Gemological Testing. *Commercial "Green Amber" Samples.* Most of the commercial "green amber" samples were yellowish green to green (some with uneven color distribution). The samples from Treasure Green Amber Ltd. had excellent transparency, with only a few inclusions (see below). The green color permeated the small pieces (1.20 and 1.31 ct) almost entirely, but it was limited to just near the surface of the largest one (5.49 ct). After the "green amber" samples were kept in the dark for several months, the green hue of two of them (i.e., TR-005 and BR-001) faded slightly.

The hardness of all the commercially treated samples was similar to that of amber (Mohs ~2–2.5), which—unlike copal—cannot be scratched with a fingernail. The SG was 1.05–1.06 and RI measurements ranged between 1.54 and 1.55, again similar to amber (see table 1; O'Donoghue, 2006). They fluoresced whitish blue and dark green to long- and short-wave UV radiation, respectively. They were warm to the touch and exhibited conchoidal surface fracture.

Samples Heat Treated for This Study. Unless stated otherwise, the information given for heat-treated samples in the remainder of the Results section refers only to the standard two-stage heat treatment process used to produce "green amber" for this study.

After the standard heating, a "lemon" yellow Colombian copal and a "honey" yellow Brazilian copal turned bright green. Pale yellow copals from Madagascar and Tanzania turned "golden" yellow and brownish yellow, respectively, with a pale green tint. Brown Kuji amber turned dark brown. Amber samples from the Baltic Sea region as well as those from Ukraine, the Dominican Republic, and Mexico turned green and yellowish green, but the colors of the Dominican and Mexican ambers were not highly saturated (figure 5).

After the two-stage heating with shorter time intervals, the 14 beads of "lemon" yellow Colombian copal (Col-04–17) turned yellowish brown (figure 6). Single-stage heating of a "lemon" yellow Colombian copal (Col-03) also yielded a brown color (figure 7).

Before heating, all copal samples could be scratched with a fingernail; the amber samples could not be scratched. After heating, none of the samples could be scratched with a fingernail. No change was seen in the RI or SG values of any of the samples after heating. However, the long-wave UV fluorescence reactions were markedly different. The

Figure 7. This 10.42 ct "lemon"-yellow Colombian copal (left) was treated by a one-stage heating process (180°C and 20 bars for one hour) that has been used routinely by Treasure Green Amber Ltd. to induce a yellowish brown color in amber and copal, as was the result here (right). Photos by A. Abduriyim.
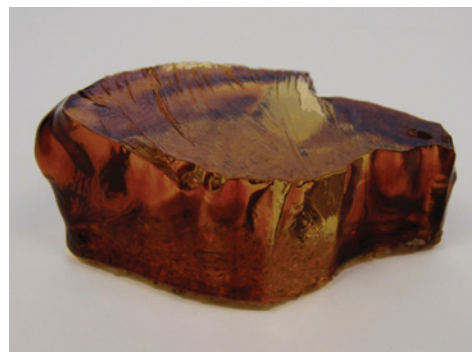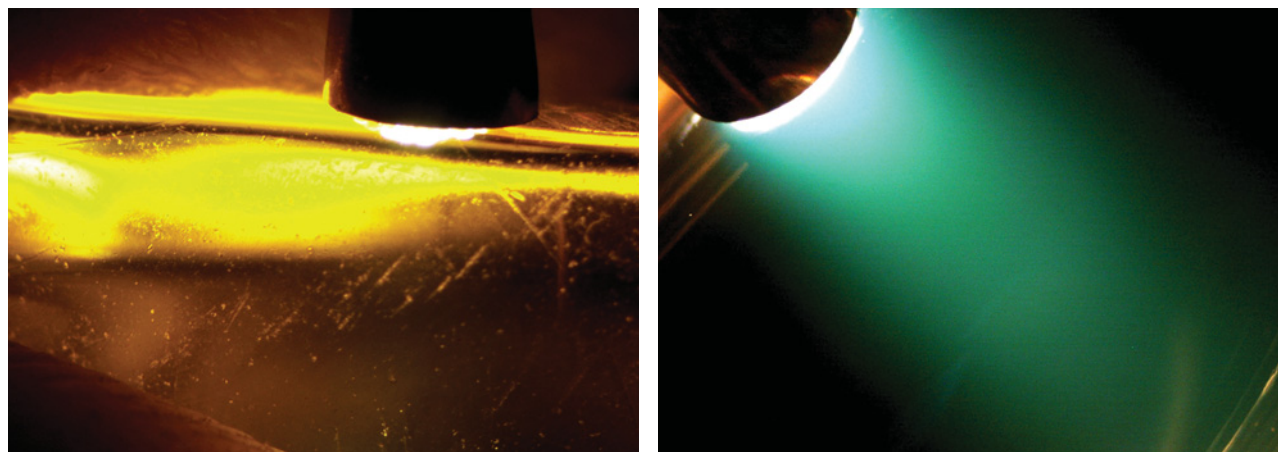
Figure 8. On the left, microscopic examination of untreated Colombian copal with fiber-optic illumination reveals no cloud-like inclusions. On the right, a fine granular cloud is illuminated in a piece of Baltic amber (Bal-01H) after heat treatment. Photomicrographs by A. Abduriyim; magnified 25× (left) and 15× (right).

untreated amber and copal fluoresced dark green or bluish green before heating, but this changed to a strong whitish blue after treatment (similar to that seen in natural "blue" amber). One exception to this was the Mexican amber, which fluoresced whitish blue to long-wave UV, both before and after heating. All samples fluoresced dark green to short-wave UV, regardless of whether they had been heat treated (again, see table 1).

Microscopic Observations. Before heating, some amber and copal samples contained small cracks or minute gas bubbles. Plant debris and insects were rarely observed. After the standard two-stage treatment, the cracks appeared larger and were disc-like (i.e., resembling the "sun spangles" or "glitter" seen in conventionally heat-treated material). The gas bubbles became smaller and migrated closer to the surface. The smaller plant debris and insects were broken up and reduced in size. A sample of milky white Ukrainian amber (Uk-02) became clear. Fine granular clouds could be seen with the use of a gemological microscope and strong fiber-optic illumination in all samples that underwent the two-stage treatment procedure (figure 8). The samples with a deeper green color contained more clouds.

Photomicrographs of various inclusions in "green amber" are available in the *G&G* Data Depository.

Alcohol Test. Before heating, all copal samples reacted to alcohol by losing their polish luster. Their surfaces became sticky and showed a fingerprint after being pressed with a fingertip. None of the heated samples—like their heated and unheated amber counterparts—showed a reaction to alcohol.

Brine Test. In the saltwater solution, amber and copal from all localities floated before and after the heating, as did the commercial "green amber."

Hot Point Test. Before heat treatment, the copal samples started to melt, while gradually giving off white smoke, when a hot point was positioned close to their surfaces. After heat treatment, none of the samples showed any melting reaction, although they all gave off white smoke when the hot point was touched to their surfaces. Untreated copal released a sweet-sour resinous odor, while untreated natural amber gave off a pungent resinous odor. Treated "green amber" produced a weaker odor than the untreated natural amber.

Static Electricity Test. All samples showed static electricity after they were rubbed with a cloth, as expected for natural resin.

FTIR Spectroscopy. The FTIR spectra of representative samples of untreated and treated amber and copal are presented in figures 9 and 10 according to their geologic age (see table 1 for ages). FTIR peak assignments are described in appendix A. The amber from Kuji in Japan represents the oldest and consequently the most structurally mature sample. Amber from the Baltic Sea region was selected for comparison in these figures because it has diagnostic spectral features for determining geographic origin (as described below and in appendix A). The Brazilian copal is shown because copal from this locality is often used as a starting material for commercial "green amber" treatment. FTIR spectra from all studied localities—and a table of FTIR spectral features

for amber and copal before and after heat treatment—can be found in the *G&G* Data Depository.

Untreated Amber. Most of the features visible in the amber spectra in figure 9 have been previously reported, including carbon single-bond absorption features near 2927 and 2867–2853 cm^{-1}, and at 1454, 1384, and 1024–975 cm^{-1} (Marrison et al., 1951; see appendix A for a discussion of the relationship between molecular structure and spectral features). The spectra of amber from the Baltic Sea region and Ukraine displayed the "Baltic shoulder"—a flat shoulder in the area between 1259–1184 cm^{-1} and an associated feature at 1159 cm^{-1}—that has been noted as characteristic of these materials in past studies (Beck et al., 1964; Langenheim, 1969). The Kuji spectrum resembled that of Baltic amber in general, but with a less-flat Baltic shoulder–like absorption at 1259–1184 cm^{-1}. Low-intensity asymmetric absorptions at 744, 698, 640, and 540 cm^{-1} may be related to aromatics or substitution in benzene rings (Broughton, 1974).

Figure 9. These FTIR spectra represent amber from Japan and the Baltic Sea region, and copal from Brazil, prior to heat treatment. They are arranged in order of geologic age, with the oldest sample on the top. Each spectrum is offset vertically for clarity. Features at 3076, 1643, and 887 cm^{-1}, which are attributed to carbon-carbon double bonds in exocyclic methylene groups, are detectable in the Ukrainian amber and Brazilian copal. Features at 1728 and 1698 cm^{-1}, and in the region from ~1260 to 1150 cm^{-1}, are due to carbon-oxygen double bonds and single bonds, respectively, in functional groups.
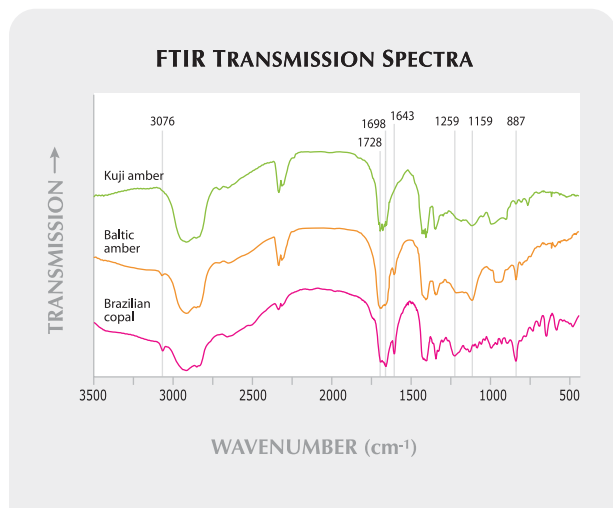
In the regions of carbon-carbon double bonding, an absorption was observed at 3076 cm^{-1}. A weak absorption at 1643 cm^{-1} was also seen, visible as a shoulder of a strong absorption at 1728–1698 cm^{-1}. In addition, there was a sharp absorption at 887 cm^{-1}.

Untreated Copal. The copal spectra (see, e.g., figure 9) contained major features at 3076, 1643, 1593, and 887 cm^{-1}, which indicate a high content of double bonds in these samples. Also, the absorption at 1698 cm^{-1} in the double-bonded carbon-oxygen region was relatively stronger than the absorption at 1728 cm^{-1}. Clearly separated small absorptions were recognized at ~2867 and ~1384 cm^{-1}. In addition, there were broad absorptions at 4720 and 4607 cm^{-1} (not shown in the figures), and intermediate-intensity absorptions at 744, 698, 640, and 540 cm^{-1}.

Heat-Treated Amber. The absorptions at 4720, 4607, 3076, 1643, and 887 cm^{-1} diminished or disappeared after treatment, while the appearance or increase in intensity of the 820 cm^{-1} absorption was observed for all amber samples (e.g., figure 10).

Figure 10. These FTIR spectra were collected after a two-stage heating process was applied to the samples in figure 9. Note that the 3076 cm^{-1} and 1643 cm^{-1} features were not detected in the copal after heat treatment, indicating that exocyclic methylene groups were destroyed in these materials during treatment. A new feature at 820 cm^{-1}, marked with red circles, was observed in all samples after heat treatment.
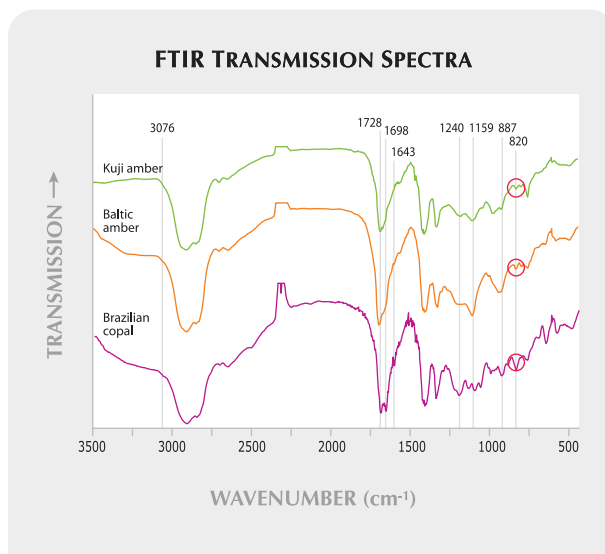
In addition, three peaks at 1172, 1147, and 1107 cm^{-1} tended to decrease and broaden in the Dominican sample. The diagnostic Baltic shoulder remained in the spectra of the Baltic and Ukrainian samples.

Heat-Treated Copal. The spectra of all copal samples showed significant changes after heating (e.g., figure 10): The absorption features at 3076, 1643, 1593, 887, 744, 698, 640, and 540 cm^{-1} were greatly diminished and those at 4720 and 4607 cm^{-1} disappeared. The absorption at 1698 cm^{-1} became notably weaker, while that at 1728 cm^{-1} became stronger. In the carbon single-bond region, the absorption at 1259 cm^{-1} shifted to 1242 cm^{-1} and three absorptions at 1172, 1147, and 1107 cm^{-1} appeared to decrease and broaden. After heating, the overall pattern of the copal spectra closely resembled those of amber but without the Baltic shoulder. Also, a small absorption formed at 820 cm^{-1} in all copal samples.

Following the experimental two-stage heating at 20 hours per stage, the spectral changes for the 14 yellowish brown copal beads (Col-04–17) were similar to those exhibited by samples for which the heating process produced a green color (see *G&G* Data Depository figure DD-6). The maximum absorption at 1698 cm^{-1} became weaker, while absorption at 1728 cm^{-1} increased, and the absorption at 1269 cm^{-1} shifted to 1242 cm^{-1}. The resulting absorption pattern resembled that of amber, except that the absorption at 820 cm^{-1} was not evident.

After the experimental one-stage heating process, copal sample Col-03 turned brown, while the absorption intensity at 4607, 4270, 3076, 1643, 1593, 887, 744, 698, 640, and 540 cm^{-1} decreased by about half. Therefore, the features that characterize it as copal could still be recognized (again, see *G&G* Data Depository figure DD-6).

Commercially Treated "Green Amber." The results for these samples were similar to the spectral patterns of the amber and copal samples after our heating experiment. Absorptions at 4607, 4270, 3076, 1698, 1643, 1593, 744, 698, 640, and 540 cm^{-1} were almost absent, a weak absorption at 887 cm^{-1} was observed, and a small absorption near 820 cm^{-1} was present in all samples (see *G&G* Data Depository figure DD-7). The spectrum of the sample from Facett Art (see FA-001 in figure DD-7) was distinctly different from those of the samples from the other two companies—Treasure Green Amber Ltd. and Amber Gallery Export-Import—with absorption features resembling a Baltic shoulder. The absorption seen at 975 cm^{-1} was stronger than that at 1024 cm^{-1}.

NMR Spectroscopy. The ^{13}C NMR spectra of amber from Kuji in Japan, amber from the Baltic Sea region, and copal from Brazil are shown in figures 11 and 12. NMR spectra from all the studied localities—and a table of NMR spectral features for amber and copal before and after heat treatment—can be found in the *G&G* Data Depository. NMR peak assignments are described in appendix A.

Untreated Amber. In general, the spectral patterns of amber from each locality were similar (again, see figure 11), though certain features showed some variation according to geologic age.

In the single-bonded region at 90–10 ppm, the ^{13}C NMR spectra showed a peak that had the largest signal intensity at 40–37 ppm. This peak is attributed to several carbon sites in the core structure of both amber and copal (Lambert and Frye, 1982) that are stable over tens of millions of years. Except for this feature, signals of carbon single-bonded to hydrogen were distributed in the 22–17 ppm range and those of carbon single-bonded to carbon were at 30–26, 36, 53–50, and 59–58 ppm. Line widths in this single-bonded carbon region tended to broaden with increasing age of the sample.

In the double-bonded carbon region at 155–105 ppm, four carbon signals were detected at 148, 139, 127, and 108 ppm. The signals at 148 and 108 ppm tended to be weaker in spectra from the older amber samples, and were absent from the Kuji amber spectrum (likely the oldest sample).

In the functional group region at 200–170 ppm, the ester group appeared only in Baltic and Ukrainian amber samples at 176–172 ppm. Note that the presence of an ester group in the amber structure is unique to material from Ukraine and the Baltic Sea region.

Untreated Copal. In the spectra of the untreated copal samples, the signals from single-bonded carbon at 49–47 ppm, 29–28 ppm, and 20–15 ppm were sharper than those of amber, and the spectral pattern of each signal was further divided into several small signals (e.g., figure 11). In the double-bonded carbon region, four main signals were resolved. The intensities of the signals at 148 and 108 ppm
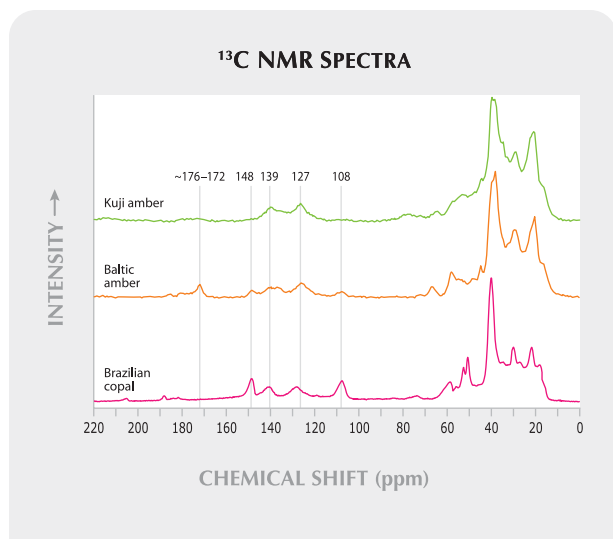
Figure 11. *^{13}C NMR spectra are shown for representative amber from Japan and the Baltic Sea region, and copal from Brazil. Peaks related to carbon atoms in the carbon skeleton are located in the 90–10 ppm region. The peaks at 148 and 108 ppm in the Baltic amber and Brazilian copal are attributed to carbons in exocyclic methylene groups. The peaks at 139 and 127 ppm, which are attributed to carbon atoms in the structural core of diterpene units, were observed in all samples. The peak at ~176–172 ppm in the Baltic amber spectrum is attributed to an ester functional group, which is characteristic of Baltic and Ukrainian material.*

Figure 12. *Shown here are the ^{13}C NMR spectra for the samples in figure 11 that were treated by the standard two-stage heating process with pressure. A new signal at 179 ppm, detected in all of these heated samples, is marked with red circles.*

were stronger than the signals at 139 and 127 ppm. In the functional group region, the spectra of all the copal samples had a clear peak at 184–182 ppm related to carboxylic acid.

Heat-Treated Amber. After heat treatment, signal intensities at 57, 48, 44, and 28 ppm generally decreased and peaks broadened in the single-bonded carbon region of all amber samples (figure 12). In the double-bonded carbon region, the signals at 148 and 108 ppm almost disappeared in all treated amber samples, and the signals at 139 and 127 ppm in the spectra from some localities increased slightly and broadened. A new signal was observed in the functional group region at 179 ppm.

Heat-Treated Copal. Unlike the heat-treated amber described above, the carbon signals in the single-bonded carbon region changed from sharp peaks for the untreated copal to broader curves for the treated

material. Even so, the peaks for the heat-treated copal were sharper than those in the spectra of the (untreated) geologically old Kuji and Baltic ambers and approximately the same as those of (untreated) young Dominican amber. The signal intensities at 148 and 108 ppm greatly diminished after heat treatment, while the signal intensities at 139 and 127 ppm generally increased. The carboxylic acid functional group signal at 184–182 ppm also disappeared after treatment, and a new signal appeared at 179 ppm (e.g., figure 12).

During the heating process using two stages with short time intervals, the spectral changes of the 14 samples of Colombian copal (Col-04–17) after treatment were almost the same as those of the Colombian sample (Col-02) heat treated with the standard set of experimental parameters, but the decrease in signal intensity at 148 and 108 ppm appeared smaller than that seen in sample Col-02 (see *G&G* Data Depository figure DD-10). In general, features in the three regions of the spectrum for Col-04–17 resembled those of unheated young amber, but with a faint signal at 179 ppm.

The Colombian copal sample (Col-03) that was heated in a one-stage treatment process showed no change in the single- and double-bonded carbon regions. In its spectra before and after heat treatment, the signal intensities at 148, 139, 127, and

108 ppm remained the same (again, see *G&G* Data Depository figure DD-10). However, the carboxylic acid functional group signal at 182 ppm disappeared and no signal was detected at 179 ppm.

Commercially Treated "Green Amber." Spectra of representative samples from the three producers are shown in *G&G* Data Depository figure DD-11. In the single-bonded carbon region, all the signals in the spectra from TR-001 and BR-001 resembled the spectrum of amber and copal samples after heat treatment, but the spectrum from FA-001 showed a less intense signal at 49–47 ppm than the spectra of those other two samples. In the double-bonded carbon region, signals at 148 and 108 ppm were barely detectable in any of these samples, and their patterns resembled the spectrum of the Kuji amber (the oldest sample studied) before and after heating. In the functional group region, a weak signal attributed to ester group carbons was detected at 172 ppm in the Facett Art sample. A signal at 179 ppm was detected in all the samples.

DISCUSSION

The main questions surrounding the green amber that has entered the market are: (1) is it "natural"; and (2) if not natural, is it produced from amber or the younger, structurally immature resin, copal? We know from the literature and our experience that green amber is extremely rare in nature and has not been reported to date in the deep peridot-like colors currently seen in the marketplace. In fact, several of the dealers offering the material readily acknowledged that it is produced by heat treatment. What is not readily apparent is whether the original material being treated is copal or its more valued fossilized counterpart, amber. We know from our heating experiments that a two-stage process involving long intervals under controlled heat, pressure, and atmosphere can produce green in both materials.

Gemological Properties. Compared to untreated amber, the heated "green amber" showed no observable differences in RI and SG, but its hot-point odor was weaker than that of natural untreated amber. The fluorescence reaction of amber and copal is potentially a very good indicator of heat treatment. A whitish blue reaction to long-wave UV radiation appears to signal treatment because, with

the exception of Mexican amber, it was observed only in amber and copal after heat treatment and in "green amber" samples that were represented as being heat treated. However, this fluorescence reaction cannot identify the starting material because heat-treated amber and copal samples had the same reaction. Destructive tests involving scratching, alcohol exposure, and a hot point may be useful for separating "green amber" from imitation amber (synthetic resin), but the reactions to these tests are not helpful in separating "green amber" from copal or amber, or in determining the starting material used to produce "green amber." The multi-stage heat treatment may improve the saturation of green color or the depth to which the color layer penetrates from the surface of the material. The green color is not always stable when the material is placed in a dark area.

Production of "green amber" in an autoclave is possible with either amber or copal, but it requires certain pressure, temperature, and time parameters. In addition, the optimal set of conditions may vary for individual starting materials, and in some cases may not exist at all. Using the Treasure Green Amber Ltd. autoclave and heat-treatment protocol, we produced "green amber" from Colombian and Brazilian copal and from amber from the Baltic Sea region, Ukraine, the Dominican Republic, and Mexico; both copal and amber samples from other localities turned greenish yellow or brown.

FTIR Spectroscopy. Our general observation of the FTIR spectra of the commercial "green amber" samples and our heat-treated "green amber" samples is that they resembled those from amber rather than copal, even when the starting material was known to be copal. Therefore, it is difficult to determine from FTIR spectra whether these "green amber" samples were originally copal or amber.

It is possible, however, that spectral features characteristic of certain localities may help identify the geologic origin of some samples and, therefore, the likelihood that the original material was copal or amber. For example, the presence of the Baltic shoulder in the FTIR spectrum indicates that amber from the Baltic Sea region or Ukraine is the likely starting material. All "green amber" samples from Facett Art showed an absorption similar to that of ester functional group carbons, which produces the Baltic shoulder in the range of 1259–1159

cm^{-1}. This feature was not seen in any of our copal material before or after heat treatment. In subsequent studies, we confirmed that several pieces of "green amber" from Treasure Green Amber Ltd. showed similar Baltic shoulder features in their FTIR spectra. These FTIR results provide supporting evidence that the Facett Art sample and at least some of the samples from Treasure Green Amber Ltd. were indeed Ukrainian or Baltic amber, as the companies claimed.

The FTIR spectra of copal from all studied localities showed peaks with strong intensities at 4720, 4607, 3076, 1643, 1541, 887, 744, 698, 640, and 540 cm^{-1}, which are related to unsaturated bonds. These peak intensities decreased after the heating protocol, which indicates that the unsaturated-bond content of the copal samples was reduced by the multi-stage heat treatment. Amber that is geologically older—or, more precisely, structurally more mature—is known to have a lower content of unsaturated bonds, since unsaturated bonds are converted to saturated bonds during fossilization processes (see appendix A). Also, after treatment the maximum absorption at 1698 cm^{-1} changed to 1728 cm^{-1} for these copal samples, causing their spectra to appear more like that of amber. This means that FTIR spectra provide evidence that the structural changes from polymerization occur in copal as a result of the multi-stage heat treatment. That is, this heat treatment essentially matures or "artificially ages" copal by causing it to undergo polymerization so that it resembles geologically older amber.

The absorption around 820 cm^{-1} was detected to varying degrees in all the amber and copal samples subjected to the standard multi-stage heat treatment and in the "green amber" from the three companies. It was not, however, present in the Colombian copal samples treated in the additional two-stage and one-stage heat treatment experiments. The presence of this signal may be a reliable indicator for multi-stage heat treatment, especially if higher-quality spectra with better signals are collected.

NMR Spectroscopy. In the ^{13}C NMR results for the commercial "green amber" from the three companies, the signals of the double-bonded carbons in the carbon skeleton at 139 and 127 ppm were comparable to those observed in amber and copal, but the signals of exocyclic methylene group carbons at 148 and 108 ppm were very weak or undetectable. However, the signals of carbon in samples from Treasure Green Amber Ltd. and Amber Gallery Export-Import at 58–57, 49–47, 36–33, 29–28, and 20–15 ppm in the single-bonded carbon region did not appear as the broad, partially resolved peaks observed in older Kuji and Baltic amber samples. Instead, they resembled spectral features of the relatively young amber from the Dominican Republic. In the functional group spectral region, we observed a signal at 179 ppm in all "green amber" samples that generally was not seen in any unheated amber and copal or in traditionally heated materials. For the "green amber" from Facett Art used in this study, the signals at 57, 48, 44, and 28 ppm in the single-bonded region were low and broad, and in the double-bonded region the signals at 148 and 108 ppm were not detectable. A weak signal due to an ester functional group was detected in the Facett Art sample at 172 ppm; this characteristic spectral feature of Baltic and Ukrainian amber indicates that the sample was likely from one of these localities.

The untreated copal samples from all studied localities showed sharper peaks at 58–57, 49–47, 36–33, 29–28, and 20–15 ppm than were seen in the untreated amber. After heat treatment of copal, peaks in the single-bonded carbon region generally broadened but did not exactly replicate the line shapes in spectra of untreated older amber. Moreover, the line shapes in the copal spectra after treatment showed less variability than was seen in untreated amber.

In the double-bonded carbon region of the spectra from the untreated copal samples, the signal intensities of exocyclic methylene group carbons at 148 and 108 ppm were greater than the signal intensities of double-bonded carbons from the carbon skeleton at 139 and 127 ppm. In the spectra of untreated amber from the Baltic Sea region, Ukraine, and the Dominican Republic, the relative signal intensities at 148 and 108 ppm were lower than those at 139 and 127 ppm, and no signals were detected in this region of the Kuji amber spectrum. After heat treatment, signal intensities at 148 and 108 ppm decreased greatly in all the samples. The molecular structure of copal is partially polymerized, meaning that individual molecules are joined into polymer chains, but bonding between polymer chains is scant and the chains are separated. Thus, exocyclic methylene groups, which are consumed during cross-linkage reactions that join polymer chains (see appendix A), are present in natural copal and their carbons (with signals at 148 and 108 ppm) are detectable in

Figure 13. Ranging from greenish yellow (shown here) to green, commercial amounts of "green amber" have entered the marketplace. This necklace consists of faceted beads that range from 1.3 to 1.8 cm in diameter. Courtesy of HotRockJewelry.com, Solana Beach, California; photo by Robert Weldon.

the corresponding spectra. However, the multi-stage heat treatment process can induce these cross-linkage reactions (see appendix A, figure App-2).

An earlier study by Kimura et al. (2006b) proposed that this cross-linkage formation was related only to the age of the amber and not to its thermal history. However, we found in the present study that the cross-linkage formation in copal and amber can be produced by a multi-stage heating process under pressure, essentially artificially aging the sample during treatment. The polymer network formation that results from the artificial aging of copal following treatment appears to be less complex than that formed during the natural aging of amber, as suggested by the broader spectral pattern of single-bonded carbon signals in the ^{13}C NMR spectrum of treated copal as compared to untreated amber. Therefore, estimating the age of "green amber" produced by heat treatment is not possible by measuring the intensities of the 148 and 108 ppm signals alone.

Identification and Cause of Color. In the functional group region, a new ^{13}C NMR absorption was observed near 179 ppm in all multi-stage heated amber and copal, as well as in all the commercial "green amber" samples, thus providing a spectroscopic index for separating samples that have been artificially and naturally aged. However, this signal cannot be used to establish the identity of the starting material. The formation of the signal is likely due to the production of a new functional group from a devolatilization reaction during the multi-stage heating process.

The small absorption around 820 cm^{-1} in the FTIR spectra was detected in all the treated amber and copal samples (except those treated by the experimental double- and single-stage processes) and in all the commercial "green amber" samples. This feature can be used to identify the treatment. Spectral evidence of the Baltic shoulder indicates that the starting material was amber; however, the absence of this feature provides no conclusive information about the starting material.

The green color exhibited by the treated material is not directly related to the molecular structure of amber or copal; nor is it derived from fluorescence. Heat treatment produced fine granular cloud inclusions that were observed throughout the treated green samples with the use of magnification and a strong fiber-optic light (again, see figure 8). The green color is likely caused by colloidal dispersion (scattering of light) of the minute grains in these clouds, as is the case with the rare Mexican green amber (Cattaneo, 2008). The mechanism by which these fine grains formed is beyond the scope of this article.

NOMENCLATURE

The "green amber" color was produced in both amber and copal by heat treatment. As a result of this process, the heat-treated copal showed changes in physical properties, such as increased hardness and improved solvent resistance, that made it more

similar to untreated amber. The "green amber" obtained from copal by this treatment is physically almost identical to amber and extremely difficult to identify by standard gemological testing. Therefore, the Laboratory Manual Harmonization Committee (LMHC) concluded that effective June 1, 2009, if the identity as amber or copal cannot be made readily, then its variety should be called *amber* and the words "Indications of heating, this resin has been processed by heat and pressure and may have been derived from copal" placed in the comment column. This statement applies to green as well as to yellow-to-brown material.

As also noted above, the presence of the Baltic shoulder feature in the FTIR spectrum proves that the starting material was amber. Identification by this method, however, requires that several milligrams be ground to a powder. In some cases, the Baltic shoulder may also be identifiable by nondestructive diffuse reflectance FTIR spectroscopy. For heated samples exhibiting this feature, the LMHC has stipulated that the following comment be used on the report: "Indications of heating, this resin has been processed by heat and pressure." This statement applies to green as well as to yellow-to-brown material.

CONCLUSION

In recent years, greenish yellow (figure 13) to peridot-like "green amber" has been circulating in the gem market. The intense color of much of this material has not been seen in untreated amber, and it possesses excellent transparency with fewer inclusions than typical amber. The hardness, SG, and solvent resistance of "green amber" are typically greater than of copal. The odor given off when "green amber" is burned with a hot point is slightly weaker than that emitted by natural, untreated amber, but its other physical properties are quite close to untreated amber.

Employing an autoclave to perform a multi-stage heating process under pressure, we successfully produced "green amber" using amber from the Baltic Sea region, Ukraine, the Dominican Republic, and Mexico, as well as copal from Colombia and Brazil. Japanese amber from Kuji turned brown, and copal from Tanzania and Madagascar turned yellow with a slight greenish hue. However, only a limited number of samples were treated, so it is possible that other material from these localities would respond differently.

Spectral analysis with FTIR and ^{13}C NMR identified structural changes in the treated copal and amber. While identification of the treated material is possible using these techniques, the drawback is that they require destructive analysis. The cause of the green color in treated green amber is not clear, but it appears to be the result of the scattering of light by minute particle clouds formed during treatment.

ABOUT THE AUTHORS
Dr. Abduriyim is chief research scientist at the Gemmological Association of All Japan (GAAJ)-Zenhokyo Laboratory in Tokyo. Dr. Kimura is a researcher at the Sophia Research Institute (SRI) Co. Ltd. at Sumitomo Rubber Group, Kobe, Japan. Dr. Yokoyama is assistant professor, Mr. Nakazono is technician, and Dr. Wakatsuki is emeritus professor, at Tsukuba University, Tsukuba City, Japan. Dr. Shimizu is group leader, Dr. Tansho is senior researcher, and Mr. Ohki is senior engineer, at NIMS in Tsukuba City.

APPENDIX A: THE STRUCTURE AND SPECTROSCOPY OF AMBER AND COPAL

Resinites are a group of organic hydrocarbons (compounds made of carbon, oxygen, and hydrogen) that are derived from plant resin. Amber and copal are the fossilized and semi-fossilized forms of resinite, respectively. Fossilization of resin involves a series of polymerization and devolatilization reactions that change its composition and structure. The measurable differences in the physical properties of copal and amber are a direct result of the structural changes that occur during fossilization processes.

In nature, fossilization takes place over long periods of geologic time at elevated temperature and pressure conditions that result from sedimentation and burial of organic materials. Fossilization reactions can also be induced in the laboratory by subjecting a resinite material to specific temperature, pressure, and time parameters so that polymerization and devolatilization can occur on the timescale of an experiment. The structure of any resinite is therefore strongly dependent on both the age and thermobarometric history of the sample—that is, its *maturity* (Anderson et al., 1992). This is quite important, since the treatment processes used to make "green amber" involve the use of temperature and pressure conditions that artificially increase the maturity of copal and amber—making the treated material difficult to identify based on its physical and spectroscopic properties.

Molecular Structure. *Individual Structural Units.* On a molecular level, resinites are composed of structural units joined together in chains of varying lengths. The precursor units that make up resinites are macromolecules called labdanoid diterpenes, which are a class of hydrocarbons with the general chemical formula $C_{20}H_{32}$. Ozic acid is a major component of resin produced by plants from the genus *Hymenaea*. Copal from Colombia, Tanzania, and Madagascar, as well as amber from the Dominican Republic, originate from the Fabaceae family (which includes *Hymenaea*). In contrast, communic acid is a major component of Baltic Sea region amber that originates from plants that may belong to the genus *Araucaria*. Both communic and ozic acid possess labdanoid diterpene molecules with similar structures (Schlee 1984; Schlee and Ayuzawa, 1993; Kimura et al., 2006a). For the purposes of this article, this appendix will discuss several key points about the molecular structure of amber and copal.

A graphic representation of a labdanoid diterpene unit is shown in figure App-1. This line-angle structure diagram provides a simplified illustration of the core structure of an organic molecule (i.e., a labdanoid carbon "skeleton"). The diagram shows only the bonds between carbon atoms. A single line represents a single bond, also known as a *saturated* bond, and a double line represents a double bond, also known as an *unsaturated* bond. Carbon atoms are located at the ends of lines and at the intersections of two lines. It is assumed that in addition to the bonds shown, each carbon participates in enough single bonds with hydrogen (C-H) so that its total number of bonds is four. Where carbon and hydrogen atoms in groups are shown at termini, it is for informational purposes.

Note that most carbons are bonded to two other carbons in the core of the structure. These carbons are bonded to two or three additional carbons by single bonds, although one double bond occurs between two carbon sites (labeled 12 and 13 in the figure). In general, the carbons in the core of the structure are not involved in the polymerization and devolatilization reactions that occur as copal matures to amber.

Other carbon sites in the labdanoid diterpene unit are terminal carbons, which are bonded only to carbon in the structural core. These terminal carbons bond with other atoms in what is called a *terminal group*. These terminal carbons are quite important to structural differences between copal and amber because they are involved in maturation reactions.

A labdanoid diterpene unit contains three *methyl groups* in its structure, which are terminal carbon bonded to three hydrogens (annotated CH_3; shown in green). It also contains one *functional group* site (shown in blue) that involves a terminal carbon bonded in one of several arrangements. These include carboxylic acid (-COOH; shown) and ester (-COO-). Carboxylic acid is present in copal, but not in amber. It is widely known that only amber originating in the Baltic Sea region and Ukraine contains ester as the functional group, so it is a useful indicator of geographic origin.

Perhaps the most gemologically relevant functional group is the *exocyclic methylene group* (shown in red); it is this group that is involved in the polymerization and devolatilization reactions that turn copal to amber. Each labdanoid diterpene unit contains one exocyclic methylene group, denoted CH_2. It consists of a terminal carbon double-bonded to a carbon in the structural core of the unit, and to two hydrogens in single C-H bonds.

Polymerization of Individual Units. As mentioned above, polymerization reactions are an important part of the fossilization process. In general terms,
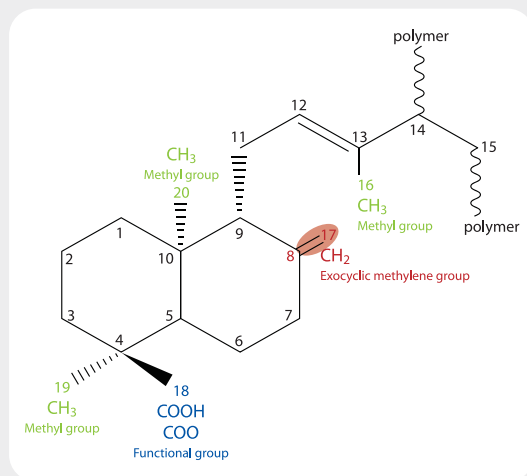
Figure App-1. This line-angle carbon skeleton structure diagram illustrates one of the macromolecules called a labdanoid diterpene that forms linkages in amber and copal. All bonds in the plane of the page are represented by straight lines. Dashed and wedged-shaped bonds are going into and out of the plane of the page, respectively. Bonds that connect individual labdanoid diterpene units to polymer chains are shown by wavy lines. Carbons that participate only in single bonds with other carbons are those labeled 1, 2, 3, 4, 5, 6, 7, 9, 11, 14, 15, 16, 19, and 20. Four of these occupy terminal sites; three of them belong to methyl groups (16, 19, and 20; shown in green), and one belongs to a functional group (18; shown in blue). Carbons involved in double bonds with other carbons are labeled 8, 12, 13, and 17. The only one of these to occupy a terminal position is part of an exocyclic methylene group (17; shown in red).

polymerization reactions involve the conversion of unsaturated (double) bonds to saturated (single) bonds. Initially, polymerization involves linking of individual labdanoid diterpene units (such as those shown in figure App-1) into polymer chains, which occurs at carbon sites 14 and 15 in immature resin. This requires breaking a double bond between sites 14 and 15 (not shown) to join individual units.

As polymerization proceeds, cross-linkage between chains of labdanoid diterpene takes place as copal changes to amber and continues as amber structurally matures (figure App-2). This cross-linkage occurs when the double bond between carbons 8 and 17 breaks, the exocyclic methylene group is destroyed, and a single bond re-forms between the carbon at site 8 and a carbon at site 12 in another labdanoid diterpene to form a three-dimensional polymer network. In copal, few cross-linkages exist and chains are separat-
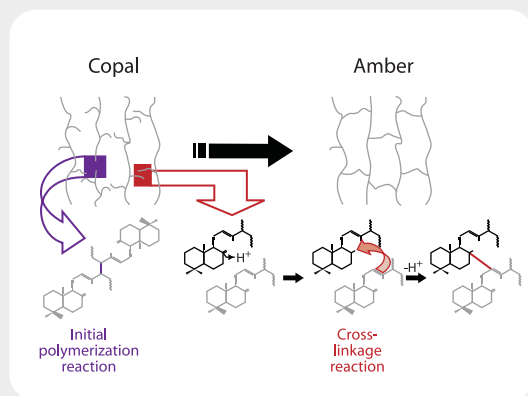

Figure App-2. This diagram illustrates the polymerization reactions involved in the formation of copal and the transition from copal to amber. During initial polymerization, individual labdanoid diterpene units in resin join together to form polymer chains and produce copal (shown in purple). Replacement of terminal exocyclic methylene groups in labdanoid diterpenes with bonds between them produces cross-linkages between polymer chains as copal matures into amber (shown in red).

ed, and thus the double bonds are present in this material. These bonds are replaced with saturated bonds as copal matures into amber. The amount of exocyclic methylene double bonds present in these materials is a rough indicator of their maturity.

Spectroscopic Methods for Investigating Structure. Fossil resins have been classified into several types (e.g., Lambert et al., 2008), using gas chromatography/mass spectrometry (i.e., Classes Ia, Ib, Ic, II, III, IV, and V) and NMR spectroscopy (Groups A, B, C, and D). These types are differentiated according to their macromolecular structure and whether they contain succinic acid within their structure. Equivalent types are Class Ia and Group C, Class Ib and Group A, Class Ic and Group D, and Class II and Group B.

FTIR and NMR spectroscopy are complementary techniques for studying the structure of amber and copal. Absorption lines in FTIR spectra correlate to bonds *between atoms*, so this technique provides information about the nature of bonds in the structure shown in figure App-1. In contrast, peaks in NMR spectra correlate *to atoms*, so this technique provides information about the individual sites shown in figure App-1.

FTIR Spectroscopy. A representative FTIR spectrum of amber studied for this article (i.e., of a Class
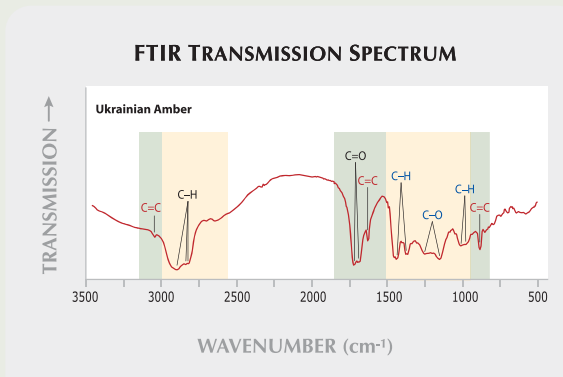
FTIR TRANSMISSION SPECTRUM

Figure App-3. In this representative FTIR spectrum of Ukrainian amber, regions corresponding to double and single bonds are shaded in green and tan, respectively. The colors of peak labels correspond to the color-coding used in figure App-1.

13C NMR SPECTRUM

Figure App-4. In this representative ^{13}C NMR spectrum of Colombian copal, the region from 90 to 10 ppm corresponds to single-bonded carbon, from 155 to 105 ppm corresponds to double-bonded carbon, and from 200 to 170 ppm corresponds to a functional group. Peaks are numbered and colored according to the carbon site in figure App-1 to which they are attributed.

Ib/Group A resinite) is shown in figure App-3. It contains features that are important to distinguishing copal from amber, and to investigating the structural changes that occur as these materials mature.

One set of important features is attributed to bonds involving terminal carbons belonging to the exocyclic methylene group described above. Single bonds between carbon (site 17) and hydrogen in the exocyclic group correlate to absorptions at ~2927, 2853, 1470, and 1380 cm^{-1}, and a band from ~1050–950 cm^{-1}. Double bonds between carbons (sites 8 and 17) correlate with absorptions at ~3070, 1640, and 887 cm^{-1}.

The second set of important FTIR features is attributed to bonds involving terminal carbons belonging to the functional group site. Carbon (site 18)-oxygen double bonds in this group are correlated with
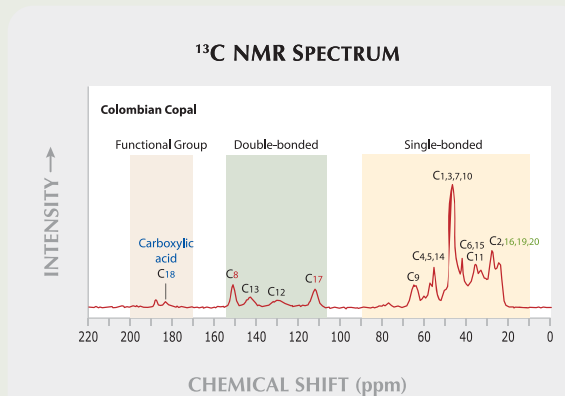
bands at ~1728 and 1698 cm^{-1}. Carbon (site 18)-oxygen single bonds are correlated with absorption features between ~1250 and 1150 cm^{-1}. When the functional group is an ester, as is the case with amber from the Baltic Sea region and Ukraine, this region displays what is termed the "Baltic shoulder." This refers to a broad horizontal shoulder from ~1250 to 1175 cm^{-1}, followed by a sharp absorption peak at ~1159 cm^{-1}.

The FTIR features correlated to the core structure of hydrocarbons comprising amber and copal are important for differentiating these materials. These features, which consist of low-intensity absorptions

REFERENCES

Anderson K.B., Winans R.E. (1991) The nature and fate of natural resins in the geosphere. I. Evaluation of pyrolysis-gas chromatography mass spectrometry for the analysis of natural resins and resinites. *Analytical Chemistry*, Vol. 63, pp. 2901–2908.

Anderson K.B., Winans R.E., Botto R.E. (1992) The nature and fate of natural resins in the geosphere—II. Identification, classification and nomenclature of resinites. *Organic Geochemistry*, Vol. 18, pp. 829–841.

Beck C., Wilbur E., Meret S. (1964) Infrared spectra and the origin of amber. *Nature*, Vol. 201, pp. 256–257.

Brody R.H., Edwards H.G.M., Pollard A.M. (2001) A study of amber and copal samples using FT-Raman spectroscopy. *Spectrochimica Acta Part A*, Vol. 57, pp. 1325–1338.

Broughton P.L. (1974) Conceptual frameworks for geographic-botanical affinities of fossil resins. *Canadian Journal of Earth Sciences*, Vol. 11, pp. 583–594.

Cattaneo G.L. (2008) L'Ambra (parte IV). *Rivista Gemmologica Italiana*, Vol. 3, No. 1, pp. 45–56.

Clifford D.J., Hatcher P.G. (1995) Structural transformations of polylabdanoid resinites during maturation. *Organic Geochemistry*, Vol. 23, No. 5, pp. 407–418.

Clifford D.J., Hatcher P.G., Botto R.E., Muntean J.V., Michels B., Anderson K.B. (1997) The nature and fate of natural resins in the geosphere—VIII. NMR and Py-GC-MS characterization of soluble labdanoid polymers, isolated from Holocene class I resins. *Organic Geochemistry*, Vol. 27, pp. 449–464.

Fujinaga T., Takenaka T., Muroga T. (1974) Origin of the archaeological amber in Japan, studied by infra-red spectra. *Nihon Kagaku Kaishi*, Vol. 9, pp. 2653–2657 [in Japanese].

Grimaldi D.A. (1996) *Amber: Window to the Past.* Harry N. Abrams, New York.

Guiliano M., Asia L., Onoratini G., Mille G. (2007) Applications of diamond crystal ATR FTIR spectroscopy to the characterization of ambers. *Spectrochimica Acta Part A*, Vol. 67, pp. 1407–1411.

Kiefert L. (2008) Treated green amber. AGTA GTC Laboratory Update, March 4.

at 744, 698, 640, and 540 cm^{-1}, are due to single carbon-hydrogen bonds involving carbons in the hexagonal rings. The positions and intensities of spectral features related to these unsaturated bonds can be used to separate mature amber from immature copal.

NMR Spectroscopy. A representative ^{13}C NMR spectrum of copal studied for this article (i.e., of a Class Ic/Group D resinite) is shown in figure App-4. NMR spectra of amber and copal are divided into three regions irrespective of resin age: single-bonded carbon (-C-) in the region of 90–10 ppm, double-bonded carbon (>C=C<) in the region of 155–105 ppm, and a functional group [(-COO-) and (>COOH)] in the region of 200–170 ppm (Lambert and Frye, 1982; Lambert et al., 1985). Individual peaks in these spectra correlate to the specific carbon sites (numbered 1–20 in figure App-1) in the structure.

In the single-bonded carbon region, peaks distributed between 22 and 17 ppm correspond to methyl group carbons (16, 19, 20) that are single-bonded to hydrogen. Peaks correlating to carbons that are part of the "labdanoid carbon skeleton" are located at 30–26, 37–40, 36, 53–50, and 59–58 ppm. The 37–40 ppm peak is attributed to several carbon sites (1, 3, 7, and 10) in the core of the structural unit (Lambert and Frye, 1982), which is stable over tens of millions of years of fossilization. Thus, this peak is quite distinct in the spectra of amber and copal of all ages. In general, peaks in this single-bonded carbon region tend to be broader with increasing age of the sample.

Spectral patterns in the double-bonded carbon region from 155 to 105 ppm are important, because of how the two different double bonds (those between 8 and 17 vs. those between 12 and 13) are affected by maturation processes. In this region, four distinct peaks at 148, 139, 127, and 108 ppm correspond to the four double-bonded carbons, at sites 8, 13, 12, and 17, respectively (Clifford and Hatcher, 1995; Clifford et al., 1997; Kimura et al., 2006a). Sites 12 and 17 are bonded to hydrogen, whereas sites 8 and 13 are bonded to carbon. The double-bonded carbons (sites 8 and 17) in the methylene group signals at 148 and 108 ppm are broken during the transition from copal to amber, as described above. The relative intensities of these two signals decrease with increasing sample maturation because their double bonds break during the transition from resin to copal to amber, until they are virtually absent in very mature samples such as the Kuji amber in this study. In contrast, the relative intensities of the 139 and 127 ppm features do not vary much with the maturity of amber and copal since the double bonds between carbons 12 and 13 are not involved in fossilization processes. Therefore, one can infer the age of natural amber from its ^{13}C NMR spectrum by setting signal intensities at 139 and 127 ppm as a standard and defining the relative signal intensities that are observed at 148 and 108 ppm (Lambert et al., 1985; Clifford and Hatcher, 1995; Clifford et al., 1997; Kimura et al., 2006a,b).

The spectral region from 200 to 170 ppm contains features of the various functional groups. The core structural units of amber and copal possess different functional groups. A peak at 176–172 ppm is attributed to carbon (site 18) from an ester functional group, which is only observed in the spectra of amber from the Baltic Sea region (Lambert and Frye, 1982; Clifford and Hatcher, 1995). In general, amber samples from other localities do not display any features in the functional group spectral region. A peak at 184–182 ppm corresponds to carbon from a carboxylic acid functional group, which is only present in copal.

Kimura H., Tsukada Y., Chujo R., Sasaki K. (2006a) Structural study of amber by high-resolution solid-state NMR. *Amber Reports, Society of Amber Studies of Japan*, No. 6, pp. 1–14 [in Japanese].

Kimura H., Tsukada Y., Mita H., Yamamoto Y., Chujo R., Yukawa T. (2006b) A spectroscopic index for estimating the age of amber. *Bulletin of the Chemical Society of Japan*, Vol. 79, No. 3, pp. 451–453.

Langenheim J. (1969) A botanical inquiry. *Science*, Vol. 163, pp. 1157–1169.

Lambert J.B. (1997) *Traces of the Past: Unraveling the Secrets of Archaeology Through Chemistry*. Perseus Books, Reading, MA, 319 pp.

Lambert J.B., Frye J.S. (1982) Carbon functionalities in amber. *Science*, Vol. 217, pp. 55–57.

Lambert J.B., Frye J.S., Poinar G.O. (1985) Amber from the Dominican Republic: Analysis by nuclear magnetic resonance spectroscopy. *Archaeometry*, Vol. 27, pp. 43–51.

Lambert J.B., Santiago-Blay J.A., Anderson K.B. (2008) Chemical signatures of fossilized resins and recent plant exudates.
Angewandte Chemie International Edition, Vol. 47, No. 50, pp. 9608–9616.

Marrison L.W., Briggs D.A.E., Polya J.B., Dennison J.C., McGilvray D.I., Mustafa A., Medhat Islam A. (1951) Notes: Characteristic absorption bands in the 10-m. period region of the infrared spectra of cycloparaffin derivatives. *Journal of the Chemical Society (Resumed)*, pp. 1614–1617.

O'Donoghue M. (2006) *Gems*, 6th ed. Elsevier, Oxford, UK.

Pedersen M.C. (2008) Natural green Caribbean amber. *Gems & Jewellery*, Vol. 17, No. 1, p. 15.

Perkovsky E.E., Zosimovich V.Y., Vlaskin A.Y. (2003) Rovno amber insects: First results of analysis. *Russian Entomological Journal*, Vol. 12, No. 2, pp. 119–126.

Rikkinen J., Poinar G. (2001) Fossilised fungal mycelium from Tertiary Dominican amber. *Mycological Research*, Vol. 105, No. 7, pp. 890–896.

Schlee D. (1984) Besonderheiten des Dominikanischen Bernsteins. *Stuttgarter Beitrage zur Naturkunde C*, Vol. 18, pp. 63–71.

Schlee D., Ayuzawa J. (1993) *In Japanese Amber*. Kitakyushu Museum of Natural History & Human History, Japan.

A CRYSTALLOGRAPHIC ANALYSIS OF THE TAVERNIER BLUE DIAMOND

Scott D. Sucher

While the Tavernier Blue has been established as the "grandparent" of the Hope diamond, the only firsthand historical documentation for it is a 17th century line drawing of questionable accuracy. It has been suggested that the diamond was crudely cut, conforming to the shape of the original crystal. If this is correct, then it should be possible to correlate the facets on the Tavernier Blue to the faces of a diamond crystal, and thus gain information on the crystallography of the original rough. This study used this information, the original drawings, and a computer model of the French Blue diamond generated from the laser scan of a recently discovered lead cast, to generate a computer model of the Tavernier Blue. This new model completely encloses the computer model of the French Blue, conforms to Tavernier's physical description, and establishes the orientation of the finished diamond within the original diamond crystal.

Recent evidence suggests that the Hope diamond was cut in the late 18th or early 19th century from the French Blue diamond, which itself was cut in the 1670s from the Tavernier Blue (see, e.g., Attaway, 2005; Farges et al., 2008, 2009). Yet the only documentation of the Tavernier Blue comes from gem merchant Jean Baptiste Tavernier (1676), who sketched three views (figure 1) of a diamond he purchased in India and sold to Louis XIV. This is the stone first referred to by Streeter (1882) as the *Tavernier Blue*. Tavernier stated that the diamond was clean, violet colored, and weighed $112^3/_{16}$ ct. The computer model of this diamond used by Attaway (2005) was derived from Tavernier's drawing as it appeared in a 1682 edition of his book and was refined using computer reconstructions of the French Blue (these based on 19th-century drawings) to determine the original diamond's volume and dimensions. Unfortunately, the drawings on which these models were based are subject to errors due to artistic interpretation, license, and skill.

The recent discovery of a lead cast of the French Blue at the Muséum National d'Histoire Naturelle (MNHN) in Paris has provided more accurate information concerning the physical attributes of that diamond. Farges et al. (2008, 2009) created an updated computer model from a laser scan of the lead cast. Since this model constituted new historical data, it had the potential to change other historical assumptions, particularly those surrounding the Tavernier Blue. The author discovered that the new French Blue model, when inserted into an unpublished model of the Tavernier Blue independently generated from Tavernier's line drawings, did not fit. This indicated that the Tavernier Blue model was not entirely accurate, suggesting that either Tavernier reported the weight incorrectly or the original line drawings contained errors.

In the 17th century, there was an important philosophical difference between European and Indian diamond cutters. Whereas the Europeans believed in symmetry and brilliance, Indian cutters thought that value resided mainly in the weight of the diamond. As Tavernier wrote, "If the stone is clean they do not do more than just touch it with the wheel above and below, and do not venture to give it any form, for fear of reducing the weight" (1682, p. 44). Since the Tavernier Blue was cut in
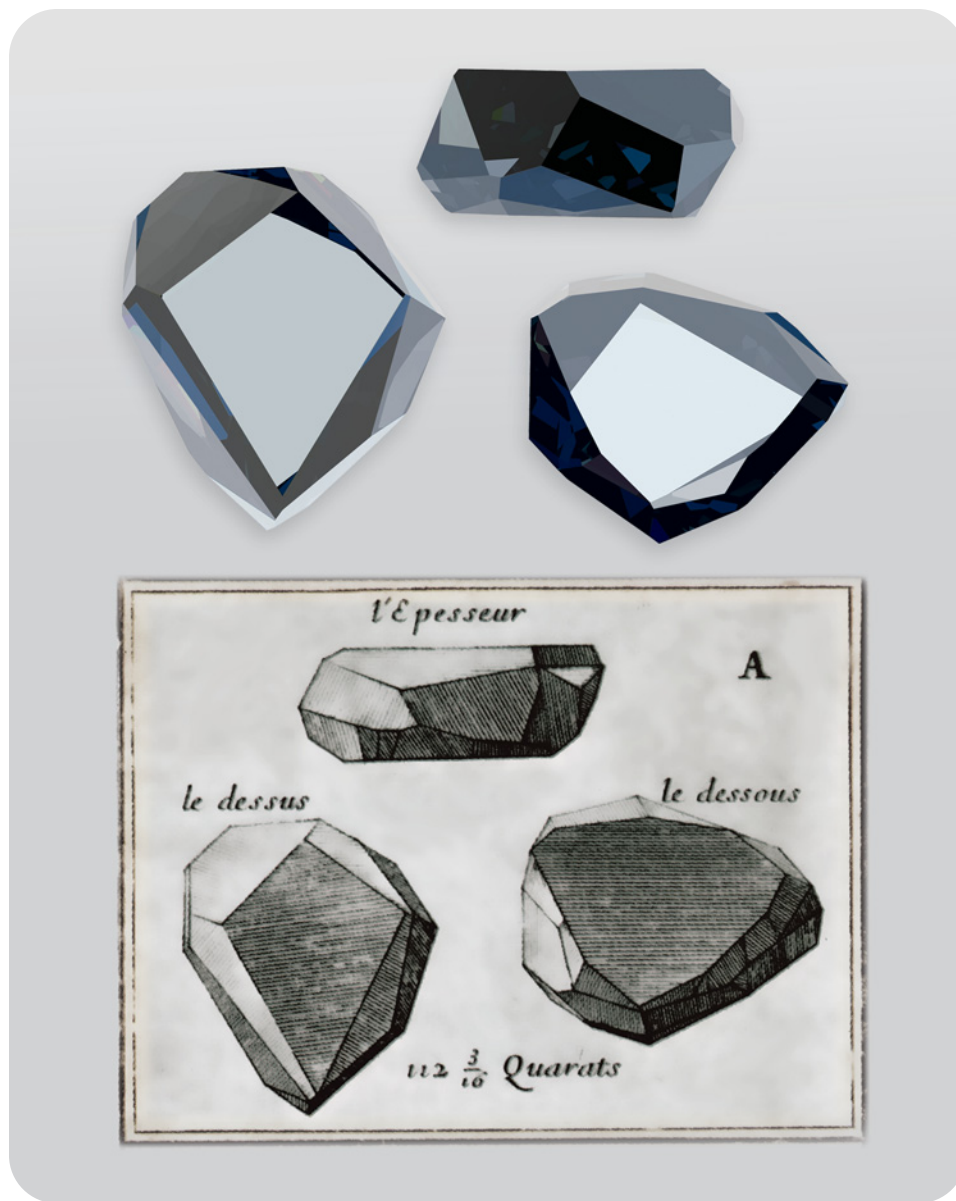
Figure 1. These line drawings (bottom) from Jean Baptiste Tavernier's 1676 memoir are the only known contemporaneous illustrations of the famed Tavernier Blue diamond before it was faceted into the French Blue. Le dessus = top; le dessous = bottom; and l'Epesseur = profile. The computer-generated images (top) emulate the appearance of the original diamond. A spectral file of the Hope diamond was imported to generate the color. The profile-view computer image does not completely match Tavernier's drawing because the profile drawing was geometrically unresolvable based on the facets in the other two views.

India, it is fair to assume that it retained much of the original crystal form. Thus, a more accurate computer model could be generated by correlating its facets to the crystal faces of a diamond. This blueprint could then be used to update the Tavernier Blue model, and previously unknown crystallographic information could be inferred.

Although similar information could be derived by X-ray diffraction analysis of the Hope diamond, there is no surviving record of XRD done on the Hope more than 30 years ago. An X-ray diffraction pattern taken then has since disappeared (J. Post, pers. comm., 2008). The Smithsonian has XRD facilities, but they are not suitable for large stones like the Hope without modification. Nevertheless, museum

staff have indicated that it may be possible to conduct XRD testing when the Hope is reset later in 2009 as part of the 50th anniversary of its donation (J. Post, pers. comm., 2009). Until such time, crystallographic data must be inferred using other methods.

MATERIALS AND METHODS

A computer model of the Tavernier Blue diamond was developed based on Tavernier's 1676 line drawing (slightly different from the 1682 version), which shows three views: *le dessus* (top), *le dessous* (bottom), and *l'Epesseur* (profile; again, see figure 1). Photogrammetric methods, using Adobe Illustrator and GemCad (a three-dimensional graphics tool for
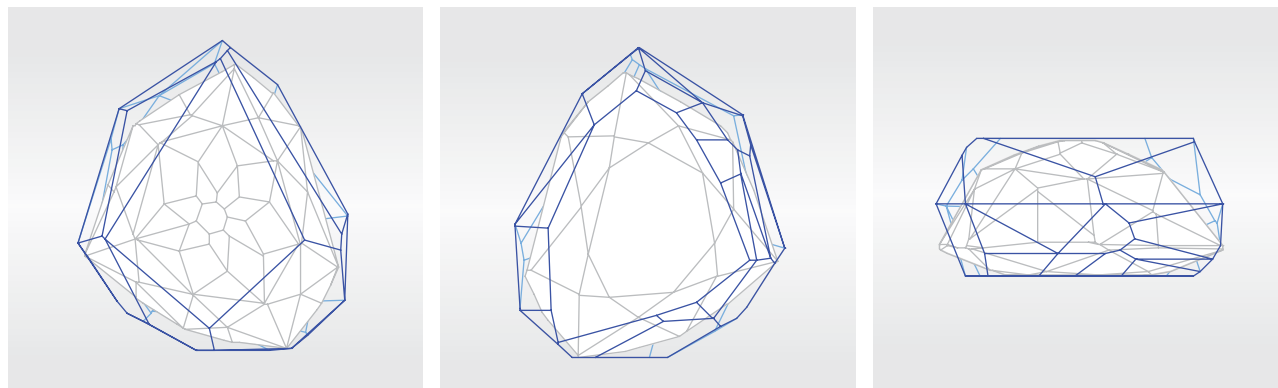
Figure 2. The most recent model of the French Blue (gray wireframe) is shown inside an older model of the Tavernier Blue (blue wireframe). Note on the far right how the French Blue protrudes on two sides, indicating an error.

planning gemstone cuts, www.gemcad.com), were employed to generate a preliminary model, as described in Sucher and Carriere (2008).

Next, GemCad was used to compare this computer model to the computer model of the French Blue described in Farges et al. (2008, 2009). The two models did not fit, as the French Blue protruded from the Tavernier Blue in a few locations, indicating that modeling errors existed (figure 2). The main difficulty in correcting modeling errors for the Tavernier Blue lay in choosing the initial assumptions. Relying on Tavernier's drawing alone was not an option, as these views were the basis of the incorrect model. But if the diamond was a crudely fashioned crystal as Tavernier's comments suggest, then crystal faces (see, e.g., figure 3) could be used to provide guidance for modeling the correct facet angle and index settings.

The crystal faces were identified by comparing the initial model to an idealized diamond crystal. Goldschmidt (1916) reported that diamond sometimes occurs as a hexoctahedral crystal, a form with 146 faces consisting of {100}, {110}, {111}, {210}, {211}, {221}, and {421} faces. This crystal form was modeled

in GemCad (figure 4), which provided sufficient crystal face candidates to correlate to the facets of the Tavernier Blue. Although diamonds are more commonly found as a mix of crystal habits and not perfect crystals, the angular relationships between the crystal faces do not change. Thus, the data from the perfect crystal were still usable for this purpose.

For this part of the study, the updated French Blue model was first oriented inside the existing model of the Tavernier Blue so that its table was parallel to the table on the bottom view and its girdle aligned with a series of facets that corresponded to the "girdle" on the Tavernier Blue. The French Blue model was then rotated one degree at a time in the X, Y, and Z directions to achieve a visual "best fit" (e.g., figure 5). Now the larger model could be revised one facet at a time using information from the faces of the crystal.

Further modeling was performed by opening a series of computer windows: (1) the hexoctahedral crystal, in GemCad, to provide angle and index settings of each face; (2) the Tavernier Blue with the French Blue model positioned inside, also in GemCad; and (3) an Adobe Illustrator file showing
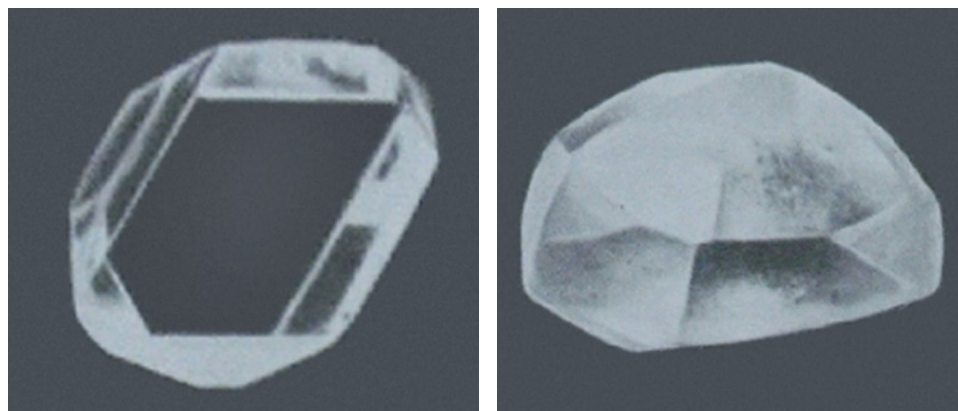

Figure 3. These photos of actual diamond crystals (Orlov, 1977) show what the Tavernier Blue may have looked like in its natural state. The crystal on the left resembles the top view, the crystal on the right the bottom view.
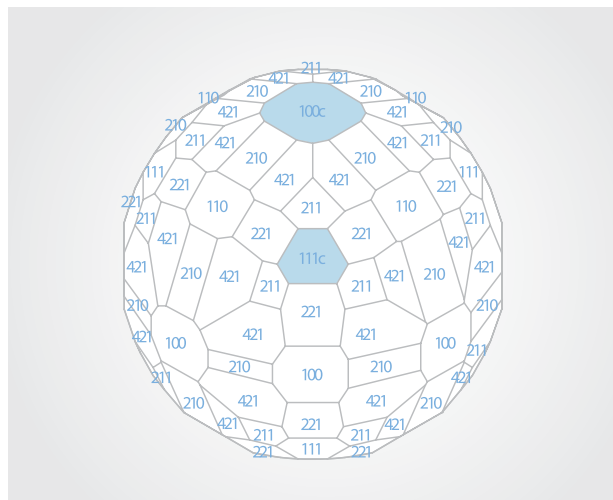
Figure 4. This GemCad model of a hexoctahedral crystal was used to select crystal faces to match to facets. The (100)c and (111)c faces (blue) remained oriented as the crystal was rotated during modeling.
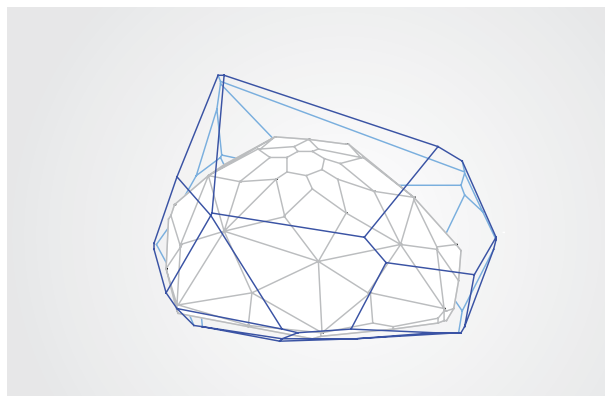

Figure 5. This GemCad view shows the French Blue enclosed within the Tavernier Blue. This model was rotated in all three directions to verify that the Tavernier Blue fully encompassed the French Blue during remodeling.

Tavernier's 1676 drawings. All windows were made semitransparent so that they would overlay each other and make all information visible at once.

NEED TO KNOW

- The Tavernier Blue was the precursor diamond to the French Blue and the Hope, but the only surviving record is Tavernier's 17th-century drawings.
- A computer model based on the drawings did not fully encompass the French Blue.
- Tavernier suggested that the diamond was a lightly polished crystal.
- The computer model was modified by assuming most facets were aligned to crystal faces.
- The revised model fully encloses the French Blue while remaining true to the original drawings and weight.

Now the original Tavernier Blue computer model had to be oriented to the hexoctahedral crystal. It was initially assumed that the table was oriented parallel to a cleavage. The hexoctahedral crystal model was rotated so that a {111} face was "face up," then a line drawing of the top was overlaid on it (figure 6). A comparison of the angle shown in the drawing at the apex of the table matched that of the surrounding faces in the crystal, so this was assumed to be a valid starting point. This was also in agreement with the lost X-ray diffraction pattern, which reportedly showed that the table of the Hope was aligned with a cleavage face (J. Post, pers. comm., 2008).

With the computer model thus oriented, corrections were made by selecting a facet and comparing it to faces on the crystal. Two methods were used to correlate crystal faces to facets:

1. Three points on the Tavernier Blue model were selected to define a particular facet, at which point GemCad could solve for angle and index settings. These were then matched to the settings for the nearest crystal face; if the crystal face settings were close, they were used to virtually cut the facet.

Figure 6. This superposition of a line drawing of the top view of the Tavernier Blue on the hexoctahedral crystal shows how the crystal faces surrounding the (111)c face form the correct angle at the apex of the "table" facet.
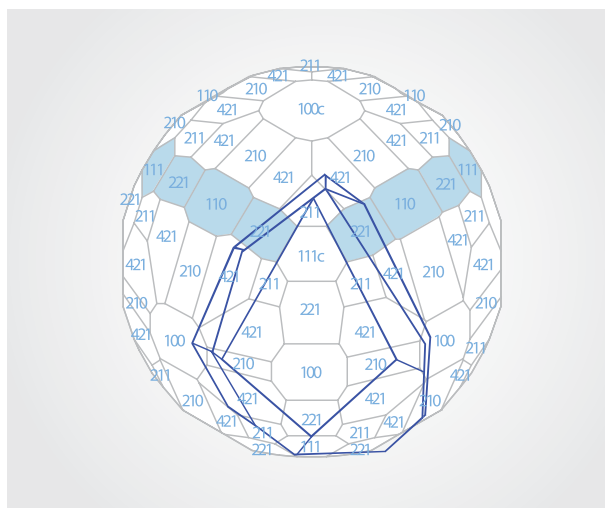
2. A likely crystal face for a facet was identified based on its position on the crystal. For instance, if the facet was on the right side, then a face on the right side of the crystal would be selected. If a low angle was required, then one closer to the top of the crystal would be selected. Then the settings for this face would be used to cut the facet. This was a highly iterative process, as face selection was based on stonecutter judgment.

Regardless of the methodology, the resultant facet was verified correct by:

1. Comparing it to Tavernier's drawing to ensure the new facet matched the drawing.

2. Rotating the Tavernier Blue and French Blue models in GemCad to ensure the modified facet removed as much material as possible from the Tavernier Blue, but did not cut into the French Blue. (This latter concern was necessary as preliminary analysis showed that the original model of the Tavernier Blue, when expanded to fully enclose the French Blue, was about 15 ct too heavy.)

3. Analyzing the result against neighboring facets on the Tavernier Blue. Since a three-dimensional solid form was being created, the settings for one facet affected the settings of adjacent facets, so any change would cascade and affect the modeling solution for the entire stone.

The top and bottom views—but not the profile view—were used to reconstruct the Tavernier Blue. There were several reasons for giving the top and bottom views preference. Attaway (2005) noted that the profile view is unresolvable given the information in the other two views. This was corroborated here by comparing various viewing angles and facet configurations. There were no facet combinations that matched this view given the facets in the other two views.

Modeling the bottom view was more problematic than the top. This view was drawn from an oblique perspective at an unknown tilt. Attaway (2005) believed that the bottom table was tilted ~15° away from the viewer to provide information concerning the side facets. This is certainly possible, but using 20° in the present study appeared to provide a better fit given the revised data (though there is no way to prove which is the better estimate). This degree of tilt greatly influences any modeling solu-

tion, since the apparent depth of the stone is affected by any tilting in the view. Determining the degree of tilt is a function of comparing length, width, and depth, tempered by changes to the facet pattern appearance due to parallax. There were modeling solutions to both perspectives (15° and 20°), but the greater tilt allowed for the use of more crystal faces, providing a better fit between the two models and Tavernier's line drawing.

The profile view shows the tables of the top and bottom to be parallel, so this was maintained for modeling the bottom. Due to the uncertainty of the bottom view's perspective, though, placing facets and correlating them to crystal faces required far more trial and error than was needed for the top view. Additionally, the area along the lower right edge of Tavernier's bottom view could not be resolved sufficiently to determine which lines indicated facets or merely shading, or were perhaps the artist's interpretation of internal reflections as surface facets (figure 7).

The facet assignments for the top and bottom views initially yielded a model for the Tavernier Blue that weighed 120 metric carats. As originally modeled, the table facets were perfectly aligned with cleavages. Tavernier did not report these as unpolished facets, so it must be assumed they were polished and, therefore oriented slightly away from the cleavage plane (which could not be polished).

However, if the table facets were indeed angled slightly away from cleavage planes, then the question of by how much and in which direction had to be resolved. There are two clues, one on each of the French and Tavernier Blue models:

1. The culet on the French Blue is oriented 3° away from parallel to its table facet. The culet facet correlates to the table in the top view of the Tavernier Blue, suggesting a similar deviation away from a cleavage plane.

2. The initial updated computer model of the Tavernier Blue had a facet pattern that was similar to Tavernier's drawing, but the two patterns did not match exactly. When the top table facet was tilted 2° in the direction suggested by the French Blue's culet facet, there was a much better visual fit to the drawing.

The bottom table was similarly remodeled to remain parallel with the top table. Although the culet of the French Blue is off-parallel approximately 3°, repositioning these facets more than 2° was phys-
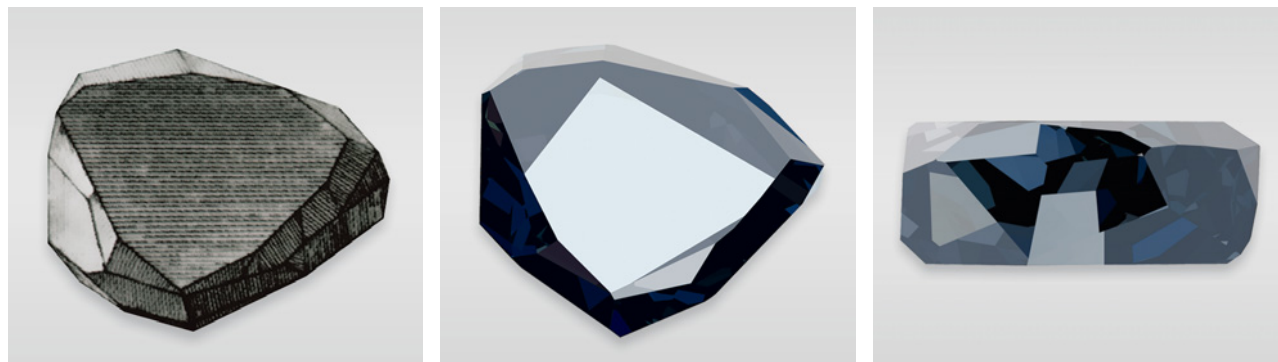
Figure 7. The fact that approximately 10–15 facets along the lower right edge of the bottom-view drawing (left) cannot be definitively interpreted affects the modeling solution. The two computer models (center and right) show the difficulty Tavernier would have had in discerning the facets and reflections.

ically impossible as the French Blue model started to protrude at the "girdle" of the Tavernier Blue. All facets were now remodeled using their established settings to allow for tilt of the table facets.

At this point, the French Blue model was tilted so that its table was parallel to the bottom table. This created more distance between some facets in the two models. Some Tavernier Blue facets were then adjusted to place them closer to the sides of the French Blue. Again, this was necessary to reduce the size of the Tavernier Blue model to better conform to its reported weight. Minor position adjustments were made to the French Blue along all three axes to accommodate changes as the larger stone was remodeled. Numerous iterations of facet combinations were performed to determine a "best fit" (as determined visually) throughout the modeling process.

Multiple iterations were tested using cubic, dodecahedral, or octahedral crystal faces as table facets of the top and bottom views. The hexoctahedral crystal model was also rotated within each table facet orientation to test different crystal face geometries to create the surrounding facets.

RESULTS

The outcome was a 116.5 metric carat (29.18 × 32.40 × 12.88 mm) model of the Tavernier Blue with 11 facets on the top, 17 on the bottom, and three at 90° along the "girdle." This revised model completely enclosed the French Blue model.

The assignments of crystal faces to facets for the top view are shown in figure 8. There was one facet that did not correlate to a crystal face (colored yellow). Additionally, the (111) facet at 2 o'clock (colored green) was rotated 3° counterclockwise to achieve the appropriate angle to the (221) facet next to the table. Some deviation was required; otherwise the facet would have been parallel to a cleav-

age face. This deviation not only satisfied this constraint but also resulted in a much better fit to Tavernier's drawing.

The table facets of the top and bottom views were oriented 2° away from the {111} crystal faces. Twenty-one of 31 facets could be directly correlated to crystal faces of a hexoctahedral diamond crystal. Of those 21 faces, three were cleavages, and rotating them 2–3° from perfect alignment achieved the necessary deviation so they could have been cut and polished.

Of the 10 facets that could not be correlated to any specific crystal face, nine were on the bottom view (again see figure 8). Of these nine facets, the angle and index settings of adjacent facets were cut within 3–5° of each other, suggesting facets that were cut near crystal faces to remove surface features/damage to the crystal with minimal weight loss.

Models using cubic {100} and dodecahedral {110} faces as the table were not physically possible. There were no facet combinations with these orientations that could be used to generate a model that matched Tavernier's description. This was true even when the hexoctahedral crystal was rotated around the "face-up" facet to generate a new set of crystal face relationships. Only the {111} orientation yielded a feasible solution.

Attempts at reconstructing the model using cubic and dodecahedral crystal faces as the table yielded the following results:

1. A cubic face–centered model resulted in three of 11 facets on the top view that could not be assigned crystal faces. Two of those that could be assigned were {421} faces, implying a higher order of crystal complexity. Additionally, one facet on the top view was geometrically impossible; adjacent facets removed the material necessary for its creation. Since the top view could not be resolved satisfactorily, modeling was not
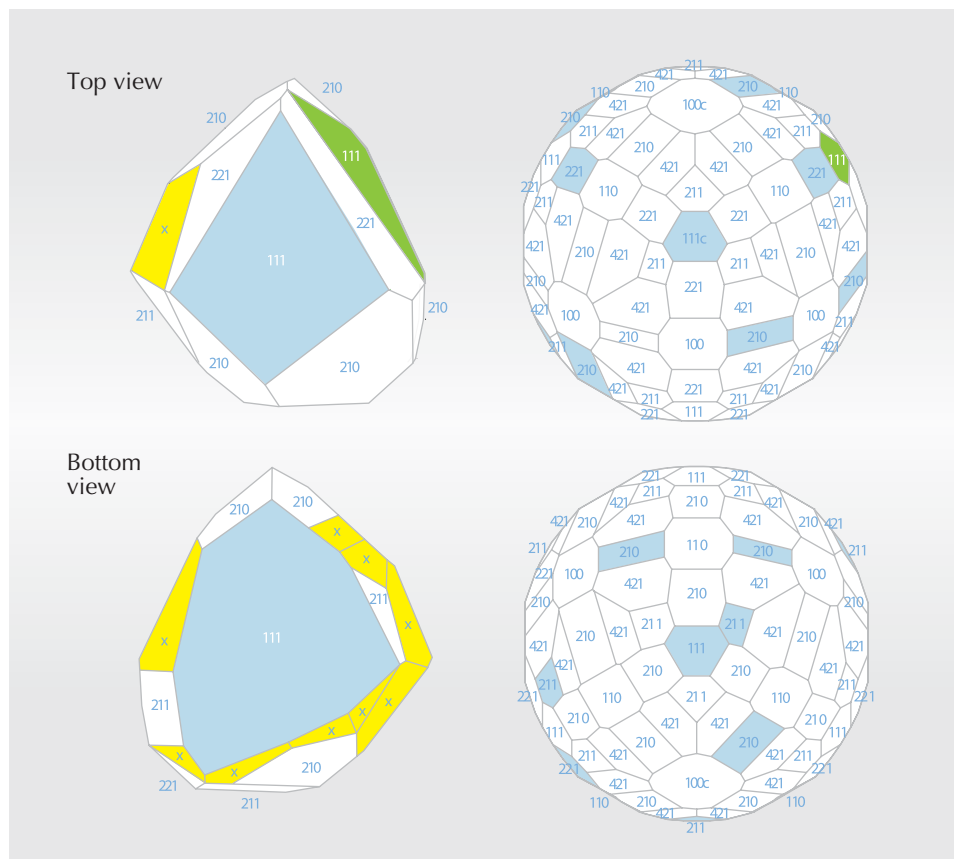
Figure 8. These illustrations show the crystal face assignments for the top and bottom-view facets. Those facets without face assignments are marked "x."

performed for the bottom view. Rotating the crystal and then assigning crystal faces also became geometrically impossible.

2. The dodecahedral face–centered model resulted in nine of 11 faces assigned to facets on the top view. Although the facet pattern matched the drawing, the angles were too shallow, yielding a model that was too blocky and heavy. A total of seven {421} crystal faces were necessary, again implying a very complex crystallization process. Modeling the bottom view resulted in seven of 14 facets without face assignments; those that were assigned did not remove enough weight. As a result, the model could not be resolved below 125.8 cts. Rotating the crystal around the dodecahedral face and then reassigning faces to facets was geometrically impossible.

DISCUSSION

The possible weight range of the Tavernier Blue affects any modeling solution. Although Tavernier reported the weight as $112\,^3/_{16}$ ct, he did not indicate whether he used Florentine carats (0.1952 g/ct [Streeter, 1898] or 0.1965 g/ct [Kunz, 1914]), French carats (0.2055 g/ct), or some other version in use at that time. As a result, conversion from old carats to metric carats (0.2 g/ct) yields a weight range from 109.5 to 115.3 ct.

The initial (erroneous) model of the Tavernier Blue that corresponded to Tavernier's 1682 drawings weighed 115.7 metric carats. There is no record of the weight of the Tavernier Blue when it was received by the French court or when Jean Pitau cut the French Blue, so Tavernier's weight cannot be independently verified. It may have been weighed at the time of the sale; however, these records have not been found. Since there is no record of any discrepancy, the weight was assumed to be correct.

The accuracy of Tavernier's drawings also cannot be verified. Historical line drawings in general should be considered suspect, given the findings of modern diamond researchers. For example, Tillander (1995) compared five drawings of the Sancy diamond from several authors, all of which differ from the actual diamond on display at the Louvre. Bauer's drawings (1968) of several diamonds are more representations of these stones and certainly not accurate depictions. Streeter's (1898) illustration of the Tavernier Blue was markedly different from Tavernier's version. Some

drawings in the English version of Tavernier's book (1682), and many subsequent versions, are mirror images of the drawings in the original French version (1676). These examples clearly demonstrate that historical line drawings must be viewed with caution.

The most important problem with Tavernier's drawings of the Tavernier Blue is that the computer model generated from them could not enclose the French Blue model by Farges et al. (2009) until it was enlarged to 130 ct. Since the lead model of the French Blue is the only surviving physical representation of this stone, the computer model of it generated by laser scanning should be considered more accurate than a computer model of the Tavernier Blue generated by a single set of line drawings. With octahedral crystal faces as the tables in the top and bottom views, the revised Tavernier Blue model satisfies historical constraints by: (1) completely enclosing the French Blue model; (2) emulating Tavernier's line drawings; (3) falling within 1% of the reported weight (a range, as discussed previously) of the original diamond; and (4) having no facet parallel to a cleavage {111} face. Importantly, no models that use the cubic or dodecahedral crystal faces as tables satisfied all four constraints.

CONCLUSIONS

The recent discovery of a lead cast of the French Blue diamond at the MNHN in Paris provides the strongest evidence to date of that diamond's physical characteristics. This cast (Farges et al., 2008, 2009) made it possible to refine a model of the Tavernier Blue that had been derived solely from line drawings; however, more information was required to generate an accurate model. This was provided by Tavernier himself, in his assertion that Indian diamond cutters conserved weight by only lightly touching up the crystal faces. Since it appears that the Tavernier Blue was a crudely fashioned diamond crystal, it became possible to assign crystal faces to many of its facets. Thus, Tavernier's drawing could be updated using crystallographic data from an idealized hexoctahedral diamond crystal. The resulting model satisfies historical physical constraints of size, weight, and facet pattern. The gem's orientation within a diamond crystal was precisely determined (i.e., with the tables parallel and offset 2° to octahedral faces), providing new crystallographic details of this historic diamond.

REFERENCES

Attaway N. (2005) The French connection. *Lapidary Journal*, Vol. 59, No. 3, pp. 24–28.

Bauer M. (1968) *Precious Stones*, Vol. 1. Transl. by L. Spencer, Tuttle, London.

Farges F., Sucher S., Horovitz H., Fourcault J.-M. (2008) Deux decouvertes majeures autour du "diamant bleu de la Couronne" (Two major discoveries about the "blue diamond of the Crown"). *Revue de Gemmologie*, No. 165, pp. 18–25.

Farges F., Sucher S., Horovitz H., Fourcault J.-M. (2009) The French Blue and the Hope: New data from the discovery of a historical lead cast. *G&G*, Vol. 47, No. 1, pp. 2–17.

Goldschmidt V. (1916) *Atlas der Kristallformen*. C. Winters, Heidelberg.

Kunz G. (1914) The new international diamond carat of 200 milligrams. In *The Mineral Industry: Its Statistics, Technology and Trade During 1913*, Vol. 22, McGraw-Hill, New York.

Orlov U. (1977) *The Mineralogy of the Diamond*. John Wiley & Sons, New York.

Streeter E. (1882) *The Great Diamonds of the World*. George Bell and Sons, London.

Streeter E. (1898) *Precious Stones and Gems*. George Bell and Sons, London.

Sucher S., Carriere D. (2008) The use of laser and X-ray scanning to create a model of the historic Koh-I-Noor diamond. *G&G*, Vol. 44, No. 2, pp. 124–141.

Tavernier J. B. (1676) *Les Six Voyages de Jean Baptiste Tavernier, Ecuyer Baron D'Aubonne, Qu'il a Fait En Turquie, En Perse, et aux Indes [The Six Voyages of Jean Baptiste Tavernier, Baron d'Aubonne, that He Made to Turkey, Persia, and the Indies]*, Vol. II. Clouzier, Paris.

Tavernier J. B. (1682) *Travels in India*, Vol. II. Transl. by V. Ball (1889), Macmillan and Co., London.

Tillander H. (1995) *Diamond Cuts in Historic Jewellery 1381–1910*. Art Books International, London.

"FLUORESCENCE CAGE": VISUAL IDENTIFICATION OF HPHT-TREATED TYPE I DIAMONDS

Inga A. Dobrinets and Alexander M. Zaitsev

HPHT-treated type I diamonds of various colors may exhibit unusually intense fluorescence at the facet edges and junctions. This effect, here named the "fluorescence cage," is observed with a fluorescence microscope as a luminous network on the diamond's surface. It was not observed in untreated diamonds or colorless type IIa HPHT-treated diamonds. This fluorescence pattern is believed to result from a high concentration of HPHT-induced optical centers, which remain on facet edges after repolishing.

The identification of high-pressure, high-temperature (HPHT) treatment of diamond poses a great challenge to gemologists (Collins, 2006). Since this enhancement was officially introduced to the diamond market in 1999, its gemological and economic implications have been discussed at length (e.g., Shigley, 2005). HPHT treatment, originally announced as undetectable, actually can be recognized in most cases by a combination of characteristic microscopic and spectroscopic features. However, most advanced spectroscopic methods are expensive and time consuming, so they cannot be used efficiently for routine characterization of every diamond. Moreover, some HPHT-treated diamonds may lack the standard identifying features. Therefore, further studies of HPHT-treated diamonds and the development of practical detection methods remain important activities at gemological laboratories.

In this article, we report on a new characteristic of faceted HPHT-treated type I diamonds: intense fluorescence on facet edges and junctions (e.g., figure 1). This feature is easily observed with a fluorescence microscope and can be used to identify HPHT enhancement.

MATERIALS AND METHODS

Fluorescence images of 60 HPHT-treated and more than 100 untreated cut diamonds of various colors and clarity grades were studied. Of the HPHT-treated stones, 50 ranged from brown to yellow to green to orange, and the other 10 were colorless and near-colorless. To our knowledge, all the stones were faceted prior to HPHT annealing and repolished after treatment. The untreated diamonds, selected from those submitted to EGL USA for grading, were colorless, near-colorless, and brown to yellow (over 30 stones in each of these three color groups).

The HPHT-treated diamonds were loaned by Nice Diamonds. They were confirmed as HPHT treated by our testing with polarized-light microscopy, Fourier-transfer infrared absorption spectroscopy (Nicolet 800 Nexus 670 FTIR spectrometer), visible-transmission spectroscopy (SAS2000 spectrometer), and photoluminescence spectroscopy (SAS2000 with PL excitation at 532 and 658 nm). The visible absorption and
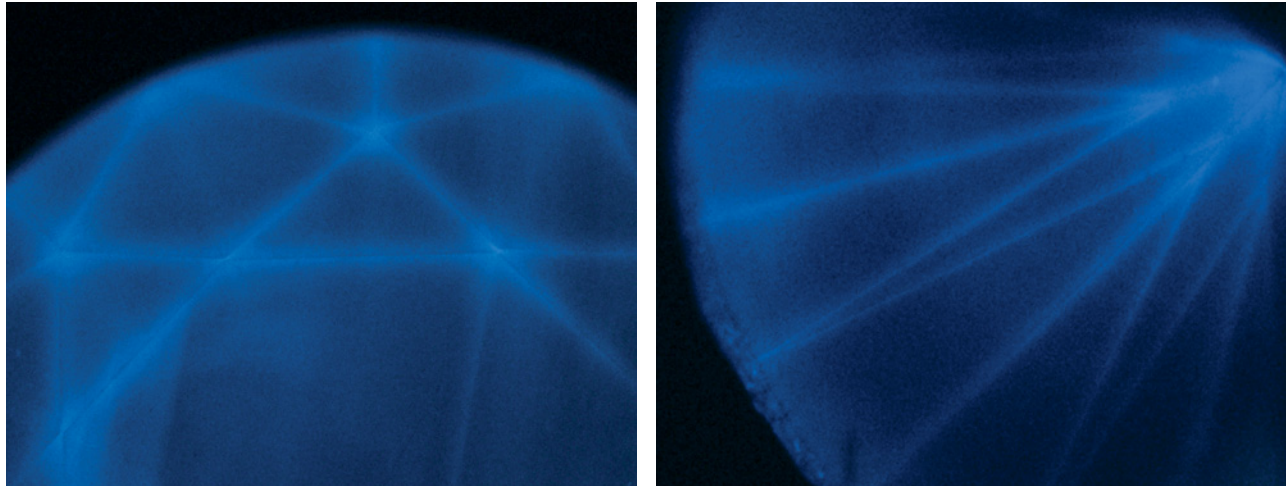
Figure 1. These face-up and table-down views of a Fancy Vivid yellow HPHT-treated type I diamond show intense fluorescence on facet edges and junctions, which is here called a "fluorescence cage." Photomicrographs by I. Dobrinets; magnified 40×.

PL spectra were measured at room and liquid-nitrogen temperatures. The same techniques were used to ascertain the untreated nature of the other diamonds.

Fluorescence images of all the diamonds were taken with a Nikon Eclipse Ti inverted fluorescence microscope equipped with a 100 W high-pressure mercury lamp and optical edge filters (Hoecht UV-2A Ex355/50 Dm400 Bar420), enabling UV excitation with Hg lines at wavelengths of 365 nm (i.e., long-wave UV; ~70% of the total excitation intensity) and 334 nm (~30% of the total excitation intensity), as well as imaging at wavelengths >400 nm (across the entire visible spectrum). Prior to the measurements, the diamonds were ultrasonically cleaned in acetone and alcohol to remove any surface contaminants that might affect the fluorescence imaging.

RESULTS AND DISCUSSION

Gemological Observations. This research stemmed from the characterization of a 0.76 ct diamond submitted to EGL USA for grading and origin-of-color determination (figure 2). The diamond received a color grade of Fancy brownish-orangy yellow and an I1 clarity grade. It was inert to long-wave UV excitation and fluoresced a faint greenish yellow with some green patterns to short-wave UV. The diamond contained a few cracks with obvious graphitization, an indication of possible HPHT treatment.

Examination with 100× magnification revealed several features characteristic of HPHT-treated diamonds in addition to the graphitized cracks: cleavages with etched surfaces, fingerprint-like inclusions, and small frosted facets (Moses et al., 1999; Smith et

al., 2000; Hall and Moses, 2001). The stone exhibited a strain interference pattern typical of natural type Ia diamond. No chips or delaminations were detected on the facets or edges, which led us to believe that this colored diamond was not coated by any films such as those documented by Shen et al. (2007).

The FTIR absorption spectra showed that the stone was a mixed type IaA/B+Ib with about 1 ppm of C defects, 25 ppm of A defects, and 45 ppm of B defects. The presence of nitrogen in both dispersed and aggregated forms—a rare occurrence in natural diamonds (Hainschwang et al., 2006)—offered further evidence of HPHT treatment. The visible

Figure 2. The fluorescence cage was first discovered during the examination of this 0.76 ct HPHT-treated diamond. Photo by Fernando Paredes.
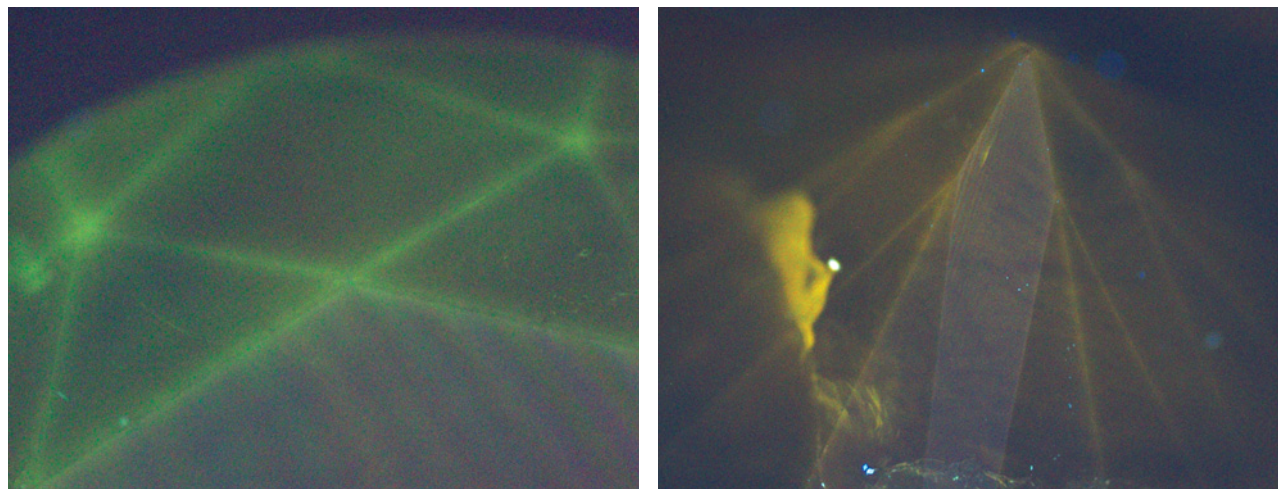
Figure 3. These images, taken with a fluorescence microscope, show the fluorescence cage on both the table (left) and pavilion (right) of the 0.76 ct HPHT-treated diamond in figure 2. The different fluorescence colors are due to the different relative intensities of nitrogen-related centers: yellowish green (dominated by H3) on the crown, and yellow (dominated by NV⁻) on the pavilion. Photomicrographs by I. Dobrinets; magnified 40×.

transmission spectrum was dominated by an absorption continuum with a threshold at 650 nm (absorption of C defects), and revealed a rather weak signal for the H3 center, which was observed in the absorption and luminescence regimes (the "green transmission" effect). Both the C-defect absorption continuum and "green transmission" are common features of mixed-type HPHT-treated diamonds. The photoluminescence spectra revealed a dominant nitrogen-related NV⁻ center with a zero-phonon line (ZPL) at 638 nm and three more centers with ZPLs at 542, 564, and 574 nm, which are believed to originate from nickel impurities. These centers are common for HPHT-treated natural diamonds with brown-to-yellow-to-orange coloration, and the latter two are also found in HPHT-treated synthetic diamonds (Yelisseyev and Kanda, 2007).

Fluorescence microscopy revealed a weak, predominantly yellowish green fluorescence, which could be a superposition of the H3 and NV⁻ center emissions. None of the cross-like patterns characteristic of synthetic diamonds were detected. The most intense fluorescence was concentrated in some cracks and—surprisingly—along the facet edges and at the table and pavilion junctions (figure 3). Because of these bright edges, the diamond looked as though it had been placed in a "fluorescence cage."

To investigate whether this fluorescence pattern was the product of HPHT treatment, we conducted a comparative study of the numerous HPHT-treated and untreated faceted diamonds described above. Spectroscopic measurements of several HPHT-treated colored, near-colorless, and colorless diamonds

revealed that the colored diamonds were type Ia with total nitrogen contents over 100 ppm and the near-colorless and colorless ones were type IIa with total nitrogen contents below a few ppm. The untreated diamonds did not show such a straightforward dependence of color on type, and those that were colorless revealed a broad range of nitrogen content.

All of the intensely colored type Ia (20 stones) and some light-colored type Ia (8 of 20 samples) HPHT-treated diamonds exhibited the fluorescence cage, whereas none of the untreated diamonds revealed any traces of it (see, e.g., figure 4). The pattern was especially distinct in those HPHT-treated diamonds that had high nitrogen concentrations and were more deeply colored (e.g., figure 5), especially those with low overall fluorescence. In contrast, the fluorescence cage was very faint in low-nitrogen near-colorless type Ia HPHT-treated diamonds, and it was not observed at all in the colorless type IIa HPHT-treated diamonds. This is consistent with our belief that the fluorescence cage is formed by nitrogen-related optical centers.

Origin of the Fluorescence Cage. Our study of the spectral content of the fluorescence cage showed that the main contributors to the luminescence were the optical centers generated during HPHT treatment: H3, NV, and some nickel-related centers. On the basis of these results, we believe that the fluorescence network is caused by HPHT-induced modification (plastic deformation) of the diamond lattice in a layer close to the surface. This modified layer contains optical centers generated by high
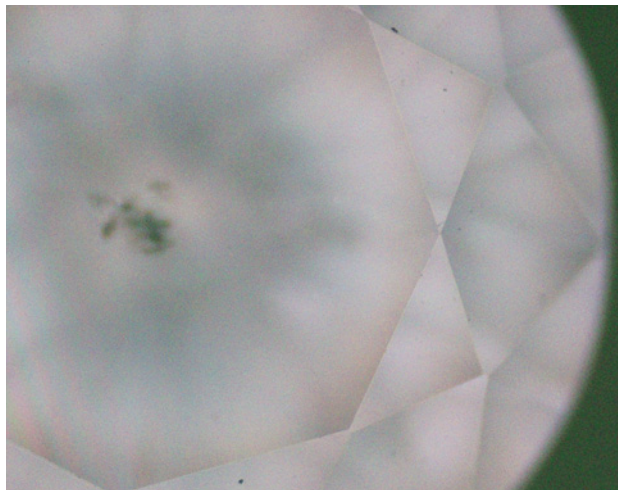
Figure 4. This untreated brownish yellow diamond exhibits whitish pink overall fluorescence and no fluorescence cage. Photomicrograph by I. Dobrinets; magnified 40×.
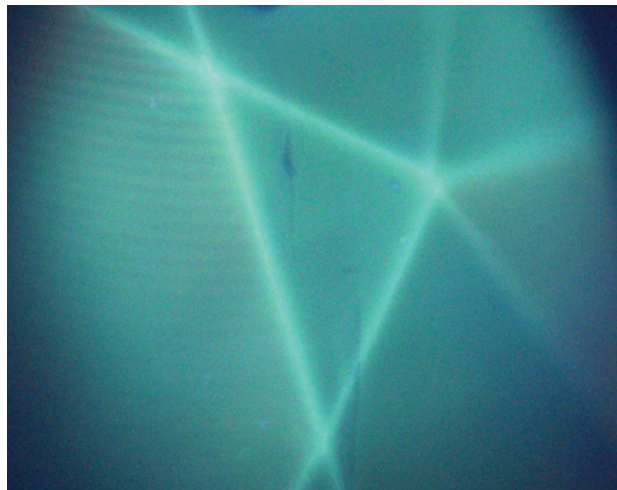

Figure 5. This deeply colored greenish yellow HPHT-treated diamond shows a strong fluorescence cage along with bluish luminescence. Photomicrograph by I. Dobrinets; magnified 40×.

mechanical stress and high temperatures. One would expect the modified layer to be thicker on protrusions such as facet edges and junctions, where the mechanical strain during HPHT compression reaches a maximum. After repolishing, the modified layer is largely removed from the flat facets, but there are remnants on the facet edges.

To support this explanation, we studied several surface-reaching cracks in one of the HPHT-treated diamonds with the fluorescence microscope. Although the area around those cracks was damaged by repolishing, it did not show strong fluorescence (figure 6). This observation confirmed that mechanical damage and plastic deformation alone did not produce strong luminescence centers: Simultaneous application of high mechanical stress and high temperature was required to generate them, as seen in the cracks of the 0.76 ct diamond, which were generated during HPHT processing.

So far, we have observed the fluorescence cage only in HPHT-treated type I diamonds. It has not been detected in any diamonds treated with irradiation alone, or with irradiation and low-pressure annealing. Indeed, it is difficult to imagine a mechanism other than HPHT annealing and repolishing that could result in the precise concentration of optical centers along facet edges. For instance, electron irradiation with energy below 1 MeV may generate optical centers of varying intensity (Fritsch and Shigley, 1989). This nonuniformity, however, is very different from that of the fluorescence cage. Neutron irradiation is very uniform and cannot

selectively produce defects at facet edges.

Important questions about the fluorescence cage are whether it can be removed from a diamond and whether it is generated by HPHT treatment of both rough and faceted type Ia diamonds. If we correctly understand the nature of this effect, the concentration of optical centers at facet edges can be enhanced by HPHT annealing of faceted diamonds only. It will not be observed on diamonds that were treated in rough form and faceted after treatment. If the cage is indeed located close to the surface, then it can be removed by a deeper repolishing. However, deep repolishing may reduce the diamond's weight to the point of being commercially impractical. Nor will it appear on type II HPHT-treated pink or blue diamonds, because their nitrogen content is too low.

Detecting the Fluorescence Cage. Fluorescence microscopes such as the one used in this study are uncommon in gem labs. As an alternative, the DiamondView instrument should be suitable to observe fluorescence images. Although the DiamondView is not an exact analogue of a conventional fluorescence microscope due to its very short excitation wavelength (<225 nm compared to 365 nm for fluorescence microscopes), we expect the fluorescence cage to be observable with the DiamondView in many stones. It must be noted, however, that the shorter excitation wavelength of the DiamondView will not excite certain HPHT-induced optical centers (e.g., the 638 nm NV$^-$ center); thus, in some cases a cage pattern that might be revealed with
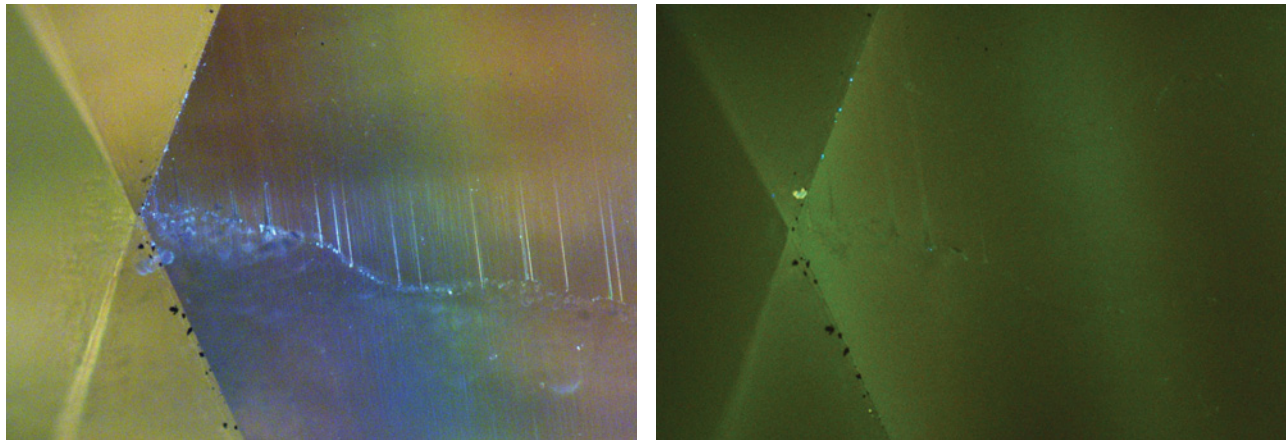
Figure 6. The conventional microscopic image of a brownish-greenish yellow HPHT-treated type I diamond on the left shows a crack surrounded by polish lines. The fluorescence image of the same area (right) shows enhanced luminescence on the facet edges and junction, but no strong luminescence around the crack and polish lines. Photomicrographs by A. Zaitsev; magnified 100×.

a fluorescence microscope will not be seen with the DiamondView.

If the fluorescence cage is strong, then it may also be seen using a standard gemological microscope while the diamond is exposed to long-wave UV radiation from a standard gemological lamp. The excitation wavelengths for such lamps are the same as those of the mercury lamps used in fluorescence microscopes. We observed the fluorescence cage in several stones using this method. However, since gemological microscopes are not designed to completely filter out UV radiation, for safety reasons we do not recommend implementing such a testing method unless the observer's eyes are properly shielded.

CONCLUSIONS

We report a new observational feature of some HPHT-treated diamonds—enhanced fluorescence on facet edges and junctions—which we term a *fluorescence cage*. On the basis of our study of numerous HPHT-treated diamonds (both colored and colorless) and their untreated counterparts, we conclude that the fluorescence cage can be readily observed on most deeply colored HPHT-treated type I diamonds with the use of a fluorescence microscope. Recognizing this feature considerably simplifies identification of HPHT treatment. We believe that the fluorescence cage cannot be generated by mechanical polishing or by other treatments such as irradiation and annealing at low pressure.

ABOUT THE AUTHORS
Dr. Dobrinets is a research gemologist at EGL USA in New York. Dr. Zaitsev is a professor of physics at the College of Staten Island, City University of New York.
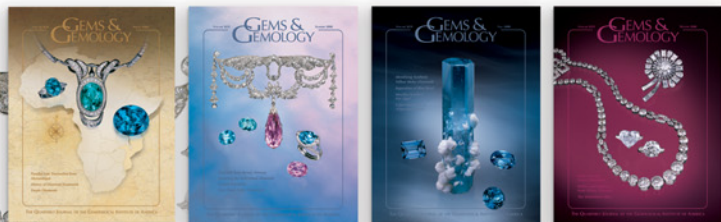
REFERENCES

Collins A.T. (2006) Identification technologies for diamond treatments. *G&G*, Vol. 42, No. 3, pp. 33–34.

Fritsch E., Shigley J.E. (1989) Contribution to the identification of treated colored diamonds: Diamonds with peculiar color-zoned pavilions. *G&G*, Vol. 25, No. 2, pp. 95–101.

Hainschwang T., Notari F., Fritsch E., Massi L. (2006) Natural, untreated diamonds showing the A, B and C infrared absorptions ("ABC diamonds"), and the H2 absorption. *Diamond and Related Materials*, Vol. 15, No. 10, pp. 1555–1564.

Hall M., Moses T.M. (2001) Lab Notes: Update on blue and pink HPHT-annealed diamonds. *G&G*, Vol. 37, No. 3, pp. 215–217.

Moses T.M., Shigley J.E., McClure S.F., Koivula J.I., Van Daele M. (1999) Observations on GE-processed diamonds: A photographic record. *G&G*, Vol. 35, No. 3, pp. 14–22.

Shen A.H., Wang W., Hall M.S., Novak S., McClure S.F., Shigley J.E., Moses T.M. (2007) Serenity coated colored diamonds: Detection and durability, *G&G*, Vol. 43, No. 1, pp. 16–33.

Shigley J.E. (2005) High-pressure and high-temperature treatment of gem diamonds. *Elements*, Vol. 1, No. 2, pp. 101–104.

Smith C.P., Bosshart G., Ponahlo J., Hammer V.M.F., Klapper H., Schmetzer K. (2000) GE POL diamonds: Before and after. *G&G*, Vol. 36, No. 3, pp. 192–215.

Yelisseyev A.P., Kanda H. (2007) Optical centers related to 3d transition metals in diamond. *New Diamond and Frontier Carbon Technology*, Vol. 17, No. 3, pp. 127–178.

UPDATE ON AMMOLITE PRODUCTION FROM SOUTHERN ALBERTA, CANADA

Keith A. Mychaluk

There have been a number of changes in Ammolite production from southern Alberta, Canada, since 2001. Korite International continues to be the dominant supplier, with a 40% increase in finished-stone production during this period. As mining focuses on Zone 4 of the host Bearpaw Formation, Korite's inventory has changed from predominantly fractured to sheet Ammolite. The Aurora Ammolite mine, operated by Rusty Pimm Enterprises, is the only other fully mechanized open-pit mine, but artisanal miners continue to be active. Dinolite— Ammolite combined with siliceous dinosaur bone—has been introduced as yet another innovative use for Ammolite.

Significant changes have occurred in the mining of Canadian Ammolite since 2001 (see Mychaluk et al., 2001), with new producers and new mines emerging. The growing industry continues to yield material for both the jewelry and specimen-collector markets (e.g., figures 1 and 2). This contributor visited the main Ammolite-producing area southwest of Lethbridge, Alberta, in September 2008 and conducted several interviews with producers through early 2009. Currently, the two main producers are Korite International and the Aurora Ammolite mine, with continuing activity by artisanal miners. In addition, a new product, Dinolite, in which

Ammolite and other gem materials are combined with dinosaur bone fragments, has been introduced.

ABOUT AMMOLITE

Ammolite is a gem material composed of aragonite that is derived from the shells of ammonites, extinct cephalopod mollusks found in marine sediments of the Bearpaw Formation (Fm) in southern Alberta, Canada. As reported in Mychaluk et al. (2001), commercial quantities of Ammolite are derived from two ammonite species (*Placenticeras meeki* and *P. intercalare*) from specific horizons within the Bearpaw Fm shale in the St. Mary River valley southwest of Lethbridge, Alberta (figure 3). Only two such horizons—labeled by Korite International as *K Zone* and *Zone 4*—are rich enough to sustain exploitation by open-pit mining methods. Ammolite can be grouped into two categories based on physical appearance: *fractured* and *sheet* (again, see figure 1). In fractured Ammolite, the original ammonite shell has been crushed and healed by natural processes, creating a "stained glass window" appearance. Fractured Ammolite is typically associated with the K Zone. Little or no crushing of the ammonite shell has occurred in sheet Ammolite; it is typically sourced from Zone 4.

MINING AND PRODUCTION

Korite International. The dominant Ammolite producer continues to be Korite International of Calgary, Alberta. As discussed by Mychaluk et al. (2001), Korite has operated several open-pit mines to recover both gem-quality Ammolite and complete ammonite fossils from the Bearpaw Fm. Pierre Paré, president of Korite, provided much of the following update on their activities.
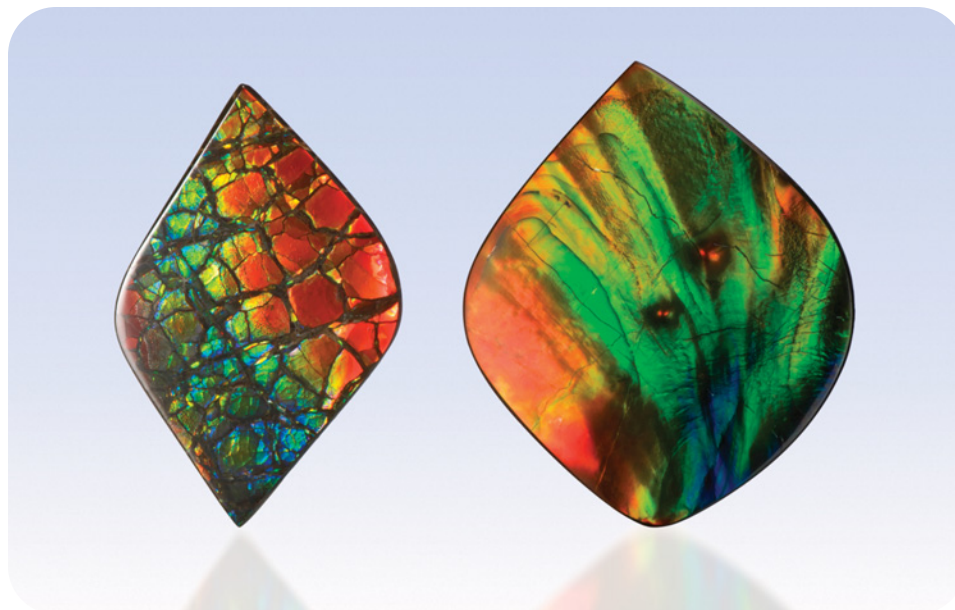
Figure 1. Alberta's St. Mary River valley continues to produce high-quality Ammolite. While fractured Ammolite (left, 4.7 × 3.0 cm) was mainly exploited in the past, today's production is dominated by sheet Ammolite (right, 5.2 × 4.4 cm). Courtesy of Korite International; photo by Robert Weldon.

The Kormos mine, the first major producer (opened in 1983), has not been reactivated since its suspension in 1994. The Oxbow mine was first opened in 1994, and exhausted by the spring of 2001. A total of 11 hectares were excavated to a maximum depth of 20 m, the economic limit of recovery. The mine exploited the "K Zone" horizon of the Bearpaw Fm, producing predominantly fractured Ammolite.

Excavation at the Zone 4 mine began in late 2000, and the economically productive portion of the deposit was exhausted in October 2003. A total of 5 hectares were exploited and, as the name implies, the mine targeted the Zone 4 horizon of the Bearpaw Fm, which primarily contains sheet Ammolite. By November 2004, both mines were totally reclaimed, with the original stockpiled topsoil backfilled and seeded with native grasses.

Korite commissioned two new open pits near the Zone 4 deposit: the Salberg and Power Pole mines. These also target Zone 4 of the Bearpaw Fm. Mining at Salberg started in 2004, but the pit was reclaimed in 2008 after yielding only 3 hectares of economical deposits. The Power Pole mine was also started in 2004, and since then approximately 5.5 hectares have been mined. Currently, this is the only active Korite mine site, although production was suspended between December 2008 and mid-July 2009 due to an unusually cold winter and the economic downturn. Korite claims that test holes on the Power Pole property indicate sufficient reserves for more than a decade of reliable production.

Of significant note is the production shift from fractured Ammolite to sheet Ammolite since 2001. As stated in Mychaluk et al. (2001), in 1999 Korite manufactured 57,025 finished gemstones from rough material derived primarily from the now-abandoned Oxbow mine. Ammolite recovered from the Oxbow mine was mostly fractured because it was produced from the K Zone of the Bearpaw Fm. Now that

Figure 2. Intensely colored fossil ammonite specimens are recovered from the Ammolite deposits. This 60-cm-diameter ammonite (P. meeki) was donated to the American Museum of Natural History in New York by Korite International and Canada Fossils Ltd. Courtesy of AMNH; photo by Craig Chesek.
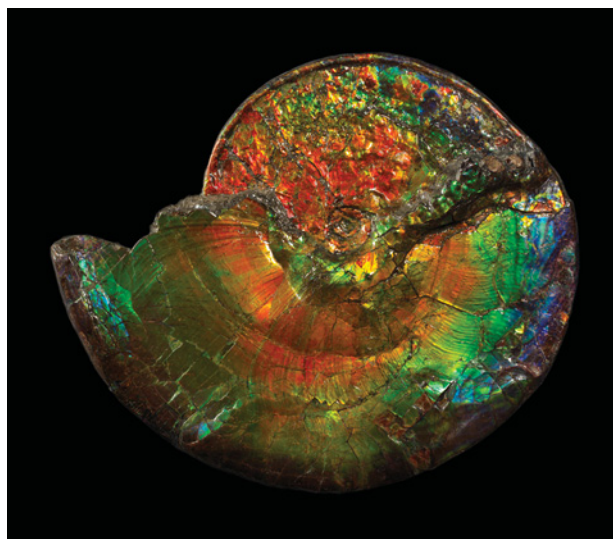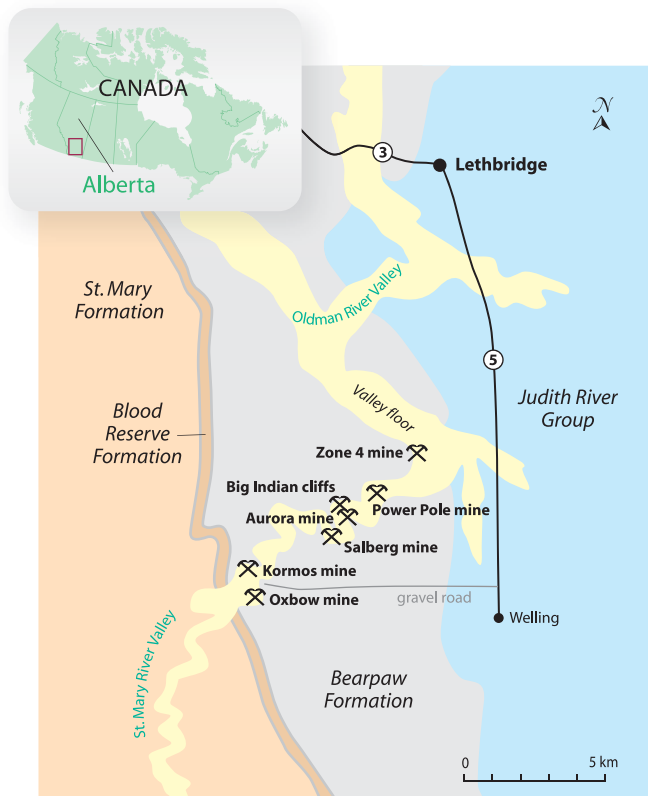
Figure 3. This map shows both the locations and subsurface bedrock of the main Ammolite-producing mines and collecting areas near Lethbridge, Alberta. Ammolite is only recovered from marine shale of the Cretaceous Bearpaw Fm. Modified from Mychaluk et al. (2001).

mining is focused on the Zone 4 horizon, Korite reports that 95% of the finished gemstones produced in 2008 were sheet Ammolite. In 2008, Korite manufactured 77,110 assembled stones (triplets) and 2,752 stabilized solids (including very few doublets) for a total of 79,862 finished gemstones. As Korite continues to be the dominant producer of Ammolite worldwide, the vast majority of Ammolite seen in today's market has switched from fractured to sheet during this decade. Korite reports, however, that it has enough stockpiled fractured Ammolite to produce 2,000–3,000 finished gemstones, to accommodate future demand for this material.

The greater availability of sheet Ammolite has helped grow the market, according to Korite, because this material tends to have stronger iridescence and more of the popular blue coloration than the fractured material. Korite, in fact, claims that revenue from Ammolite sales grew by more than 130% from 2001 to 2008. Sales in Asia (mainly Singapore, Hong Kong, China, and Japan) have grown three-fold since 2001. Much of this growth is from those practicing the ancient Chinese system of *feng shui*. These customers

are reportedly purchasing more Ammolite gemstones as well as ammonite fossils because the colors and shell shape of these materials are symbolic and auspicious in the *feng shui* tradition. Korite has opened further markets for Ammolite through the cruise ship industry.

Korite's sister company, Canada Fossils, has discovered some significant fossils (*Placenticeras meeki*) in the new Salberg and Power Pole mines. Korite donated an exceptional specimen to the American Museum of Natural History in New York in 2007; it is on display in the museum's "Grand Gallery" (again, see figure 2).

Due to the size of Korite's operation in the marine sediment of the Bearpaw Fm, the chances of finding Cretaceous-age marine reptile skeletons are quite good. Since 2001, Korite has unearthed three mosasaurs and one plesiosaur at its Salberg and Power Pole mines. These specimens are among the best preserved from Alberta. The fossils excavated were turned over to the Royal Tyrell Museum of Paleontology in Drumheller, Alberta, where they are being restored and studied.

Aurora Ammolite Mine. Located within the St. Mary River valley between Korite's Salberg and Power Pole mines, the Aurora is the only fully mechanized Ammolite mine not operated by Korite. Owner Rusty Pimm took the author on a tour of this open-pit mine in September 2008 (figure 4). First opened in 2004, the pit is slightly larger than 1.2 hectares and has been excavated to a depth of 18 m (60 ft) on the west end and to 12 m (40 ft) on the east. The pit is being expanded (along strike) to the south and is being backfilled and reclaimed as mining moves southward. Reserves appear to be significant. The author believes the Aurora mine is exploiting Zone 4 of the Bearpaw Fm based on pay zone thickness (~1.5 m), proximity to Korite's new mines, relative stratigraphic position within the Bearpaw Fm, and the production of sheet Ammolite.

Mining is done by a two-person team (Rusty's sons) consisting of a backhoe operator and a "spotter" (see Mychaluk et al., 2001, for more on Ammolite mining techniques). The Bearpaw Fm shale, fortunately, is quite friable above the pay zone, while it is hard and sandy below this horizon.

The Aurora mine operated for a total of 40–60 days in 2007, mainly in the summer months, while Korite's operations are typically year-round. The 2008 season was much shorter than previous years due to heavy rains in June that flooded the Aurora pit and

required pumping before operations could resume.

Highly localized faulting within the Bearpaw Fm has created a number of hazards at the Aurora mine. Shortly after a fault with 4.5 m (15 ft) of displacement was exposed, a significant pit-wall collapse occurred. Although no one was injured, some minor equipment was buried and the pit had to be cleaned out. The faults are also problematic because they alter the depth at which the pay zone is located, thereby increasing mining time and cost. Most significantly, they serve as conduits for water percolation from the surface into the pay zone, causing damage to the Ammolite within (e.g., iron-oxide staining). The faults may have formed when the weight of overlying glaciers caused the Bearpaw shale to buckle during the last ice age.

Within the pay zone, four to five complete ammonite fossils (generally situated horizontally and compressed laterally) are found per backhoe set (defined as the volume a backhoe can excavate from one set location). Rough material is sent to Edmonton, Alberta, for manufacture into gemstones (eventually marketed by Aurora Canadian Jewelry) or for restoration into display specimens.

Artisanal Mining. Surface collecting of Ammolite (and complete ammonite fossils) has been ongoing since the late 1960s, but some localities are more challenging to access than others. Tom Chant—president of Enchanted Designs, an independent manufacturer of Ammolite jewelry—purchases much of his rough material from members of the Blood Indian Tribe who collect from the west banks of the St. Mary River (located on reservation lands opposite Korite and Rusty Pimm's operations). Mr. Chant arranged a tour for the author of a key collecting area with Edward "Ed" Eaglechild of the Blood Tribe. The site, locally called "Big Indian" or "Kings," is an imposing 80 m (260 ft) high cliff overlying the St. Mary River (figure 5).

Mr. Eaglechild and other freelance collectors like him rappel down these cliffs, swinging back and forth along the face at various levels in search of Ammolite and complete fossil ammonites. The ropes are either tied to the axle of a truck or to metal stakes driven deep into the ground at the top of the cliff. Mr. Eaglechild has been collecting for over nine years, and reported that there are many individuals and groups from the Blood Tribe who are involved in artisanal mining–based businesses (such as Raw Ammonite, Black Horse Mines, and Buffalo Rock Mining Co.). Most collecting is weather dependent and usually per-

Figure 4. Outside of Korite International, only newcomer Rusty Pimm Enterprises has been successful at continuous mechanized mining for Ammolite. In this view, looking west, topsoil can be seen stockpiled on the north and west sides of the pit. Photo by K. Mychaluk.

formed during the summer, but he stated that he was one of two collectors who worked through the Canadian winter last year. He typically collects five times per week and finds, on average, one good-quality fossil ammonite (sometimes with Ammolite attached) per day. Mr. Eaglechild reported that there are six productive cliff areas on the Reserve including Big Indian. The exposed surface area of the cliffs is significantly larger than that of the open-pit mines and, when combined with high erosion rates, yields a con-

Figure 5. The cliffs at Big Indian can only be accessed by Blood Indian Tribe members. The top buff layer consists of glacial lake sediments, which overlie weathered Bearpaw Fm shale (light brown). The majority of the cliff face exposes unweathered gray Bearpaw shale that hosts Ammolite and ammonite specimens. View is upstream to the southwest. Photo by K. Mychaluk.

Figure 6. Dinolite is a composite of Alberta dinosaur bone and Ammolite with sugilite, turquoise and/or malachite, as seen in these pendants (22 × 32 mm on the left). Courtesy of Enchanted Designs; photo by Robert Weldon.

sistent supply of material to collect. The author was also shown two pits on the Blood Reserve that had formerly been excavated with mechanical equipment. Results and production history were not provided, and other such pits may also exist. Additional photos are available in the G&G Data Depository at www.gia.edu/gandg.

Rough production from the Blood Tribe is typically sold to Enchanted Designs and Korite, although there are many other small buyers and jewelry manufacturers in the area.

FOSSIL POACHING

Theft (locally called "fossil poaching") continues to be a problem for all mine operators. Shortly before the author's field visit, burglars had cut locks and gained access to a field office at the Aurora mine. The Ammolite miners interviewed report that, as a matter of policy, they remove all gem material (including high-quality fossil specimens) from their mine sites at the end of each day. As a further deterrent, miners routinely comb their pits and exposed outcrops for

any trace of Ammolite regardless of quality. As erosion rates of the Bearpaw Fm are quite fast, most operators typically scour these surfaces on a daily basis. Korite also conducts truck patrols to dissuade would-be thieves. During the author's one-day visit, a Korite vehicle was observed intercepting trespassers on two occasions. Thieves are also active at night, when they make small excavations.

DINOLITE

Lapidaries continue to find innovative ways to use Ammolite. Due to its typically thin and sheet-like nature, Ammolite has been used in mosaics, such as on watch faces. Enchanted Designs manufactures two products in which Ammolite is used in a mosaic or composite fashion. Keeping with a Canadian theme, one product consists of polished mammoth ivory pieces from the Yukon Territory inlaid with Ammolite and other gem materials such as turquoise or sugilite. The other, a new product called "Dinolite," combines siliceous dinosaur bone fragments from Alberta with pieces of Ammolite, sugilite, turquoise, and malachite using an undisclosed process (figure 6). The Canadian Intellectual Property Office granted trademark status to Dinolite on July 23, 2008.

CONCLUSION

Production of Ammolite has grown significantly since 2001. Notwithstanding the current global economic slowdown, the author predicts this trend will continue for the next decade.

ABOUT THE AUTHOR
Mr. Mychaluk (kmychaluk@shaw.ca) is a geologist in Calgary, Alberta, Canada.

REFERENCE

Mychaluk K.A., Levinson A.A., Hall R.L. (2001) Ammolite: Iridescent fossilized ammonite from southern Alberta, Canada. *G&G*, Vol. 37, No. 1, pp. 4–25.

POLYMER-FILLED AQUAMARINE

Li Jianjun, Sun Yuan, Hao Wangjiao, Luo Han, Cheng Youfa, Liu Huafeng, Liu Ying, Ye Hong, and Fan Chengxing

The authors have encountered hundreds of polymer-filled aquamarines in the Chinese jewelry market. This treatment can be identified with a standard gemological microscope, since it has characteristics such as a flash effect and relief lines. In addition, some of the filled fractures fluoresce chalky white to long-wave UV radiation. FTIR spectroscopy reveals diagnostic features at ~3100–2850 cm^{-1} that are related to benzene and ethylic C-H bonds in a polymer.

Clarity enhancement of beryl is not new, though by far most attention has been focused on emerald (e.g., Johnson et al., 1999a,b). However, aquamarine has been treated by oiling for some time, and more recently with wax and resin-based fillers such as Opticon (Eliezri, 1998; Johnson et al., 1999a,b). Within the last few years, large quantities of filled aquamarine have entered the Chinese market. Of ~10,000 jewelry pieces tested at the National Gold & Diamond Testing Center of China (NGDTC), we encountered more than 200 items that contained >400 pieces of polymer-filled aquamarine of varying quality. So far, these have been in the form of beads (figure 1), cabochons, and carvings; no filled faceted gems have yet been encountered.

Materials and Methods. For this report, we examined an aquamarine bracelet obtained from a jewelry wholesaler that consisted of 17 reportedly polymer-filled bluish green beads (11.28–12.46 ct; again, see figure 1). The bracelet was disassembled to ensure that there was no interference from the string. In addition, we studied two faceted aquamarines (one oiled and one untreated) for comparison of spectral features.

At NGDTC, we performed standard gemological testing and Fourier-transform infrared (FTIR) spectroscopy on all the samples. FTIR was conducted with a Nicolet Nexus 470 instrument at room temperature and relative humidity below 40%. Spectra were collected in the range 6000–400 cm^{-1} at a resolution of 8 cm^{-1}, with eight scans per sample at a fixed gain of 1.0. Both transmission and specular reflectance FTIR spectroscopy were performed.

To check whether a lead-based glass such as that used for filling corundum might be present, we performed qualitative chemical analysis of the samples at NGDTC with a Thermo QuantX EC energy-dispersive X-ray fluorescence (EDXRF) spectrometer using parameters optimized for the detection of heavy elements. Operating conditions were 100 second live time, voltage of 20 kV, Rh target, vacuum, and no filter.

Figure 1. These bracelets are typical of the filled aquamarine jewelry currently being encountered in the Chinese market. The beads in the bracelet on the far left (11.28–12.46 ct) were the subject of this study. Photo by Li Jianjun.
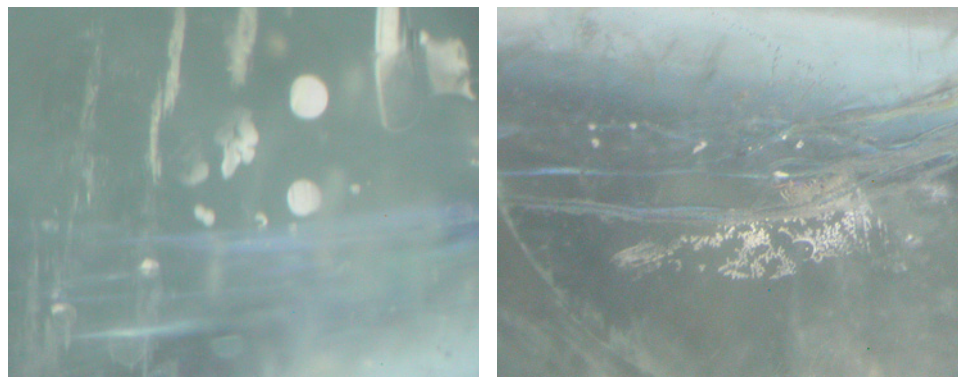
Figure 2. Blue flash effects, high-relief areas, and surface-reaching fissures with cloudy white-appearing regions of reduced transparency were observed in the filled aquamarine beads. Photomicrographs by Li Jianjun; magnified 30× (left) and 15× (right).

Results and Discussion. *Physical and Optical Properties.* The physical and optical properties of the polymer-filled, oiled, and untreated samples are reported in table 1. With the unaided eye, the filled beads exhibited no significant features to arouse suspicion. They were translucent and contained abundant fissures. However, the fractures in a few beads showed a weak, chalky white fluorescence to long-wave UV radiation. This is a good indicator for the presence of a polymer filling (Kammerling and Koivula, 1991). All samples were inert to short-wave UV.

Microscopic Features. With 10× magnification, we observed flash effects in almost every filled bead; some other common microscopic features were high-relief areas (representing incomplete filling) and cloudy areas of reduced transparency that appeared white (figure 2). These are all classic signs of polymer filling (Kammerling et al., 1991; Johnson et al., 1999a; Hainschwang, 2002). Some fractures in the beads showed iridescence (figure 3) as well as a flash effect. When viewing a sample in the direction of the flash, we also observed relief lines where the filling

Figure 3. This aquamarine bead exhibited iridescence in the unfilled portion of an incompletely filled fracture. Photomicrograph by Li Jianjun; magnified 30×.
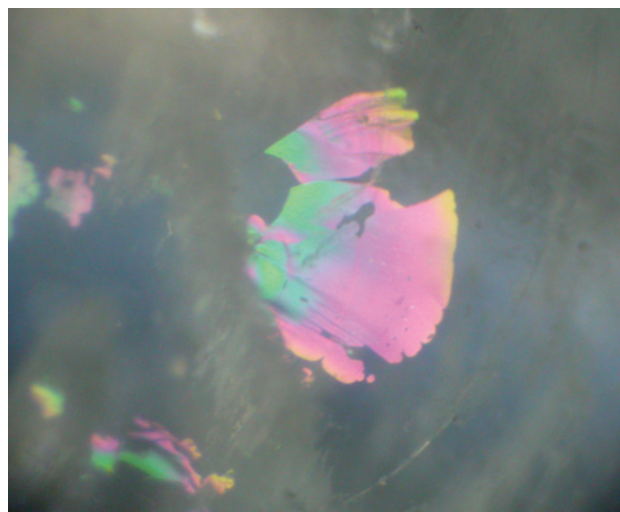
reached the polished surface (figure 4). The underlying fissures did not show a reflective appearance.

Infrared Spectroscopy. FTIR spectroscopy was successful in determining the type of filler material in the beads and in the oiled comparison stone. In spectra taken from the beads (figure 5), the region between 3100 and 2850 cm^{-1} showed features that are diagnostic for polymers. The peaks at 3051 and 3035 cm^{-1} belong to the benzene C-H bond, while those at 2962, 2927, and 2873 cm^{-1} belong to the ethylic C-H bond (Stuart, 2004). The strength of the

TABLE 1. Physical and optical properties of the aquamarine samples studied for this report.

Property	Polymer-filled (17 samples)	Oiled (1 sample)	Untreated (1 sample)
Weight	11.28–12.46 ct	2.27 ct	1.45 ct
Color	Bluish green	Very light blue	Light blue
Pleochroism	Moderate, gray-blue and green-blue	Moderate, blue and greenish blue	Moderate, blue-green and blue
Luster	Vitreous	Vitreous	Vitreous
RI	1.57 (spot reading)	1.575–1.582	1.577–1.583
Birefringence	Not determined	0.007	0.006
SG	2.69–2.73^a	2.71	2.71
UV fluorescence	Fractures chalky white to long-wave (in a few beads)	Inert	Inert
Microscopic features	Liquid-gas inclusions, fractures and fracture plane reflections, flash effects, iridescent fractures, cloudy areas of reduced transparency, surface relief lines	Liquid-gas inclusion	Three-phase inclusions
Mid-IR absorption features	3051, 3035, 2962, 2927, and 2873 cm^{-1}	2923 and 2858 cm^{-1}	No significant peaks between 3100 and 2850 cm^{-1}

^{a} *Seven of the 17 samples were selected randomly for hydrostatic SG measurements.*
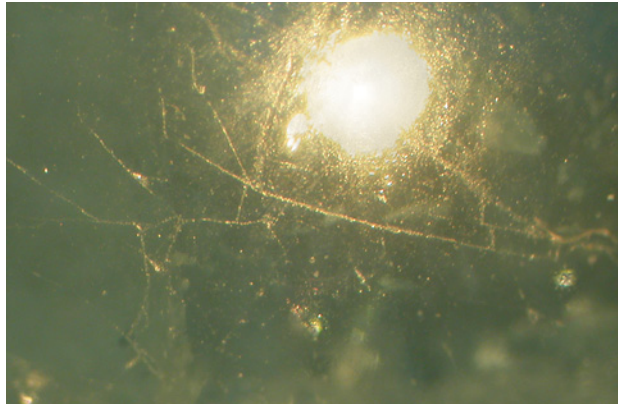
Figure 4. Filled fractures were visible on the surface of the aquamarine beads as relief lines. Photomicrograph by Li Jianjun; magnified 15×.

Figure 5. This representative mid-IR spectrum of the polymer-filled beads shows distinct features from polymer impregnation, particularly between 3100 and 2850 cm^{-1}, that are not seen in the oiled and untreated aquamarine comparison samples. The absorption features at 3051 and 3035 cm^{-1} are due to the benzene C-H bond in a polymer. The bands from 3250 to 3100 cm^{-1} are characteristic of beryl. Spectra are offset and shifted vertically for clarity.

filler-related absorption was rather high in some samples, suggesting that some residual substance was present on the surface. We suspect these polymers might be Opticon-like resins or Araldite (Johnson et al., 1999a; Hainschwang, 2002; Lowry, 2006). The differences between these spectra and those of the oiled comparison sample and the untreated stone were apparent (again, see figure 5).

Chemical Analysis. No heavy elements such as lead were detected by EDXRF spectroscopy (Li et al., 2008). Thus, it does not appear that any lead-based glass was used in our samples.

Conclusions. A few of the filled aquamarines in our study revealed abnormal long-wave UV fluorescence, which is a good indicator for polymer filling. Microscopic evidence of polymer filling also included surface relief lines with no corresponding reflective internal features, as well as flash effects when the samples were viewed nearly parallel to filled fractures.

In our experience, about 15% of the aquamarines with poor clarity (i.e., mostly beads, cabochons, and carvings) currently in the Chinese market have been filled. Although we have not yet encountered polymer-filled faceted samples in the marketplace, this treatment could easily be used on included faceted gems.

ABOUT THE AUTHORS

Mr. Li Jianjun (geoli@vip.sina.com), Mr. Cheng Youfa, and Mr. Liu Huafeng are with the National Gold & Diamond Testing Center of China (NGDTC), Jinan, Shandong. Ms. Sun Yuan, Ms. Hao Wangjiao, and Ms. Luo Han are in the Earth Sciences Department, Gems Testing & Appraisal Center (GTAC), Sun Yat-Sen University, Guangzhou. Ms. Liu Ying is with the National Gem Testing Center of China (NGTC), Beijing. Ms. Ye Hong is at the Shenzhen laboratory of NGTC. Mr. Fan Chengxing is with the National Jewellery Quality Supervision and Inspection Center of China (NJQSIC), Beijing.

REFERENCES

Eliezri I.Z. (1998) Address at the First World Emerald Congress, Bogotá, Colombia, *ICA Gazette*, July/August, pp. 7–10.

Hainschwang T. (2002) The identification of clarity enhancements of emeralds. *Gemlab Research Newsletter*, June 1, www.gemlab.net/website/gemlab/fileadmin/user_upload/publications_old/emeraldtreatmentsengl.pdf.

Johnson M.L., Elen S., Muhlmeister S. (1999a) On the identification of various emerald filling substances. *G&G*, Vol. 35, No. 2, pp. 82–107.

Johnson M.L., Elen S., Muhlmeister S. (1999b) Characterization of some emerald filling substances. *G&G*, Vol. 35, No. 3, pp. 149–151.

Kammerling R.C., Koivula J.I., Kane R.E., Maddison P., Shigley J.E., Fritsch E. (1991) Fracture filling of emeralds: Opticon and traditional "oils." *G&G*, Vol. 27, No. 2, pp. 70–85.

Koivula J.I., Kammerling R.C., Eds. (1991) Gem News: Colored Opticon for emeralds. *G&G*, Vol. 27, No. 1, pp. 52–53.

Li J., Liu X., Cheng Y., Liu H. (2008) The characteristics and identification of filled aquamarine [in Chinese]. *China Gems*, Vol. 17, No. 1, pp. 187–189.

Lowry S. (2006) Analysis of emeralds by FT-IR spectroscopy: Identifying treated and synthetic emeralds. Thermo Fisher Scientific, Application Note 51123, www.thermo.com/ethermo/cma/pdfs/articles/articlesfile_2442.pdf.

Stuart B.H. (2004) *Infrared Spectroscopy: Fundamentals and Applications*. John Wiley & Sons, New York.

GEM-QUALITY YELLOW-GREEN HAÜYNE FROM OLDOINYO LENGAI VOLCANO, NORTHERN TANZANIA

Anatoly N. Zaitsev, Olga A. Zaitseva, Alexander K. Buyko, Jörg Keller, Jurgis Klaudius, and Andrei A. Zolotarev

Yellow-green to green-yellow gem-quality haüyne was found for the first time in an alkaline plutonic rock from the active Oldoinyo Lengai volcano in northern Tanzania. The mineral has optical and physical properties that are typical for sodalite-group minerals. Infrared and Raman spectroscopy showed that in addition to the $(SO_4)^{2-}$ group, the haüyne also contains $(NO_3)^-$, $(CO_3)^{2-}$, and water in its structure. SEM-EDS and EDXRF analyses confirmed the presence of Na, Ca, Al, and Si as major cations, with minor amounts of K.

Oldoinyo Lengai volcano, located in the Gregory Rift, northern Tanzania, is the only active carbonatite volcano in the world (Dawson, 1962; Keller and Krafft, 1990; Mitchell and Dawson, 2007). It is a typical stratovolcano and 2,952 m high (figure 1). It consists of unusual silica-undersaturated volcanic rocks including nephelinite and phonolite, as well as natrocarbonatites. The rocks occur as ash, lapilli, tuff, and agglomerates interlayered with lava flows. The agglomerates contain blocks of unusual feldspathoid-rich plutonic rocks such as urtite and ijolite.

While visiting Oldoinyo Lengai volcano in 2003, researchers from Freiburg University in Germany found a block of plutonic rock ~0.35 m in longest dimension, which proved to have a composition intermediate between ijolite and urtite. The block was coarse-grained and pegmatitic, consisting primarily of nepheline and diopside with subordinate amounts of magnetite, apatite, and perovskite. It also contained large (up to 7 cm) anhedral gem-quality pale greenish yellow crystals that were subse-

quently identified as haüyne (figure 2), ideal formula $Na_6Ca_2(Al_6Si_6O_{24})(SO_4)_2$. However, published data on haüyne show that it is characterized by variable contents of Ca and Na, typically contains some K, and in addition to $(SO_4)^{2-}$ also contains Cl and S^{2-} (e.g., Deer et al., 2004). Thus, a more general formula of haüyne can be written as $(Na,Ca,K)_{4-8}(Al_6Si_6O_{24})(SO_4,S,Cl)_{1-2}$.

Materials and Methods. Haüyne samples measuring 10–15 mm were extracted from the Oldoinyo Lengai block and cut into three faceted stones ~1.5 ct each (e.g., figure 3). The faceted gem shapes, all brilliant cut, were round, antique square cushion, and triangle. Gemological properties were determined on all three of the faceted stones (RI with a refractometer, hydrostatic SG, and UV fluorescence) and on some anhedral grains (RI with the immersion method) at St. Petersburg State University, Russia, using standard equipment. Hardness was determined on a rough fragment using a Mohs hardness mineral set.

Chemical composition was determined on rough fragments at the Natural History Museum in London by: (1) scanning electron microscopy–energy dispersive spectroscopy (SEM-EDS), and (2) combustion analysis (gas analysis after the sample is combusted to break it down into components) for C, H, and N. In addition, energy-dispersive X-ray fluorescence (EDXRF) analysis of a powdered sample was performed at Freiburg University. One faceted stone was also investigated by variable pressure SEM-EDS (no sample coating required). Powder X-ray diffraction analysis, single-crystal structure determination, and IR spectroscopy of the rough samples were performed at St. Petersburg State University. Raman spectroscopy of both rough and cut specimens was undertaken at the School of Earth Sciences and Geography, Kingston University, London.

Results and Discussion. The mineral was identified as haüyne on the basis of its X-ray diffraction pattern (unit-cell parameter a = 9.040 ± 0.001 Å), and its optical and physical properties, which are similar to those reported for haüyne and other sodalite-group minerals (e.g., Deer et al., 2004; Ballirano and Maras, 2005). However, the RI values were lower, and SG values were higher, than those reported

Figure 1. At 2,952 m high, Oldoinyo Lengai volcano in northern Tanzania is the only active carbonatite volcano in the world. Photo by E. O. Zaitseva.

for gem-quality blue haüyne by Kiefert and Hänni (2000). Nevertheless, the identification as haüyne was confirmed by data from the single-crystal structure determination.

The yellow-green color of our samples is quite different from that of the well-known gem-quality blue haüyne from Eifel, Germany (Kiefert and Hänni, 2000) and Dattaw, Myanmar (Grobon and Hainschwang, 2006). Other color variants of haüyne are white and shades of gray, green, yellow, and red (Roberts et al., 1990). The gemological properties of the Oldoinyo Lengai material are shown in table 1.

The infrared spectra of the Oldoinyo Lengai haüyne in the 1300–350 cm^{-1} region were similar to spectra for haüyne and SO_4-bearing sodalite from other localities (e.g., Ballirano and Maras, 2005). In addition, the IR spectra for

Figure 2. A large haüyne crystal (up to 7 cm) is embedded in this rock, which is composed of ijolite-urtite. Photo by A. N. Zaitsev.

Figure 3. This silver ring is set with a 1.53 ct round brilliant-cut haüyne that was faceted for this study. Photo by A. A. Antonov.

the Oldoinyo Lengai samples contained single peaks at 1364 cm^{-1} [(NO$_3$)$^{2-}$ groups], 1499 and 1412 cm^{-1} [(CO$_3$)$^{2-}$ groups], and 1692 cm^{-1}, as well as a broad band at 3600–3400 cm^{-1}; the latter two bands correspond to water molecules (Buhl and Löns, 1996; Ballirano and Maras, 2005).

Raman spectroscopy showed that the haüyne from Oldoinyo Lengai contains (SO$_4$)$^{2-}$ groups, as indicated by the presence of peaks at 990–980 and 449–446 cm^{-1}. No peaks were observed at ~1089 and 543 cm^{-1}, which are related to the S^{3-} group, as seen in the Raman spectra of blue haüyne from Eifel (e.g., Kiefert and Hänni, 2000; Di Muro et al., 2004).

SEM-EDS, EDXRF, and combustion analyses confirmed the very unusual composition of some of the anions in the haüyne. The analyses showed significant amounts of sulfur (6.6–7.1 wt.% SO$_3$); minor nitrogen (1.1–1.3 wt.% N$_2$O$_5$), water (0.9–1.0 wt.% H$_2$O), chlorine (0.6–0.7 wt.% Cl), and carbon (0.4–0.5 wt.% CO$_2$); and traces of phosphorous (0.1 wt.% P$_2$O$_5$). In addition to the major cations in haüyne (Na, Ca, Al, and Si), we found minor amounts of K (1.6–1.8 wt.% K$_2$O), and traces of Fe (0.2–0.3 wt.% Fe$_2$O$_3$) and Mg (0.1 wt.% MgO). The analytical results are given in table 2, from which we calculated an average empirical formula of: (Na$_{6.75}$Ca$_{0.87}$K$_{0.37}$)$_{\Sigma7.99}$(Al$_{5.97}$Fe$^{3+}_{0.03}$Si$_{6.00}$O$_{24}$) [(SO$_4$)$_{0.89}$(OH)$_{0.54}$(NO$_3$)$_{0.23}$Cl$_{0.20}$(CO$_3$)$_{0.12}$]$_{\Sigma1.98}$. To our knowledge, this is the first naturally occurring nitrogen-bearing mineral from the sodalite group.

Conclusions. Gem-quality haüyne has been found at the active Oldoinyo Lengai volcano. This haüyne has a very unusual yellow-green color and a complex chemical composition (including the presence of N and C). The future production of the haüyne is uncertain, but with growing numbers of visitors to this part of Tanzania, it is likely that more samples of this gem mineral may be found.

TABLE 2. Chemical composition of haüyne from Oldoinyo Lengai.[a]

Oxide (wt.%)	SEM-EDS		EDXRF	Combustion analysis	
	Average (10)	Range		Average (3)	Range
SiO$_2$	34.24	33.89–34.34	34.01	na	
TiO$_2$	bdl		0.02	na	
Al$_2$O$_3$	28.95	28.68–29.37	28.91	na	
Fe$_2$O$_3$	0.23	0.20–0.29	0.30	na	
MnO	bdl		bdl	na	
MgO	bdl		0.09	na	
CaO	4.62	4.58–4.65	4.47	na	
Na$_2$O	19.88	19.67–19.91	19.00	na	
K$_2$O	1.66	1.57–1.79	1.57	na	
SO$_3$	6.78	6.63–7.05	na	na	
P$_2$O$_5$	bdl		0.13	na	
CO$_2$	na		na	0.49	0.45–0.54
N$_2$O$_5$	na		na	1.20	1.08–1.34
H$_2$O	na		na	0.92	0.85–0.99
Cl	0.68	0.63–0.72	na		
-O=Cl$_2$	0.15				
Total	96.89		88.50	2.61	

[a] *Notes: Carbon, nitrogen, and hydrogen were analyzed as elements and recalculated into oxides. Calculation of the empirical formula was performed using SEM-EDS and combustion analyses and considering all Fe as Fe$_2$O$_3$. Abbreviations: bdl = below detection limit; na = not analyzed.*

REFERENCES

Ballirano P., Maras A. (2005) Crystal chemical and structural characterization of an unusual CO_3-bearing sodalite-group mineral. *European Journal of Mineralogy*, Vol. 17, pp. 805–812.

Buhl J.-C., Löns J. (1996) Synthesis and crystal structure of nitrate enclathrated sodalite $Na_8[A1SiO_4]_6(NO_3)_2$. *Journal of Alloys and Compounds*, Vol. 235, pp. 41–47.

Dawson J.B. (1962) The geology of Oldoinyo Lengai. *Bulletin Volcanologique*, Vol. 24, No. 1, pp. 349–387.

Deer W.A., Howie R.A., Zussman J., Wise W.S. (2004) *Rock-Forming Minerals—Framework Silicates*, 2nd ed., Vol. 4B. Geological Society, London, 982 pp.

Di Muro A., Bonaccorsi E., Principe C. (2004) Complex colour and chemical zoning of sodalite-group phases in a haüynophyre lava from Mt. Vulture, Italy. *Mineralogical Magazine*, Vol. 68, No. 4, pp. 591–614.

Grobon C., Hainschwang T. (2006) Gem News International: Massive haüyne-sodalite from Myanmar. *G&G*, Vol. 42, No. 1, pp. 64–65.

Keller J., Krafft M. (1990) Effusive natrocarbonatite activity of Oldoinyo Lengai, June 1988. *Bulletin of Volcanology*, Vol. 52, No. 8, pp. 629–645.

Kiefert L., Hänni H.A. (2000) Gem-quality haüyne from the Eifel district, Germany. *G&G*, Vol. 36, No. 3, pp. 246–253.

Mitchell R.H., Dawson J.B. (2007) The 24th September 2007 ash eruption of the carbonatite volcano Oldoinyo Lengai, Tanzania: Mineralogy of the ash and implications for formation of a new hybrid magma type. *Mineralogical Magazine*, Vol. 71, No. 5, pp. 483–492.

Roberts W.L., Campbell T.J., Rapp G.R. Jr. (1990) *Encyclopedia of Minerals*, 2nd ed. Van Nostrand Reinhold, New York.

AQUAMARINE FROM THE MASINO-BREGAGLIA MASSIF, CENTRAL ALPS, ITALY

Rosangela Bocchio, Ilaria Adamo, and Franca Caucia

Aquamarine from granitic pegmatites of the Masino-Bregaglia Massif, Central Alps, Italy, is investigated by classical gemological methods, LA-ICP-MS chemical analyses, and UV-Vis-NIR and mid-IR spectroscopy. This beryl has typical gemological properties for aquamarine, including iron absorption features, and is characterized by a low alkali content and both types I and II water molecules. Although so far only a small amount of this aquamarine has been polished into gems, it represents an attractive gem material of potential economic interest.

The Masino-Bregaglia Massif (also known as the Bergell Massif) contains numerous granitic pegmatites hosting a remarkable variety of minerals—including aquamarine (figure 1)—that have attracted the interest of mineralogists and collectors since the late 18th century (e.g., Bedogné et al., 1995). Beryl from this area was initially mentioned by Repossi (1916) and Staub (1924). Subsequently, many other beryl occurrences were discovered in the massif. In their listing of the locations of historical beryl-bearing pegmatites, Hügi and Röwe (1970) indicated that the most important Italian deposits occurred in the areas of Val Bregaglia (Bregaglia Valley), Valle Mello, Cima di Zocca, Val Masino, Val Codera, and Alpe Vazzeda. In the 1970s, a limited amount of gem-quality aquamarine was recovered and cut from the Filone Silvana (Silvana dike), located in Val Codera.

Masino-Bregaglia aquamarine crystals typically show a prismatic habit and measure several centimeters long, although some crystals attain ~15–20 cm in length. They range from light to dark greenish blue to blue or yellow-green. Some gem- and carving-quality aquamarine has

been recovered, although the fact that most of the crystals contain numerous inclusions and fractures makes such material rare (Bedogné et al., 1995).

To our knowledge, a gemological characterization of this aquamarine is lacking, except for the recent work of Caucia et al. (2008, in Italian). The present article builds on that work by supplying additional data obtained on a larger number of samples from four pegmatites in this area.

Geologic Setting. Masino-Bregaglia is a composite pluton located at the border of Italy and Switzerland (figure 2). It consists mainly of a medium-grained tonalite at the margin and a coarse-grained granodiorite in the core (Trommsdorff and Nievergelt, 1983), which crystallized 32 and 30 million years ago, respectively (von Blanckenburg, 1992). Younger cross-cutting granitic pegmatites and aplites are found throughout the pluton, and some of the pegmatites contain beryl, garnet, tourmaline, and a suite of rare minerals (Wenger and Armbruster, 1991; Bedogné et al., 1995).

Figure 1. This 2.33 ct aquamarine is from the Masino-Bregaglia Massif, Italy. Courtesy of Francesco Bedogné; photo by Roberto Appiani.

Materials and Methods. We examined 14 aquamarine samples from the Masino-Bregaglia Massif: five cabochons (0.30–5.79 ct) and three crystals (4.8–12.0 g, obtained from three different rough specimens) from Val Codera (e.g., figure 3); one faceted (0.26 ct) and one rough (9.6 g) sample from Cima di Zocca; one faceted (0.90 ct) and one unpolished sample (4.0 g) from Val Bregaglia; and one faceted (2.44 ct) and one rough (8.7 g) sample from Alpe Vazzeda. The studied samples are in the collection of the Earth Sciences Department Museum of the University of Milan.

All cut samples were examined by standard gemological methods to determine their optical properties, hydrostatic specific gravity, UV fluorescence, and microscopic features.

Chemical analyses were performed on the six rough specimens by laser ablation–inductively coupled plasma–mass spectrometry (LA-ICP-MS), using an Elan DRC-e mass spectrometer coupled with a Q-switched Nd:YAG laser source, with a fundamental emission (1064 nm) that was converted to 266 nm by two harmonic generators. Helium was used as a carrier gas, mixed with Ar gas downstream of the ablation cell. The calibration was performed using NIST SRM 610 glass and Si as external and internal standards, respectively. The precision and accuracy estimated on the basaltic glass BCR2 standard were better than 10%. Four analyses per sample were collected using a spot size of 40 μm.

Nonpolarized UV-Vis-NIR spectra of three aquamarines (two crystals from Val Codera and one faceted gem from Val Bregaglia) were collected with a Lambda 950 PerkinElmer spectrometer, equipped with an integrating sphere, over the 250–1300 nm range.

Mid-infrared (4000–400 cm^{-1}) spectra of the six rough samples were collected in transmission mode by a Nicolet Nexus FTIR spectrometer, with a resolution of 4 cm^{-1}, using KBr pellets consisting of 2 mg of powdered sample mixed with 200 mg KBr.

Results and Discussion. The cut stones ranged from light to medium blue to greenish blue, and were transparent to opaque. Gemological testing gave the following properties: RI—n_o = 1.580–1.590 and n_e = 1.572–1.579, birefringence—0.008–0.009, optic character—uniaxial negative, SG—2.67–2.72, and inert to both long- and short-wave UV radiation. These observations are consistent with those reported in the literature for aquamarine (O'Donoghue, 2006). The samples were fairly heavily included; they contained fractures, partially healed fissures with fluid and two-phase (fluid and gas) inclusions (figure 4), and growth lines.

LA-ICP-MS measurements (table 1) showed a distinct amount of the chromophore Fe (0.46–0.74 wt.%), as is present in all aquamarines (see, e.g., Adamo et al., 2008, and references therein). Other possible coloring elements (Ti, V, Cr, Mn) were present at very low trace levels (<<0.1 wt.%), as were the alkaline earth metals (Ca and Mg) and the alka-
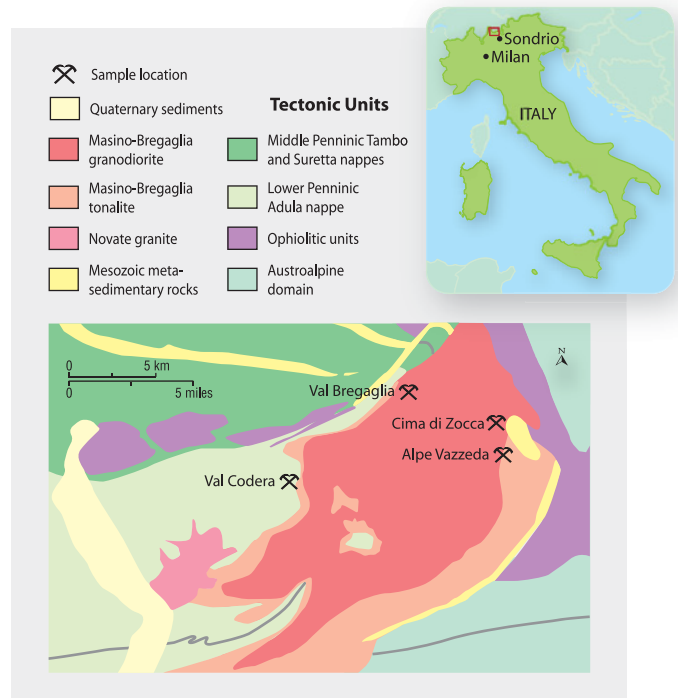
Figure 2. This simplified geologic map illustrates the composite pluton of the Masino-Bregaglia Massif, Central Alps, Italy, and the locations of four of the granitic pegmatites where the beryl samples studied were found.

li metals (Li, Rb, Cs). The only exception was Na, which ranged from 0.22 to 0.39 wt.%. On the basis of these data, our samples can be considered low-alkali-bearing beryls, per the classification of Schmetzer and Kiefert (1990).

Figure 3. These aquamarine crystals (~3.5–4 cm long) from Italy's Val Codera pegmatite were among those investigated in the present study. Photo by R. Bocchio.
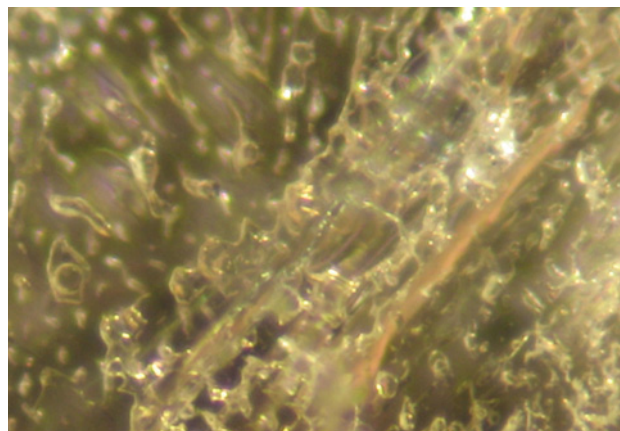
Figure 4. Fluid inclusions (some containing a gas bubble) are common features in aquamarine from the Masino-Bregaglia Massif (here, from Val Codera). Photomicrograph by I. Adamo; magnified 45×. The brown color is an artifact of the lighting conditions.

Figure 5. As is typical for aquamarine, this UV-Vis-NIR spectrum (top) of the faceted specimen from Val Bregaglia is characterized by absorption features related to iron, which is responsible for the blue color. The representative mid-IR spectrum in transmission mode (bottom) shows the region of water-stretching vibrations (3800–3500 cm^{-1}) and is characterized by absorption features of water molecules in both type I (at 3699 cm^{-1}) and type II (at ~3660 and 3597 cm^{-1}) configurations in the structural channels.

The UV-Vis-NIR spectra were typical for aquamarine (e.g., figure 5, top), with a general absorption below ~300 nm, two peaks at 370 and 426 nm related to Fe^{3+}, and a strong and broad absorption band centered at about 820 nm that was due to Fe^{2+} (Wood and Nassau, 1968; Burns, 1993; Taran and Rossman, 2001; Spinolo et al., 2007). A sideband at about 600 nm has been attributed to an Fe^{2+}-Fe^{3+} intervalence charge-transfer process (Schmetzer, 1990; Burns, 1993; Taran and Rossman, 2001), although some authors (e.g., Wood and Nassau, 1968; Viana et al., 2002) have assigned it to Fe^{2+}.

The mid-infrared spectra (e.g., figure 5, bottom) contained absorption bands below 1200 cm^{-1} intrinsic to the beryl structure, as well as features originating from both type I (3699 cm^{-1}) and type II (~3660 and 3597 cm^{-1}) water molecules trapped in the structural channels (Wood and Nassau, 1967, 1968; Charoy et al., 1996; Fukuda and Shinoda, 2008). In agreement with the chemical composition, the IR spectrum is typical of low-alkali-bearing beryl, both natural and synthetic (Schmetzer and Kiefert, 1990; Adamo et al., 2008).

Conclusions. Aquamarine from the Masino-Bregaglia Massif shows typical gemological properties. The studied specimens consist of low-alkali-bearing beryl that contains water molecules in both type I and II configurations. Iron is the chromophore, as is typical for aquamarine. This area is one of the most significant localities for gem-quality aquamarine in Italy, although fine material has been found only in limited amounts and only a few pieces have been set into jewelry (e.g., figure 6). Local mineral collectors continue to work the deposits, and it is likely that small amounts of gem-quality aquamarine will continue to be produced in the future.

TABLE 1. Average LA-ICP-MS analyses of six aquamarine samples from the Masino-Bregaglia Massif, Central Alps, Italy.

Minor and trace elements (ppm)	Val Codera			Cima di Zocca	Val Bregaglia	Alpe Vazzeda
	1	2	3			
Li	58	62	126	267	275	116
Na	2187	2625	2500	3930	3838	2939
Mg	644	638	579	1067	1033	411
Ca	310	245	155	176	176	123
Ti	29	30	40	56	52	57
V	1.6	1.7	2.5	0.40	0.92	0.80
Cr	5.7	4.0	1.6	1.60	1.68	1.40
Mn	50	48	88	91	85	158
Fe	4666	4633	7273	6361	6280	7444
Zn	543	535	317	381	375	177
Rb	34	34	92	46	47	49
Cs	661	662	613	729	735	1228

Figure 6. This 8.5 ct aquamarine cabochon from the Masino-Bregaglia Massif is set with diamonds. Photo by, and specimen courtesy of, Pietro Nana.

REFERENCES

Adamo I., Pavese A., Prosperi L., Diella V., Ajò D., Gatta G.D., Smith C.P. (2008) Aquamarine, Maxixe-type beryl, and hydrothermal synthetic blue beryl: Analysis and identification. *Gems & Gemology*, Vol. 44, No. 3, pp. 214–226.

Bedogné F., Maurizio R., Montrasio A., Sciesa E. (1995) *I minerali della Provincia di Sondrio e della Bregaglia Grigionese. Val Bregaglia, Val Masino, Val Codera e Valle Spluga*. Bettini Typography, Sondrio, Italy, 300 pp. [in Italian].

Burns R.G. (1993) *Mineralogical Applications of Crystal Field Theory*, 2nd ed. Cambridge Topics in Mineral Physics and Chemistry, Cambridge University Press, Cambridge, UK.

Caucia F., Bocchio R., Adamo I., Tarantola E. (2008) Carat-terizzazione di berilli in pegmatiti del plutone di Val Masino-Bregaglia (Alpi Centrali). *Rivista Gemmologica Italiana*, Vol. 3, No. 1, pp. 25–32 [in Italian].

Charoy B., De Donato P., Barres O., Pinto-Coelho C. (1996) Channel occupancy in an alkali-poor beryl from Serra Branca (Goiás, Brazil): Spectroscopic characterization. *American Mineralogist*, Vol. 81, No. 3/4, pp. 395–403.

Fukuda J., Shinoda K. (2008) Coordination of water molecules with Na+ cations in a beryl channel as determined by polarized IR spectroscopy. *Physics and Chemistry of Minerals*, Vol. 35, No. 6, pp. 347–357.

Hügi Th., Röwe D. (1970) Berylliummineralien und Beryl-liumgehalte granitischer Gesteine der Alpen. *Schweizerische Mineralogische und Petrographische Mitteilungen*, Vol. 50, No. 3, pp. 445–480 [in German].

O'Donoghue M., Ed. (2006) *Gems*, 6th ed. Butterworth-Heinemann, Oxford, UK.

Repossi E. (1916) La bassa Val Mera. Studi petrografici e geologici. Parte II. *Memorie Società Italiana Scienze Naturali e Museo Civico Storia Naturale Milano*, Vol. 8, No. 2, 138 pp. [in Italian].

Schmetzer K. (1990) Hydrothermally grown synthetic aquamarine manufactured in Novosibirsk, USSR. *Gems & Gemology*, Vol. 26, No. 3, pp. 206–211.

Schmetzer K., Kiefert L. (1990) Water in beryl—a contribution to the separability of natural and synthetic emeralds by infrared spectroscopy. *Journal of Gemmology*, Vol. 22, No. 4, pp. 215–223.

Spinolo G., Fontana I., Galli A. (2007) Optical absorption spectra of Fe2+ and Fe3+ in beryl crystals. *Physica Status Solidi B*, Vol. 244, No. 12, pp. 4363–4370.

Staub R. (1924) Zur Kenntnis der Bergeller Berylle. *Schweizerische Mineralogische und Petrographische Mitteilungen*, Vol. 4, pp. 364–367 [in German].

Taran M.N., Rossman G.R. (2001) Optical spectroscopy study of tuhualite and a re-examination of the beryl, cordierite, and osumilite spectra. *American Mineralogist*, Vol. 86, No. 9, pp. 973–980.

Trommsdorff V., Nievergelt P. (1983) The Bregaglia (Bergell) Iorio intrusive and field relations. *Memorie Società Geologica Italiana*, Vol. 26, pp. 55–68.

Viana R.R., Jordt-Evangelista H., Magela da Costa G., Stern W.B. (2002) Characterization of beryl (aquamarine variety) from peg-matites of Minas Gerais, Brazil. *Physics and Chemistry of Minerals*, Vol. 29, No. 10, pp. 668–679.

von Blanckenburg F. (1992) Combined high-precision chronome-try and geochemical tracing using accessory minerals: Applied to the Central-Alpine Bergell intrusion (central Europe). *Chemical Geology*, Vol. 100, pp. 19–40.

Wenger M., Armbruster T. (1991) Columbite (Fe,Mn)(Nb,Ta)$_2$O$_6$ in the pegmatites of the calc-alkaline Bergell intrusion (south-east Central Alps). *Schweizerische Mineralogische und Petrographische Mitteilungen*, Vol. 71, pp. 349–369.

Wood D.L., Nassau K. (1967) Infrared spectra of foreign molecules in beryl. *Journal of Chemical Physics*, Vol. 47, No. 7, pp. 2220–2228.

Wood D.L., Nassau K. (1968) The characterization of beryl and emerald by visible and infrared absorption spectroscopy. *American Mineralogist*, Vol. 53, No. 5/6, pp. 777–800.

DIAMOND

Fancy Red, Irradiated and Annealed

The most notable feature of the 0.28 ct round-cut diamond in figure 1, submitted to the lab for scientific examination, was its pure color, graded as Fancy red. This color grade (without modifying hues) is extremely rare, even for treated-color diamonds. Treated diamonds in this color range usually have a strong purplish hue and are typically not dark enough to be graded as *red*. This stone had an uneven color distribution, with an obvious concentration at the culet (figure 2). With magnification, it displayed well-developed linear graining and a group of tiny needle-like inclusions. The diamond fluoresced strong orangy red to long-wave ultraviolet (UV) radiation and weak orangy red to short-wave UV.

Infrared absorption spectroscopy revealed features typical of type Ib diamond, with a weak but sharp absorption at 1344 cm^{-1}. The strength of this absorption was ~0.14 cm^{-1}, corresponding to a nitrogen concentration of ~5 ppm. No A- or B-form nitro-

Figure 1. This treated 0.28 ct diamond was graded Fancy red, a very rare color grade.

Figure 2. A distinct pink color zone is present at the culet of the red diamond, indicating irradiation and annealing at moderate temperatures to introduce NV centers.

gen was detected. In addition to a moderate "amber center" absorption at ~4110 cm^{-1}, irradiation-related absorptions such as H1a (1450 cm^{-1}) and H1b (4935 cm^{-1}) were present in the IR spectrum. The UV-Vis-NIR spectrum at liquid-nitrogen temperature showed strong NV absorptions at 575.0 [(NV)^0] and 637.0 [(NV)$^-$] nm and their related side bands, which were the main cause of the red color. Moderately strong absorptions at 503.1 nm (H3) and 594.3 were also detected.

These gemological and spectroscopic properties suggested a natural type Ib diamond that was originally yellow or orange with some brown component. High concentrations of

NV centers were formed by irradiation and annealing at moderate temperatures. This singular color was achieved by introducing the proper concentration of defects to suitable starting material, under ideal treatment conditions.

The NV centers, composed of one nitrogen atom and a nearby vacancy, are common point defects in diamond. These defects occur in natural diamonds and when present can induce a pleasing pink hue, but they can also be induced by laboratory treatment. Such treated stones have become much more prevalent in recent years, as exemplified by this treated-color red diamond.

Wuyi Wang

With Hydrogen Cloud and Etch Channels

Diamonds containing hydrogen clouds or etch features are fairly common (see, e.g., Lab Notes: Summer 1994, pp. 115–116; Spring 1999, pp. 42–43; Summer 1999, pp. 137–138; and Spring 2009, pp. 54–55). Hydrogen clouds in natural diamonds usually have an irregular shape, and the most common etch features associated with diamonds are trigons (see T. Lu et al., "Observation of etch channels in several natural diamonds," *Diamond and Related Materials*, Vol. 10, 2001, pp. 68–75).

Recently, the New York laboratory examined a 0.63 ct (7.98 × 7.88 × 0.76 mm) square blocked diamond with an X-shaped hydrogen cloud and narrow, hollow etch channels symmetrically located on each side of the cloud (figure 3). The stone was polished to display a clear view of the interior. The "X" pointed to the four corners of the diamond along the [100] direction, where the stone exhibited four-fold symmetry. Approximately 16 linear etch channels were present, measuring ~0.3–1.35 mm long and ~0.1–0.4 mm wide, tapering with depth. Most of the channel apertures were angular and teardrop-shaped (figure 4), indicating that they were roughly parallel to the [111] direction; etch channels following this direction tend to be elliptical. Angular patterns observed on the channels pointed to a natural origin (Summer 1994 Lab Notes, pp. 115–116), as did the radiation staining. All the channels terminated prior to reaching the cloud.

Infrared and photoluminescence spectra revealed the diamond to be hydrogen rich, and spectra collected from two regions (within and outside the cloud) revealed clear differences in H content. The cloud region showed the two fundamental absorptions for hydrogen, at 3107 and 1405 cm^{-1}, as well as H-related peaks at 3236, 3153, and 3050 cm^{-1} (W. Wang and W. Mayerson, "Symmetrical clouds in diamond—the hydrogen connection," *Journal of Gemmology*, Vol. 28, No. 3, 2002, pp. 143–152). In contrast, the region outside the hydrogen cloud had only a 3107 cm^{-1} peak with much

Figure 3. This 0.63 ct diamond has an X-shaped hydrogen cloud in its center, with symmetrical etch channels on all four sides of the cloud.

Figure 4. These etch channels display teardrop-shaped apertures, along with radiation staining and angular patterns on the body of the channel. Magnified 80×.

lower intensity, proving the cloud had a higher hydrogen content. Both regions showed a characteristic type IaA spectrum for nitrogen content. Photoluminescence spectra obtained from the cloud revealed strong H-related peaks at 693 and 700 nm, which were not seen in the cloudless region (figure 5).

The termination of the etch channels at the cloud could have resulted from chemical resistance to the etchant, or perhaps the channel met a point defect, such as an impurity, that impeded dissolution. However, as the hydrogen cloud occurred along the {100} plane and the channels followed the [111] direction, there was not suf-

Figure 5. Photoluminescence spectra for (A) the hydrogen cloud and (B) the region outside it demonstrate clear differences in H content. The spectra are normalized to show relative intensities.

PHOTOLUMINESCENCE SPECTRA
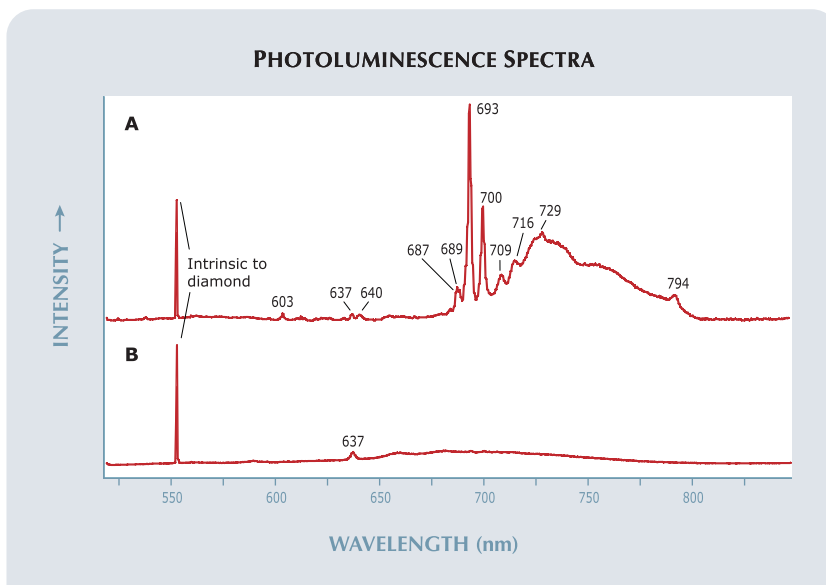
ficient evidence to prove that the hydrogen cloud disrupted etch channel formation.

Erica Emerson

Large Type Ib Yellow Diamond Colored by Isolated Nitrogen

Some natural yellow diamonds are colored by trace amounts of isolated nitrogen, which causes strong selective absorption in the blue region of the visible spectrum. Historically, these diamonds have been called "true canaries" for the purity and intensity of their color. Generally, such diamonds are small and contain clouds, fractures, or other inclusions. However, the New York laboratory recently examined a very large type Ib diamond that had some unusual features.

The 12.01 ct (18.66 × 12.38 × 8.11 mm) pear-shaped brilliant was color graded Fancy Vivid yellow and clarity graded VS2 (figure 6). It is one of the largest natural type Ib diamonds the GIA Laboratory has ever tested, and its attractive color made it especially noteworthy. The color distribution was slightly patchy when viewed with

Figure 6. This 12.01 ct Fancy Vivid yellow diamond is exceptionally large for a type Ib stone and has some unusual characteristics.

magnification. Parallel lines of surface graining from "glide planes" were easily seen with the microscope, as was a small crystal inclusion surrounded by tiny graphite flakes, but no other distinct internal features were observed. The IR absorption spectrum revealed a weak but sharp peak at 1344 cm^{-1} and a broad band at 1130 cm^{-1} from isolated nitrogen, which proved it was a type Ib diamond. After normalization, the intensity of the 1344 cm^{-1} peak was about 0.093 cm^{-1}, which corresponds to ~2.3 ppm of nitrogen. This concentration is very low compared to most natural type Ib diamonds we have tested. It is interesting to note that such a low concentration of isolated nitrogen still introduced intense yellow color. In fact, the nitrogen occurred almost exclusively in isolated form, with no A- or B-aggregated N detected; type Ib diamonds often contain some A aggregation. Gemological and spectroscopic features confirmed that the color was natural.

When exposed to the ultra-short-wave UV radiation of the Diamond-View, the stone displayed numerous

Figure 7. Numerous orange-red fluorescence lines, caused by highly localized concentrations of NV centers in the yellow diamond, are visible with the DiamondView. Field of view is 3.7 mm high.
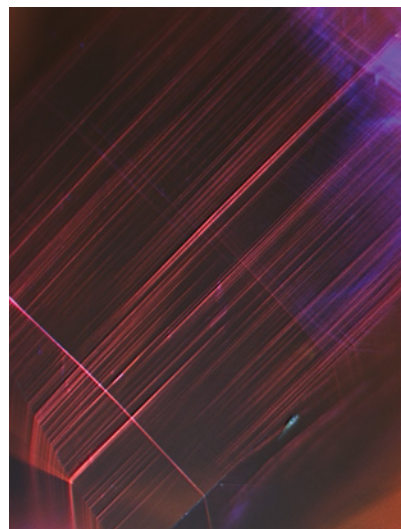
orange-red fluorescence lines and irregular blue fluorescence (figure 7). The orange-red lines were very sharp and straight, and were aligned parallel to one another within each of two perpendicular groups. The orange-red fluorescence can be attributed to relatively high concentrations of NV centers in very localized regions along the glide planes. Distortion in these regions was so localized that it could not be seen with the microscope, but vacancies released from the dislocations could have combined with preexisting isolated nitrogen to form NV centers, which produced strong emissions in the photoluminescence spectrum. Most natural type Ib diamonds show sharp green fluorescence lines due to the H3 defect, and its absence in this diamond is consistent with the absence of A-aggregated nitrogen.

Nitrogen is a common impurity in diamond, and it typically occurs in aggregated forms. It is widely accepted that nitrogen in natural diamonds is initially incorporated in isolated form, with the aggregation process following over a long period of geologic time at high temperature. However, a predominance of isolated nitrogen, as in this diamond, does not necessarily mean the host diamond is young or was crystallized and preserved at low temperature. Many other factors, such as pressure and the occurrence of other defects, can affect the nitrogen aggregation rate. A natural diamond of this size, color, and clarity, with isolated nitrogen as the main impurity, is extremely rare.

Wuyi Wang

Patterned Green Radiation Stains

Green and brown radiation stains are common features on rough diamond surfaces. They are produced when minerals or fluids containing radioactive elements remain in contact with the crystal for an extended time. Natural radioactive decay processes generate alpha particles that cause structural damage visible as green or brown spots. The radiation stains
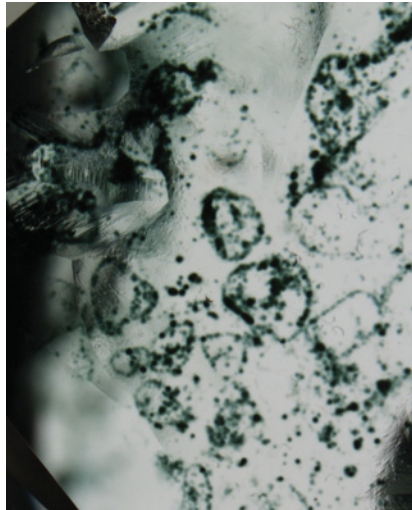
Figure 8. These green radiation stains, observed on the surface of a Fancy gray-green faceted diamond, exhibit patterns that resemble the outlines of grains that likely surrounded the stone while it was buried in an alluvial deposit (left). A DiamondView image from a different part of the same stone shows an overall blue fluorescence with inert zones corresponding to the location of the radiation stains (right). Left field of view is 3.23 mm high.

often occur with round outlines and may appear to "bleed" into the diamond from the surface. These stains are thought to be green at first, only changing to brown with relatively low-temperature heating (either while buried in the ground or from the heat of a cutting wheel).

Most radiation stains are very shallow and are typically removed during faceting. When preserved in a cut stone, they are usually seen as isolated spots on the girdle or as small zones around natural surface-reaching fractures. Recently, the Carlsbad laboratory examined a diamond with a fascinating pattern of green radiation stains (figure 8, left). The 6 ct rectangular modified brilliant was found to be type Ia using infrared absorption spectroscopy, and it was color graded Fancy gray-green. Most of the color, however, was caused by the green radiation stains on naturals and indented naturals that were not removed during faceting. The interior of the diamond appeared to be near-colorless.

Interestingly, the green stains were arranged so that several rounded shapes were outlined. The most likely expla-nation for the pattern is that the origi-nal crystal was surrounded by grains of varying sizes; the diamond was proba-bly mined from an alluvial deposit where natural weathering would have produced a mixture of rounded mineral fragments. We speculate that the boundaries of the larger grains (outlined by the stains) were more porous and so filled with radioactive fluids, whereas the unstained areas of the crystal were in contact with finer grains that were tightly packed or cemented and thus less porous.

DiamondView fluorescence imag-ing revealed another interesting fea-ture: While most of the diamond fluo-resced blue, the radiation-stained spots and outlines were inert (figure 8, right). This suggests that radiation damage might have destroyed the defects that caused the fluorescence. More work is required to fully inves-tigate this effect. While radiation stains are common on diamond, it is rare to find them preserved with pat-terns that give clues to the geologic history of the original crystal.

Christopher M. Breeding and
Virginia A. Schwartz

Pumpellyite in QUARTZ

The Carlsbad laboratory recently had the opportunity to examine a 6.64 ct polished quartz crystal from Mada-gascar (figure 9) that had an interesting inclusion scene. Initial observation showed a phantom quartz crystal defined by small clusters of a green mineral. Magnification revealed an intricate arrangement of planes of fibrous green crystal clusters punctu-ated by larger (~0.5 mm in diameter) brown crystal clusters (figure 10). These brown clusters displayed a well-developed radial structure nucleated by a central core crystal.

The client permitted us to grind down part of the sample (on lapidary equipment using diamond abrasives) until examples of both the green and brown minerals were exposed at the surface, so they could be analyzed by Raman microspectroscopy. The green mineral inclusions were identified as fuchsite, the chromium-rich variety of muscovite, which has been previ-ously identified in quartz. However, the spectral data for the brown miner-al were consistent with pumpellyite. A literature search did not reveal any prior reference to this mineral inclu-sion and host combination. To our knowledge, pumpellyite has not been previously reported as an inclusion in quartz.

Nathan Renfro

Figure 9. This striking 6.64 ct pol-ished quartz crystal proved to have some very rare inclusions.
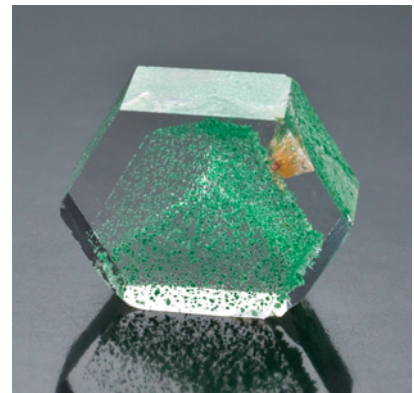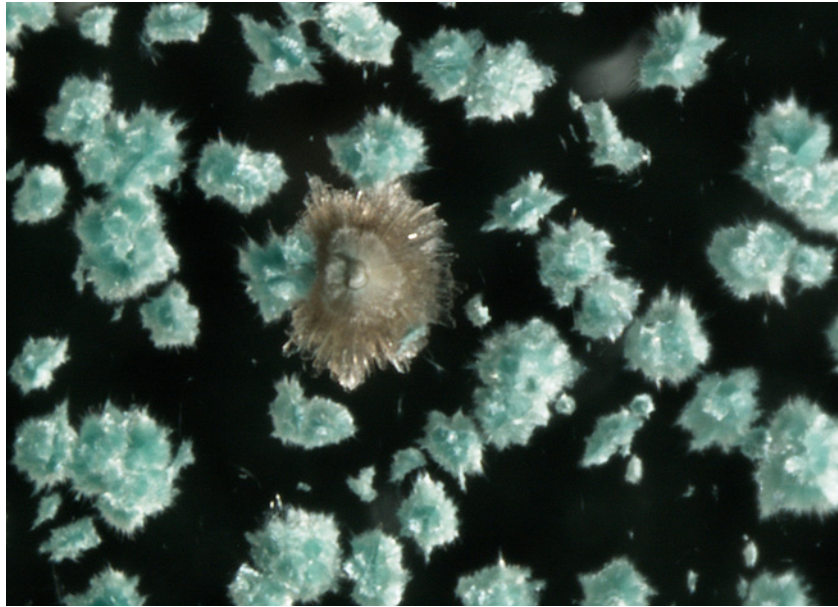
Figure 10. This brown cluster of pumpellyite crystals is surrounded by multiple clusters of green fuchsite in quartz from Madagascar. Magnified 40×.

taneous reflections indicated the crystallographic alignment of the inclusions with the ruby host, evidence that supports their identification as negative crystals.

This simple technique illustrates how light control can be used to enhance the arsenal of tools available for gemological investigation.

Nathan Renfro

"Textbook" Columbite in TOPAZ

In any gem, opaque black inclusions are generally more difficult to identify visually than inclusions of transparent, brightly colored minerals such as azurite, cinnabar, or some species of tourmaline. Colorful inclusions may be more recognizable because they tend to draw attention and may seem more interesting at the outset. At the same time, opaque black inclusions in diamonds have an adverse effect on value, a negative association that has carried over to other gem materials.

Yet some black inclusions are both

A Useful Technique to Identify Negative Crystals in RUBY

Although negative crystals in corundum are common, they are often mistakenly assumed to be crystals of a foreign material. By combining a little knowledge of crystalline materials with a useful technique for microscopic examination, we can find clues that reveal their true identity. In particular, since the host mineral's crystal structure defines the shape of these negative spaces, when several of them are clustered together their identity is often revealed by their congruent arrangement.

Recently, a very good example of this was observed in a ruby submitted to the Carlsbad laboratory for a Ruby Report (figure 11, left). To verify the inclusions in question as negative crystals, a simple tool was constructed to induce or block reflections on their internal faces by controlling their exposure to light. A small square (~one inch, or 2.5 cm) of black electrical tape was affixed to a pointer probe and inserted between the well light of the microscope and the ruby. As the tape was moved in and out of the well

to partially block the light, a uniform change in reflections throughout the numerous negative crystals was observed (figure 11, right). The simul-

Figure 11. When viewed with normal darkfield lighting (left), these negative crystals in ruby (arrows) are difficult to identify precisely. By partially blocking the light with a square of tape, the uniform change in appearance confirms their crystallographic alignment with the host. Magnified 40×.
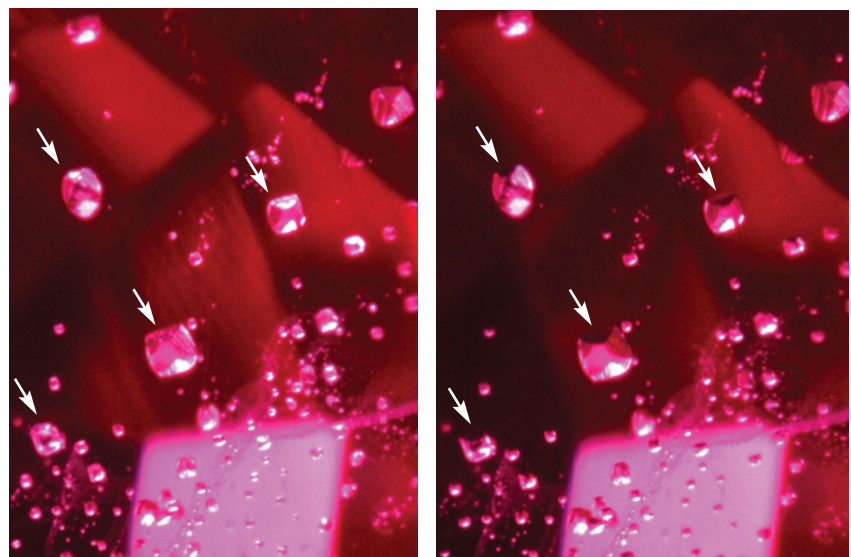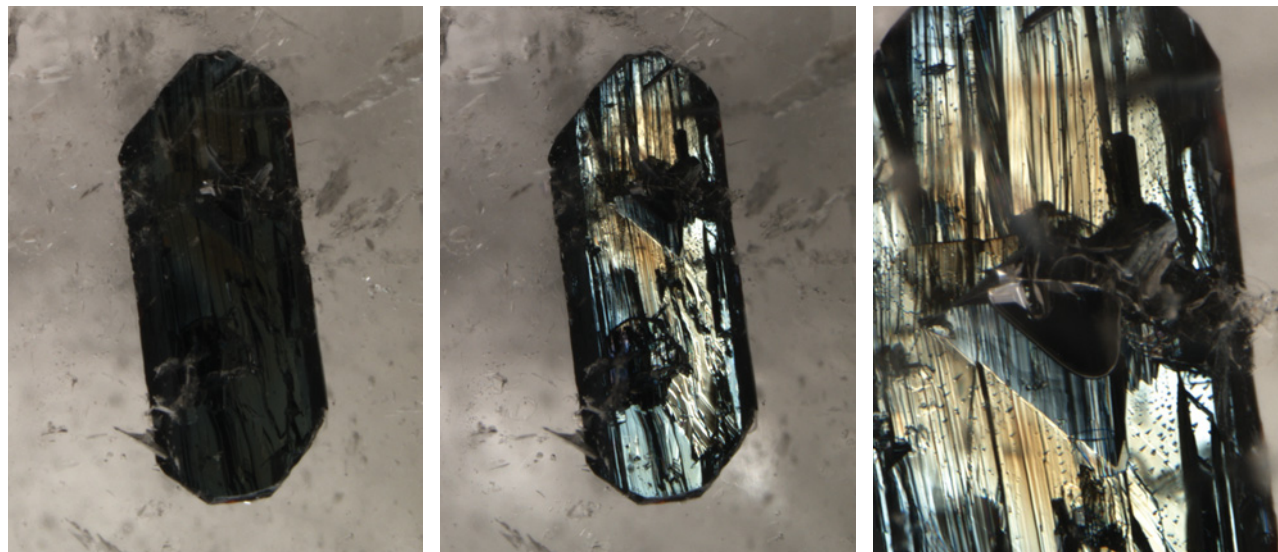
Figure 12. Showing excellent crystal form, this 2.62-mm-long doubly terminated columbite inclusion (left, darkfield illumination) was discovered in a colorless topaz from Pakistan. With incident fiber-optic illumination, an iridescent interface clearly reveals the surface texture (center) and a large primary fluid inclusion with an ~0.28 mm vapor bubble trapped between the crystal and the topaz (right).

attractive and form classic associations with their host gem mineral. Such is the case with the doubly terminated crystal in figure 12, which was discovered in a 1.6 cm terminated colorless topaz crystal from Gilgit, Pakistan. The topaz was sent to the Carlsbad laboratory by Jack Lowell (Colorado Gem & Mineral Co., Tempe, Arizona), who had obtained it from a longtime contact in Pakistan.

The most perfectly formed of two small inclusions, this 2.62 mm crystal was clearly orthorhombic and doubly terminated. It was situated near the surface of the topaz, parallel to a prism face and aligned along the c-axis of the host. In incident fiber-optic lighting, this inclusion revealed an iridescent interface (figure 12, center) that clearly displayed its surface texture. Under this lighting, it also became apparent that a relatively large primary fluid inclusion, with a vapor bubble, was trapped along the interface between the inclusion and the topaz (figure 12, right). Morphologically, this inclusion resembled columbite-(Fe) or columbite-(Mn), as its crystal habit was similar to that illustrated in V. Goldschmidt's *Atlas der Krystallformen* (Vol. 2, C. Winters, Heidelberg, Germany, 1913–1923). On a thin edge at one termination, it displayed the red-brown color typically caused by manganese, so columbite-(Mn) seemed like the logical choice.

Also observed was a much larger, 6.9 mm long, singly terminated crystal that was only partially enclosed at the base of the topaz. In general appearance, this larger crystal was virtually identical to the smaller inclusion. Raman microanalysis of this larger crystal, which was easily targeted, confirmed the visual identification of the smaller "textbook" crystal as columbite.

*John I. Koivula and
Karen M. Chadwick*

For regular updates from the world of GEMS & GEMOLOGY, visit our website at:

www.gia.edu/gemsandgemology

DIAMONDS

A greenish yellow diamond with glass filling and HPHT treatment. Diamond treatments are now routine, and stones with multiple forms of treatment have been reported. These include diamonds that have been clarity enhanced by laser drilling and glass filling (R. C. Kammerling et al., "An update on filled diamonds: Identification and durability," Fall 1994 *G&G*, pp. 142–177), and others that were color enhanced by a combination of high-pressure, high-temperature (HPHT) processing, irradiation, and/or annealing (see, e.g., Winter 2005 Lab Notes, pp. 341–343). Recently, we examined a diamond that had been subjected to both color and clarity enhancement.

The 1.02 ct greenish yellow heart-shaped brilliant mounted in a ring (figure 1) was submitted to the National

Figure 1. This 1.02 ct greenish yellow diamond proved to be both color- and clarity-treated. Photo by Zhonghua Song.

Gemstone Testing Center in Beijing for grading and identification. Preliminary visual inspection of the stone raised suspicions about the origin of its color, which appeared quite similar to that seen in HPHT-treated diamonds. In addition, the stone fluoresced a strong yellow-green to long-wave UV radiation and a weak yellow-green to short-wave UV. No phosphorescence was observed.

The Fourier-transform infrared (FTIR) spectrum showed a strong platelet-related peak (1371 cm^{-1}) and a large, saturated absorption band between 1350 and 1050 cm^{-1}, typical of type Ia diamond with a small concentration of hydrogen. The ultraviolet-visible (UV-Vis) absorption spectrum, recorded at room temperature, showed a strong N3 center, a strong broad absorption band between 450 and 500 nm, and two weak but distinct absorption lines at 503 nm (H3) and 494 nm. The Raman photoluminescence (PL) spectrum (figure 2), recorded at liquid-nitrogen temperature with a 514.5 nm laser, showed a very strong peak at 637 nm related to the $(NV)^-$ center; three moderate-intensity peaks at 575 $[(NV)^0]$, 588, and 679 nm; two weak peaks at 612 and 773 nm; and two broad peaks at 604 and 659 nm. Features such as the strong yellow-green luminescence to long-wave UV, the distinct absorption lines at 494 and 503 nm, and the strong photoluminescence peak at 637 nm proved that the stone was HPHT treated (A. T. Collins, "The colour of diamond and how it may be changed," *Journal of Gemmology*, Vol. 27, No. 6, 2001, pp. 341–359).

Microscopic examination revealed signs of additional

PHOTOLUMINESCENCE SPECTRUM
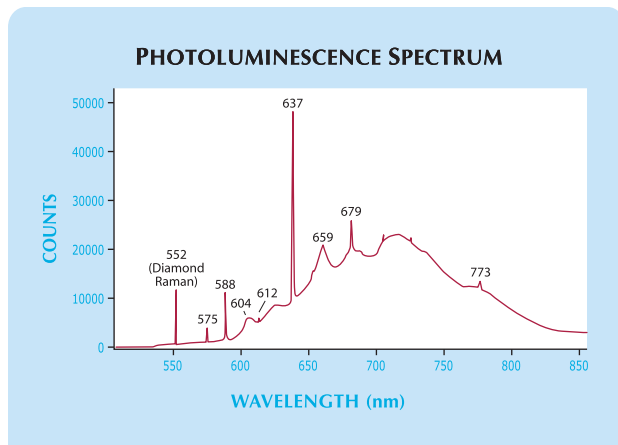
Figure 2. The 637 nm peak in the Raman PL spectrum of the diamond was one feature that indicated HPHT treatment.

treatment. Two large fractures displayed flash-effect colors typically associated with glass filling (figure 3). In darkfield illumination, distinct purple and green flashes were visible in one fracture, and subtle purple flashes were seen in another. Usually, one predominant color (violet, purple, or pink) was noted, though sometimes we saw a flash that was simultaneously purple and green. No distinct flow structure or trapped bubbles were visible. Because the diamond was mounted, we could not test for the presence of Pb that would be expected in the glass filling.

Based on these results, we concluded that the diamond was both color enhanced by HPHT processing and clarity treated by glass filling. Since glass fillers are unstable at high temperature (see Kammerling et al., 1994), the diamond likely underwent color enhancement first.

<div align="right">
Zhonghua Song (songzhh@ngtc.gov.cn),
Jun Su, and Taijin Lu
National Gemstone Testing Center (NGTC), Beijing
</div>

Figure 3. Purple and green flash-effect colors can be seen in this filled fracture in the greenish yellow diamond. Photomicrograph by Zhonghua Song; magnified 32×.
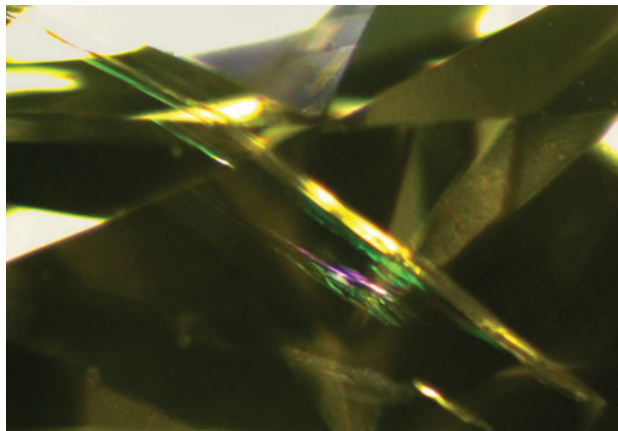
Figure 4. This aquamarine crystal (80.9 mm long), reportedly from Pakistan, proved to have an interesting inclusion scene. Photo by Jian Xin (Jae) Liao.

COLORED STONES AND ORGANIC MATERIALS

Aquamarine with ocean-themed inclusions. Recently, this contributor had the opportunity to examine an unusual aquamarine crystal (figure 4), reportedly from Pakistan, that was brought to our attention by Jordan Bogel, a gem collector from Oregon. The specimen, 80.9 mm long and 140.8 g, was readily identifiable as aquamarine from its color and crystal structure, though this was confirmed by standard gemological testing.

The crystal displayed an interesting growth pattern along one of its faces, but the most striking feature of this aquamarine was its inclusion scene, which gave the impression of exploring the ocean's depths. Transmitted light revealed "fingerprints" composed mostly of two-phase inclusions. The image of an irregular ocean floor was evoked by yellowish green moss-like inclusions, close to the crystal's surface, which resembled seaweed at higher magnification (figure 5). Despite several attempts to identify these inclusions, they proved too thin for Raman microanalysis.
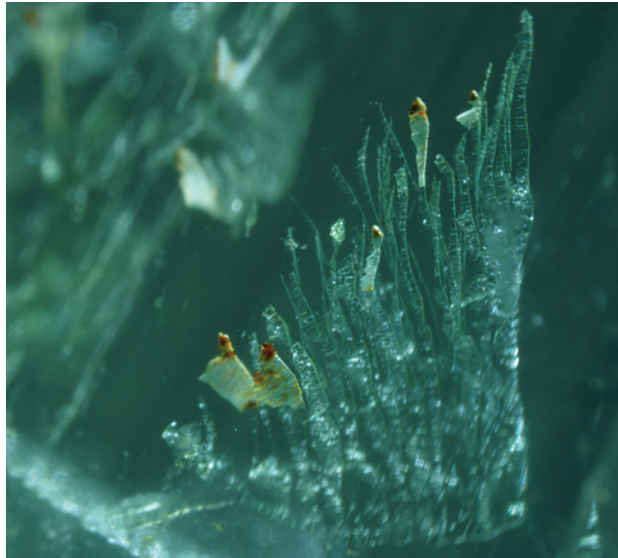
Figure 5. Seaweed-like forms contributed to the oceanic scene in the aquamarine crystal. Photomicrograph by R. Befi; image width 3.0 mm.

Figure 6. This striking stingray-shaped inclusion in the aquamarine crystal proved to be a zircon that is partially surrounded by a tension fracture. Photomicrograph by R. Befi; image width 2.3 mm.

Small crystals visible in different areas of the aquamarine resembled stingrays composed of tapered crystals partially surrounded by tension fractures (see, e.g., figure 6). One "stingray" was exposed at the surface, and the crystal was identified as zircon by Raman spectroscopy. Zircon inclusions have been previously documented in aquamarine from Pakistan (E. J. Gübelin and J. I. Koivula, *Photoatlas of Inclusions in Gemstones*, Vol. 2, Opinio Publishers, Basel, Switzerland, 2005, p. 322), but we could find no report of zircon inclusions with this unusual morphology.

No other name is better suited to this ocean-themed crystal than *aquamarine*.

Riccardo Befi (riccardo.befi@gia.edu)
GIA Laboratory, New York

"Smoky" gray beryl. Recently, the Gem Testing Laboratory in Jaipur, India, examined the 71.57 ct step-cut stone in figure 7. It had a gray color with moderate saturation and slightly brownish gray reflections near the corners, which were stronger in one corner than the other three. When the stone was tilted in standard lighting against a white background, subtle zones of pale brown color were observed at some angles.

The color appearance and brown zones were reminiscent of smoky quartz. However, although the specimen displayed a uniaxial optic figure, it did not show the characteristic "bull's-eye" pattern of quartz. This did not rule out quartz, but it did raise sufficient doubt to warrant further testing. The results were surprising: The refractive indices were 1.590–1.598, with birefringence of 0.008, values that are consistent with beryl. Although beryl occurs in a variety of colors—green, blue, red, pink, yellow, orange, brown, and colorless are all known—gray is quite unusual.

The stone had a hydrostatic SG of 2.81, which is high for aquamarine but low for pink beryl (e.g., 2.66–2.80 and 2.80–2.90, respectively; see M. O'Donoghue, Ed., *Gems*, 6th ed., Butterworth-Heinemann, Oxford, UK, 2006, pp. 163–164). No absorption features were visible with the desk-model spectroscope, and the sample was inert to long- and short-wave UV radiation. It displayed weak gray and pinkish brown dichroism (figure 8). No features were observed with the microscope, other than some angular and planar growth zones. The presence of these growth zones indicated the stone was natural.

FTIR spectra were typical for natural beryl, while qualitative energy-dispersive X-ray fluorescence (EDXRF) analysis revealed the presence of Al, Si (major), Ca, Mn, Fe (trace),

Figure 7. This beryl specimen (32.90 × 20.52 × 12.14 mm) is unusual for its gray color. Photo by G. Choudhary.
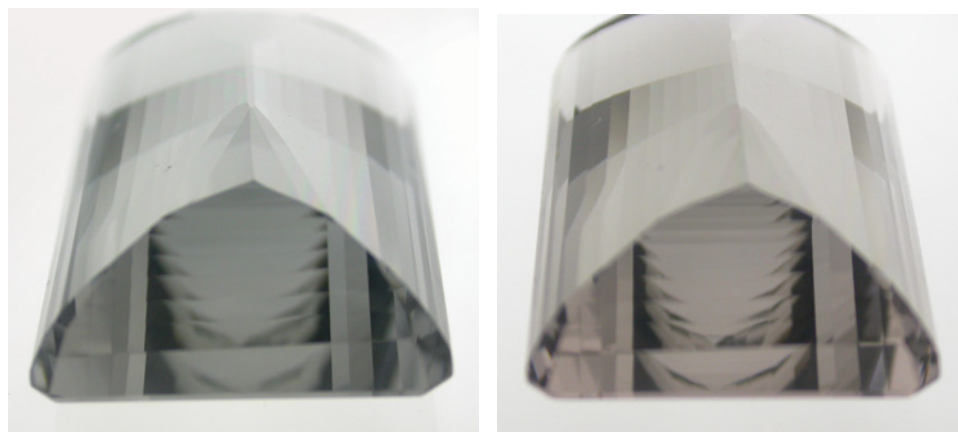
Figure 8. The beryl displays weak dichroism; the gray component (left) turns pinkish brown (right) when the polarizing filter is rotated 90°. Photos by G. Choudhary.

and Cs (minor). The presence of Cs would explain the relatively high specific gravity compared to aquamarine.

The cause of color in this unusual specimen remains unknown. John Sinkankas's *Emerald and Other Beryls* (Chilton Book Co., Radnor, Pennsylvania, 1981) noted that a beryl that had been previously heated in oxidizing conditions turned deep gray when subsequently heated in reducing conditions, although the cause of color was not determined.

Gagan Choudhary (gtl@gjepcindia.com)
Gem Testing Laboratory, Jaipur, India

Chalcedony from Oregon with pyrite and cloud-like green areas. In June 2008, Steve Perry (Steve Perry Gems, Davis, California) informed GIA about an attractive green gem material from Oregon. He believed that it consisted of a mixture of gray chalcedony with green uvarovite and pyrite or marcasite. It was sold to him as "old material" from the Applegate Valley in Jackson County, southern Oregon. From a small parcel of rough, Mr. Perry has cut about two dozen cabochons, ranging from 0.54 to 13.38 ct.

The following properties were determined on four cabochons (2.31–13.38 ct; see, e.g., figure 9) that Mr. Perry loaned to GIA: color—variegated green and dark gray; spot RI—1.54 (from both green and gray areas); hydrostatic SG—2.70–2.80; Chelsea filter reaction—none; and fluorescence—inert to long- and short-wave UV radiation. These properties are generally consistent with those reported for chalcedony by M. O'Donoghue, Ed. (*Gems*, 6th ed., Butterworth-Heinemann, Oxford, UK, 2006, pp. 306–307), except for the lower SG values reported by that source (2.57–2.64). Two absorption lines, at ~680 and ~690 nm, which are related to the presence of chromium, were visible with the desk-model spectroscope.

The chalcedony contained discrete areas of cloud-like bright yellowish green to green material, as well as surface-reaching metallic "golden" yellow crystals that appeared to be pyrite (figure 10), but no other significant inclusions. Raman spectroscopy confirmed the metallic yellow inclusions as pyrite, but no Raman signals other than those of chalcedony were detected from the green clouds, which suggests they are probably not in a crystalline form. Laser

ablation–inductively coupled plasma–mass spectrometry (LA-ICP-MS) analysis of the surface-reaching green areas showed Si, Na, Mg, Al, and Cr as the main components. This composition is not consistent with uvarovite, and the identity of the green material remains unknown.

This is the first time that we have encountered chalcedony with this combination of inclusions.

Wai L. Win (wwin@gia.edu)
GIA Laboratory, New York

Figure 9. These attractive chalcedony samples (2.31–6.01 ct) are reportedly from southern Oregon. Photo by Robert Weldon.
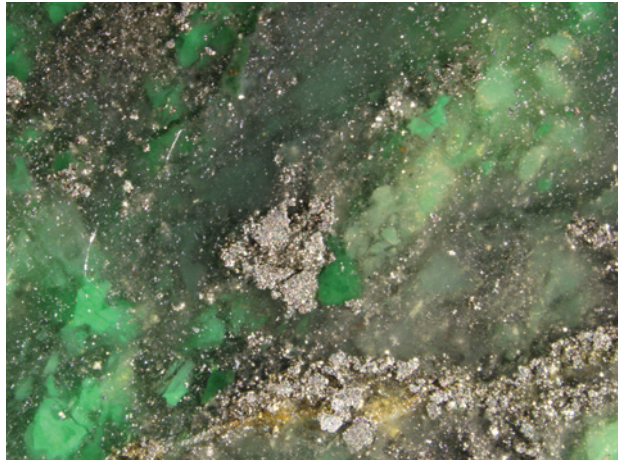
Figure 10. Microscopic examination of the cabochons revealed patches of pyrite and massive green cloud-like areas, while the host chalcedony appeared light gray. Photomicrograph by W. L. Win; field of view 5.2 mm.

Demantoid from Ambanja, Madagascar. In mid-2008, crab fishermen in northern Madagascar reportedly found some green stones in a mangrove swamp. These were brought to Antananarivo, where they were identified as demantoid. Eventually, sapphire diggers from Ambondromifehy heard the news and started to work the area. Beginning in April 2009, rumors of a new find of expensive green "sapphire" spread from cell phone to cell phone, and several hundred miners, buyers, and brokers—both Malagasy and foreign—rushed to the site (figure 11). As of late May 2009, when this contributor initially visited the deposit, about 2,000 miners were digging and 5,000–10,000 people were living in the nearby village of Antetezambato. The deposit is

Figure 11. Thousands of miners have descended on a new demantoid deposit that was found in mid-2008 in a mangrove swamp near Ambanja in northern Madagascar. Photo by F. Danet.

located 22 km northeast of Ambanja, and the eastern border of the main workings has coordinates 13°30.426′ S, 048°32.553′ E.

Using hand tools (crowbars, buckets, etc.), the miners dig pits 6–11 m deep in the mangrove swamp at low tide. Pumps and dikes are employed by some miners to keep the pits from flooding, while others have explored the dry land adjacent to the swamp. The deposit measures ~500 × 500 m, and observations by this contributor suggest that the demantoid is hosted by an altered whitish skarn layer, surrounded by clays and crystalline rocks. The crystals are found lining fractures or cavities (of decimeter dimensions). The host rock can be quite hard, although it is typically completely weathered. According to the miners, some pockets have yielded a half-bucket of crystals.

The demantoid crystals are sharp and lustrous, and some faces are striated. They form truncated rhombododecahedrons or trapezohedrons (e.g., figure 12), ranging up to 25 mm. Their green hue commonly has a blue or yellow component in day or fluorescent light; the latter stones appear "olive" green in incandescent light. Also recovered are yellow and brown andradite crystals, with gem-quality areas weighing up to 2 g. Quartz is associated with the garnet, and consists of thin opaque crystals up to 4 cm long. Many other minerals were seen in the Antetezambato market, but the dealers may have brought them from other deposits in northern Madagascar.

This contributor examined 16 pieces of rough demantoid (23.6 g total weight; again, see figure 12) weighing up to 3.1 g, with the largest clean stone weighing 1.2 g. The following properties were recorded: RI—over the limits of the standard refractometer; hydrostatic SG (five stones)—3.79–3.88 (the lower measurements were due to abundant impurities); strong anomalous birefringence in the polariscope; and spectroscope spectrum—cutoff in the blue region, diffuse bands at 621 and 640 nm, but no lines in the

Figure 12. The Madagascar demantoid is recovered as well-formed crystals. The largest shown here weighs 3.1 g and measures 16.5 × 12.3 × 8.6 mm. Photo by F. Danet.

red region (i.e., those due to Cr at 693 or 701 nm). Microscopic examination revealed fractures and fingerprint-like inclusions, as well as a few isometric crystals. Although no "horsetails" were seen in these samples, this contributor has noted some curved acicular inclusions in a few stones examined subsequently.

While it is difficult to estimate the production, this contributor suspects that at least 20 kg of mine-run demantoid is recovered each week (probably much more), with several kilograms in the 1–3 g range. Larger sizes are rare, as are eye-clean stones weighing >1 g. About 5% of the material is facetable. Initial cutting of the demantoid has yielded some attractive stones weighing 1–3+ ct, while more-included gems range up to 7 ct. Eye-clean stones of good "emerald" green color are scarce above 2 ct, while those with "olive" green coloration are more frequently seen in the 2–5 ct range.

This demantoid discovery has created a great deal of excitement in Madagascar, and gem buyers and brokers are at least as numerous as the miners at the deposit. In mid-June, for security reasons, the provincial government prohibited buyers from visiting the deposit and mandated that all trading take place at a nearby "comptoir," as was done at the well-known Ilakaka gem deposit in 1999.

Additional images to accompany this report are available in the *G&G* Data Depository at www.gia.edu/gandg. Chemical analyses of the Madagascar demantoid, as well as additional gemological data, are available online at www.gemnantes.fr/recherche/autre/demantoide_mada.php.

Fabrice Danet (fabdanet@moov.mg)
Style Gems, Antsirabe, Madagascar

Enstatite from Pakistan. At the 2009 Tucson gem shows, Syed Iftikhar Hussain (Syed Trading Co., Peshawar, Pakistan) displayed a parcel of small, dark yellow-green crystals and broken fragments that he had obtained as "diopside or garnet" from Baluchistan, Pakistan, in 2007. The parcel weighed 105 g, and a few of the pieces were transparent enough to facet. Mr. Hussain donated several rough samples to GIA for examination.

Initial analysis of the samples with Raman spectroscopy identified them as enstatite. Enstatite is an orthorhombic pyroxene with an end-member composition of $MgSiO_3$ that forms a solid-solution series with ferrosilite ($FeSiO_3$). It ranges from colorless to yellow, green, or brown; these various colorations are associated with the presence of chromophores such as Cr, Mn, V, and Fe. Iron-bearing enstatite has often been referred to as *hypersthene*, though the International Mineralogical Association now simply classifies it as enstatite.

Enstatite has a Mohs hardness of 5–6, and it is quite brittle and considered difficult to facet (J. Sinkankas, "Some freaks and rarities among gemstones," Fall 1955 *G&G*, pp. 199–200). GIA had three of the pieces donated by Mr. Hussain faceted (0.42–1.29 ct; e.g., figure 13) for further examination, and the following properties were recorded: color—dark yellow-green, RI—1.665–1.675 from the table
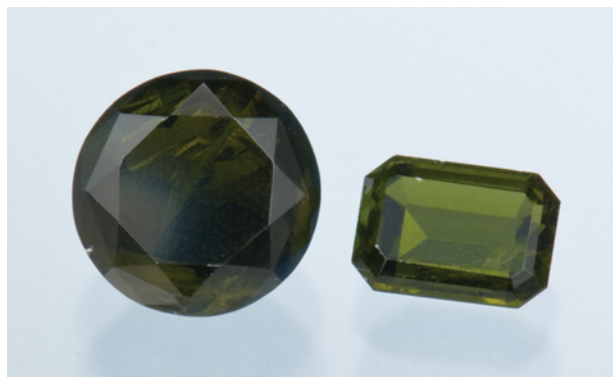
Figure 13. These dark yellow-green gems (0.42 and 1.29 ct) from Baluchistan, Pakistan, were identified as enstatite. Photo by Robert Weldon.

face (and a higher value of 1.730 from the pavilion of one stone), birefringence—0.010, hydrostatic SG—3.31, and no UV fluorescence. The desk-model spectroscope showed a strong and sharp absorption line at 505 nm and a broad band near 550 nm. These properties are consistent with those reported for enstatite (M. O'Donoghue, Ed., *Gems*, 6th ed., Butterworth-Heinemann, Oxford, UK, 2006, p. 408). Microscopic observations revealed typical fractures and "fingerprints" (see the *G&G* Data Depository).

Visible-range spectroscopy showed a sharp peak at 505.8 nm and a broad band centered at 548 nm (see the *G&G* Data Depository), which correlate well with the absorptions seen with the spectroscope. A weak feature near 680 nm was also present, due to Cr^{3+}. Some similar features have been observed with the spectroscope in dark green enstatite from Arizona and in medium green enstatite from East Africa (G. R. Crowningshield, "Enstenite!" [sic], Fall 1965 *G&G*, pp. 334–335; C. M. Stockton and D. V. Manson, "Peridot from Tanzania," Summer 1983 *G&G*, pp. 103–107).

Chemical analysis of one of the cut samples by LA-ICP-MS indicated a composition of $(Mg_{0.79}Fe_{0.17}Ca_{0.04})SiO_3$, along with trace amounts of Cr and Mn. The Fe concentration is relatively high for gem-quality enstatite, with a ratio of Fe/(Mg+Fe) = 0.18—compared to a ratio of 0.12 for the East African sample documented by Stockton and Manson (1983)—and is apparently responsible for the material's dark tone.

The highest RI value of 1.730 is significantly higher than that of typical magnesium end-member enstatite, which has RIs ranging from 1.649 to 1.680, and is consistent with the appreciable iron measured in the chemical analysis. By comparison, RI values for iron end-member ferrosilite range from 1.755 to 1.788 (J. W. Anthony et al., *Handbook of Mineralogy*, Vol. 2—Silica, Silicates, Part 1, Mineral Data Publishing, Tucson, Arizona, 1990, p. 255). The high transparency and yellow-green color of this iron-bearing enstatite are quite unlike the "hypersthene" documented in the Summer 2003 GNI section (pp. 160–161).

Ren Lu (ren.lu@gia.edu) and Chandana Samararatne
GIA Laboratory, New York
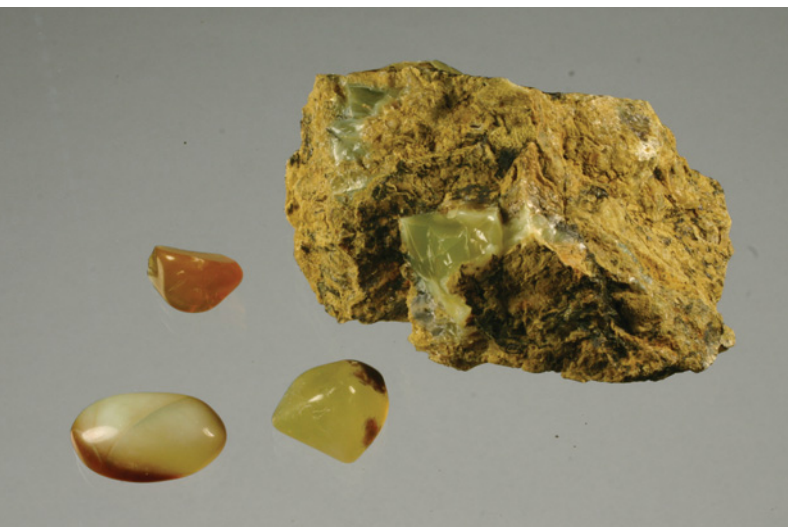
Figure 14. This new opal-CT comes from Argentina. The largest polished stone weighs 16.6 ct. Photo by B. Rondeau.

Figure 15. This spherulitic inclusion in a greenish yellow Argentine opal seems to have absorbed the iron staining around it. The inclusion consists of quartz and iron compounds. Photomicrograph by E. Fritsch; magnified 16×.

Common opal from Argentina. At the 2009 Tucson gem shows, Jorge Raul Dascal (Patagonia Minerals, Buenos Aires) displayed some new common opal from Argentina. The material was opaque to transparent, and ranged from yellow-green to orange (approximating fire opal) to brown (e.g., figure 14). The color and transparency were often layered.

We measured RI and SG values on three polished samples representing a range of typical color and transparency (again, see figure 14). The RIs were 1.440–1.445, and SG values were 2.02–2.04. Out of six pieces tested for UV fluorescence, four were inert. However, the two chalkiest samples fluoresced very weak whitish green to long-wave UV radiation and even weaker to short-wave UV, with no phosphorescence. Raman analysis of the three polished samples using a Bruker RFS100 Fourier-transform spectrometer confirmed that the material was opal-CT, with an apparent maximum for the main peak ranging from 345 to 325 cm^{-1}. Chemical analyses of three pieces performed on a JEOL 5800LV scanning electron microscope (SEM) equipped with a Princeton Gamma Tech energy-dispersive IMIX-PTS detector determined that the material was essentially SiO_2 with traces of Al in two stones (0.05 and 0.25 wt.%) and Fe in all three (0.30–2.5 wt.%). The Fe content qualitatively correlated with the greenish yellow to brown component of the color.

Four of the six samples showed breadcrumb-like inclusions that appeared white in reflected light. Larger inclusions with similar texture sometimes had a disc-like or spherulitic appearance. One such inclusion in a dark brown zone was surrounded by a lighter rim (figure 15). SEM microchemical analysis of the inclusion revealed major amounts of Si and O (with at least some of these elements contributed by the surrounding opal), as well as ~5 wt.% Fe and ~2 wt.% Al—both more concentrated in the core—and traces of Mg, Ca, and Mn. A Raman spectrum of the inclu-

sion obtained with a Jobin-Yvon T64000 dispersive spectrometer showed a series of weak bands at about 690, 550, 394, and 301 cm^{-1}, as well as a sharper band at about 463 cm^{-1}. These were consistent with a mixture of quartz and an iron oxide or hydroxide, possibly hematite or goethite. As in other common opals, the yellow-to-brown bodycolor of the Argentine samples is likely related to submicroscopic-to-nanometric Fe-bearing inclusions.
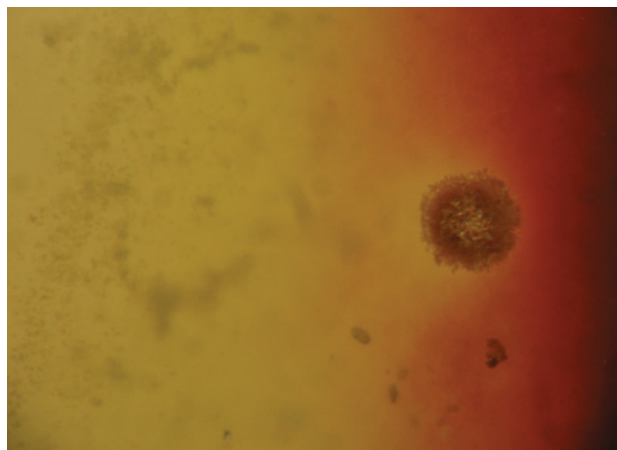
Figure 16. These cabochons of opal from Argentina (4.26–8.06 ct) illustrate some of the colors that have been recovered from the new deposit. Photo by Robert Weldon; GIA Collection nos. 37967–37969.

The opal structure was investigated on freshly broken surfaces of three yellow-green and orange samples using a JEOL 6400 field-effect SEM. It consisted of coalesced nanograins 20–45 nm in apparent diameter, as is typical for common opal-CT from many localities worldwide.

The Argentine opal deposit was found in some remote undisclosed foothills in late December 2008. The opal was first discovered as loose gravel in dry riverbeds, which was traced several kilometers upstream to veins in a very hard volcanic rock. The matrix of some of the specimens was quite altered, and was apparently rich in silica and clays. Because of the cold, arid climate, the deposit can only be worked five or six months of the year. In April 2009, Mr. Dascal reported finding some yellow-green opal in the same area. By that time, he had collected a total of ~140 kg of gem-quality material, and 11 kg was being tumbled in pieces ranging up to ~10 × 7 × 7 cm. In addition, a few cabochons of the opal had been cut (e.g., figure 16).

Emmanuel Fritsch
Yves Lulzac
Centre de Recherches Gemmologiques, Nantes, France

Benjamin Rondeau
CNRS, Team 6112, Laboratoire de Planétologie et Géodynamique
University of Nantes, France

Mabe pearls from Vietnam with seashell nuclei. At the 2009 Tucson gem shows, VanTuyen Tran (Ferjenni Co., Fullerton, California) showed this contributor some recently harvested mabe (assembled cultured blister) pearls from Vietnam that were produced using seashell nuclei. Although they debuted at the 2008 Tucson gem shows, the 2009 material (from the company's second harvest) included a wider range of shapes and better nacre coverage. Ms. Tran reported that she came up with the concept, and then collaborated with a pearl farm in Vietnam owned by Cuc Nguyen (Boi Ngoc Co. Ltd., located near Ben Tre). The several varieties of shells used as nuclei were gathered from beaches in the Indo-Pacific region. For the most recent harvest, they were implanted into 9,000 *Pteria penguin* oysters in April–May 2008, and in January 2009 they obtained 625 high-quality mabe pearls. The relatively low yield resulted from incomplete nacre coverage on many of the shell nuclei and the fact that 15% of the oysters died after implantation.

After harvesting, the mabes were cleaned and polished, then trimmed to remove excess shell material (e.g., figure 17). Mabes up to ~5 cm long have been produced, but most range from 2 to 4 cm. Some of those from the first harvest—which had thinner nacre—were polished to reveal the color of the underlying shell nucleus (see the two cowrie mabes on the far right in figure 17). Even for those that were completely covered with nacre, the surface textures of the underlying seashell nuclei were remarkably evident (figure 18). Marketed as *mabe shell pearls*, some have been set into pendants and earrings (figure 19).

Brendan M. Laurs

Figure 17. *These Vietnamese mabe pearls, which came from the first harvest, were produced using seashell nuclei consisting of coiled gastropods (left, 3.4–4.1 cm long) and cowries (right). Some of the nacre on the cowrie mabes has been polished off to expose the underlying shell colors. The inset shows the shell nucleus within an unbacked mabe pearl. Photo by Robert Weldon.*

Characterization of some pearls of the Pinnidae family. Pearls of the Pinnidae family (classified by Leach, 1819) are produced by bivalves belonging to the genera *Pinna* (Linnaeus, 1758) and *Atrina* (Gray, 1847), and are known as "pen shell" pearls. Pinnidae bivalves are widely distributed in the Mediterranean Sea as well as the Red Sea, the Indo-Pacific Ocean (including the region circumscribed by southeastern Africa, Melanesia, New Zealand, Australia, and northern Japan), and in American waters (e.g., the Pacific coast of Baja California, Mexico). Those found in the

Figure 18. *A diversity of forms and textures is shown by these large Vietnamese mabes (3.8–5.1 cm in maximum dimension), which were produced from the second harvest. Photo by Robert Weldon.*
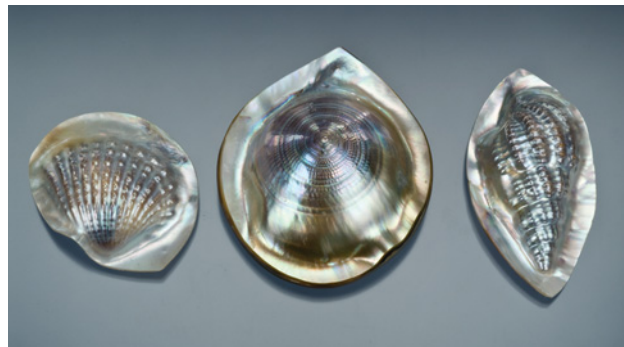
Figure 19. Vietnamese mabe pearls are featured in these earrings (2.2 cm long) and a pendant with amethyst (3.4 cm long) that were manufactured by Randall Otten, Otten, Vallot & Co., Huntington Beach, California. Photo by Robert Weldon.

Figure 20. This collection of nacreous and non-nacreous Pinnidae family pearls shows various colors and shapes. The largest specimen is 13.7 mm in diameter (10.42 ct). Courtesy of the Gübelin Gem Lab; photo by Eric Erel.

Mediterranean and Red Sea have probably reached the highest popularity after pearls from *Pinctada* species (E. Strack, *Pearls*, Rühle-Diebener-Verlag, Stuttgart, Germany, 2006). Pen shell pearls commonly attain sizes of 7 mm (rarely up to 16 mm), and can range from grayish white to various shades of orange and brown as well as black. Both nacreous and non-nacreous varieties exist (e.g., figure 20); the nacreous Pinnidae pearls are aragonitic.

Several years ago, one of the authors (J-PG) collected some nacreous and non-nacreous pearls from *Pinna* mol-

lusks harvested from the bays of Hyères (Var, France), Sagone (Corsica, France), and Olbia (Sardinia, Italy). Some of these were orange, and they included near-round and teardrop shapes (figure 21). Microscopic observation revealed that they were translucent in transmitted light and had columnar structures (figure 22). Similar patterns were seen in non-nacreous pearls described in the Fall 2007 GNI section (pp. 259–260). As was the case for the pearls described in that entry, the columnar structures in the present samples were typically due to a radial arrangement of

Figure 22. Columnar calcitic structures were observed with transmitted illumination in this pen shell pearl. Photomicrograph by S. Karampelas; image height 1 mm.

Figure 21. These five non-nacreous pen shell pearls are also from Pinnidae family mollusks. The smallest pearl is about 3.2 mm in diameter (0.39 ct), and the largest is 16.4 mm long (2.17 ct). Photo by S. Karampelas.
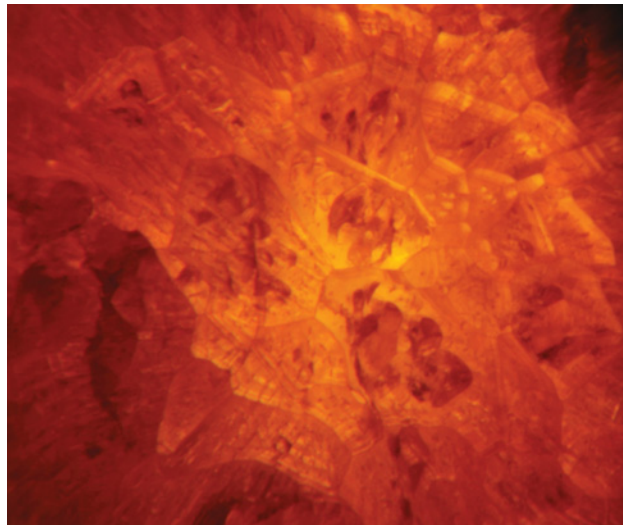
calcite. One of the teardrop-shaped pearls had no visible structures in the bulbous part but displayed columnar structures in the tail. Raman spectroscopy revealed that the bulb consisted of aragonite and the tail was composed of calcite.

Raman spectroscopy of the samples in figure 21, using five different excitation wavelengths, also showed that they contained a mixture of carotenoid pigments. Similar pigments have been observed in *Stylaster* gem corals (S. Karampelas et al., "Identification of the endangered pink-to-red *Stylaster* corals by Raman spectroscopy," Spring 2009 *G&G*, pp. 48–52).

UV-Vis-NIR reflectance spectra of Pinnidae pearls showing gray, orange, brown, and black coloration (in various combinations of hue, tone, and saturation) revealed a gradual absorption continuum from the UV to the NIR region. This continuum is responsible for the gray (less intense) to black (more intense) coloration. Further, carotenoid pigments absorb in the violet-blue portion of the spectrum and are responsible for the orange hue. To our knowledge, Pinnidae pearls are the only gem-quality natural pearls that can consist of calcite and contain carotenoid pigments.

Stefanos Karampelas (s.karampelas@gubelingemlab.ch)
Gübelin Gem Lab, Lucerne, Switzerland

Jean-Pierre Gauthier
Centre de Recherches Gemmologiques, Nantes, France

Emmanuel Fritsch

Franck Notari

Cat's-eye phenakite. In May 2009, a prismatic crystal of phenakite was mined from central Madagascar (probably Anjanabonoina) and subsequently cut into three cabochons that showed chatoyancy (7.03, 8.98, and 50.36 ct; e.g., figure 23). Since cat's-eye phenakite is not well known, the following properties were documented on these three stones: color—light brownish yellow; dichroism—moderate; RI—1.654–1.670; birefringence—0.016; optic character—uniaxial positive; hydrostatic SG (two measurements)—2.96; and no absorption features seen with the handheld spectroscope. These properties are consistent with those reported for phenakite by M. O'Donoghue, Ed. (*Gems*, 6th ed., Butterworth-Heinemann, Oxford, UK, 2006, pp. 436–437), who also mentioned that "the occasional chatoyant specimen is reported."

The stones contained fine needles (probably very thin empty tubes) oriented perpendicular to the c-axis, which were responsible for the unusual chatoyancy exhibited by this material. No other inclusions were seen in the stones with the microscope.

Fabrice Danet

Color-change pyrope-spessartine from Kenya. Color-change pyrope-spessartine has been reported from East Africa, Sri Lanka, and more recently Madagascar (see D. V. Manson and C. M. Stockton, "Pyrope-spessartine garnets with unusual color behavior," Winter 1984 *G&G*, pp. 200–207;

Figure 23. This unusual phenakite from Madagascar (50.36 ct) exhibits chatoyancy. Photo by F. Danet.

Summer 1998 GNI, p. 138; K. Schmetzer and H.-J. Bernhardt, "Garnets from Madagascar with a color change of blue-green to purple," Winter 1999 *G&G*, pp. 196–201).

A new deposit of color-change garnet, in Kenya, was recently reported to GIA by Amarjit Saini (Mobu Gems, Los Angeles). According to his partner, Peter C. L. Pereira (Isle of Gems, Arusha, Tanzania), the garnet is found in the Taita Hills, at a village called Kamtonga, which is close to the Mwatate tsavorite mining area. This region typically produces brown-to-red material, but some remarkable green/red color-change garnet was found in January 2009. Most of the rough weighs <1.5 g, yielding cut stones <2 ct, although some attractive clean gems with a good color change that range up to 8–10 ct are known to both gentlemen. Production has been intermittent due to disputes over mining claims in the area.

Mr. Saini donated two color-change garnets from this deposit to the GIA Collection. The 1.32 and 1.39 ct stones were fashioned as rectangular and square cut-cornered step cuts, respectively. Their coloration was observed in a Gretag Macbeth Judge II light box under both daylight-equivalent and incandescent illumination. Their color changed from dark bluish green to dark violet, and from grayish bluish violet to purple, respectively (figure 24). The garnets appeared more blue under other nonstandard "daylight-equivalent" fluorescent light sources. No significant color variation between reflected and transmitted light was observed.

Gemological examination revealed the following properties (with those for the smaller stone indicated first): RI—1.762 and 1.765; SG—3.88 and 3.91; fluorescence—inert to both long- and short-wave UV radiation; Chelsea filter reaction—moderate red; and absorption bands at ~485, 505, and 575 nm with the desk-model spectroscope. Magnification revealed oriented, fine reflective needles (figure 25), as previously observed in color-change garnets from East Africa and Madagascar (Summer 1998 GNI; Schmetzer and Bernhardt, 1999). Vis-NIR spectroscopy (figure 26) confirmed two distinct areas of transmission in

Figure 24. These garnets (1.32 and 1.39 ct) are from a new deposit in Kenya. The stone on the left displays a stronger color change. Photos by Robert Weldon; daylight-equivalent light (left), incandescent light (right); GIA Collection nos. 37962 and 37963.

the visible range that are characteristic of color-change gems, one centered at ~475 nm (blue range) and the other above 650 nm (red region). Distinct absorption features were present at 486, 505, and 577 nm, with very weak features centered at 464, 524, and 688 nm.

LA-ICP-MS analysis revealed Mg and Mn, indicating a pyrope-spessartine mixture; the gemological properties were more consistent with the spessartine end member. The presence of small amounts of Fe and Ca confirmed small almandine and grossular components, respectively. Color-causing agents included Fe (average 12,000 ppm), V (4300 ppm), and Cr (500 ppm).

Donna Beaton (donna.beaton@gia.edu)
GIA Laboratory, New York

Preliminary observations on new rubies from Mozambique. GIA recently examined two groups of transparent faceted rubies that were represented as coming from new localities in Mozambique. The first group of five rubies

(2.03–2.73 ct; e.g., figure 27, left) was brought to us in May 2009 by J. Blue Sheppard of Millennium Inc., Pala, California. These were represented to Mr. Sheppard as being from "Lusingha," and having been heated to "drive-out the silk." The locality was subsequently identified as the Lichinga area, near the village of Msawizi (or M'sawize), in Mavango District, Niassa Province, north-central Mozambique. The second group of 19 rubies (0.70–4.62 ct; e.g., figure 27, right) was supplied in July 2009 by Tommy Wu of Shire Trading Ltd., Hong Kong. These stones were reportedly unheated, and consisted of a mixture of those from Lichinga and a newer mine reported to be in the Montepuez area of Cabo Delgado Province, ~225 km north of Nampula in northeastern Mozambique.

GIA examined all 24 rubies by standard gemological methods and EDXRF spectroscopy. The stones from both localities were similar in visual appearance as well as gemological properties. Their color was primarily red to

Figure 25. Oriented needles were present in the Kenyan color-change garnets. Photomicrograph by D. Beaton; field of view 2.6 mm.

Figure 26. Vis-NIR spectroscopy of the 1.39 ct garnet confirmed two distinct areas of transmission (centered at ~475 nm and above 650 nm) that are characteristic of color-change gems, as well as several distinct features from color-causing ions.
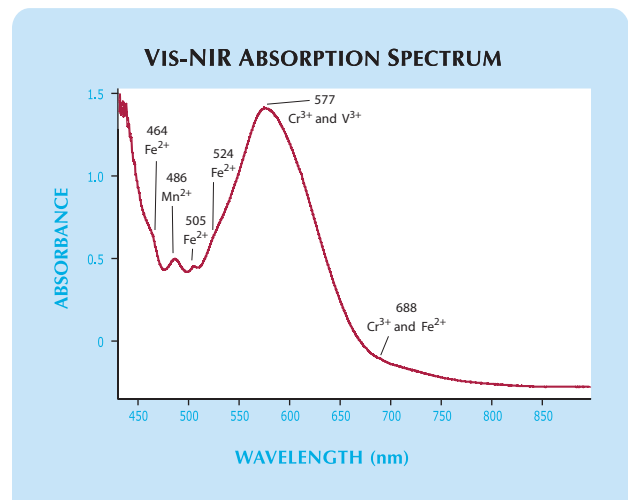
Figure 27. The heat-treated rubies on the left (2.03–2.50 ct) are reportedly from Lichinga, Mozambique. The unheated rubies on the right (1.07–4.62 ct) are a mixture of stones said to be from Lichinga and Montepuez, Mozambique. Photos by Robert Weldon.

purplish red, with none of the orangy component that is commonly seen in many other African rubies. The stones Mr. Wu provided did not show any evidence of heat treatment when examined with the microscope and analyzed by FTIR spectroscopy. Chemical analysis by EDXRF revealed iron contents ranging from 0.09 to 0.31 wt.% Fe_2O_3, with an average value of ~0.16 wt.%. Also present was 0.13–0.76 wt.% Cr_2O_3 and minute traces of Ti, Ga, and V.

The inclusion scenes in these stones showed some of the features noted in rubies from other East African localities, but in combinations that made them somewhat different in our experience. Most were fairly included. Strong laminated twinning with networks of intersection tubules were common. Some tubules were naturally stained orange with what appeared to be epigenetic iron compounds (figure 28, left). Dense clouds of reflective platelets, similar to those seen in sapphires from Umba, Tanzania, were present in many of the rubies (again, see figure 28, left). Within some of the clouds were needle-like inclu-

sions that appeared to be rutile. A few stones also contained clouds that had a more particulate appearance (figure 28, center). In addition, dense particulate planar clouds were seen in some samples (figure 28, right).

Perhaps the most interesting inclusions we noted—in two stones—were rounded blue-gray to grayish blue transparent crystals (e.g., figure 29) that gave a Raman signal of an amphibole very close to that of pargasite. Their visual appearance was identical to the pargasite crystals found in rubies from Winza in Tanzania. It is unclear if this is a coincidence or represents contamination with Winza material. However, the inclusions in the other stones in this sample set did not resemble those documented in rubies from Winza.

Shane F. McClure (smcclure@gia.edu) and
John I. Koivula
GIA Laboratory, Carlsbad

Yogo sapphire update. The Vortex sapphire mine at Yogo Gulch, Montana, has reopened under the consolidated

Figure 28. Some of the Mozambique rubies hosted epigenetically stained tubules and dense clouds consisting of reflective platelets and short needles that were reminiscent of sapphires from Umba (left, image width 1.8 mm, by J. I. Koivula). Also seen were particulate clouds made up of small disk-shaped inclusions (center, image width 1.6 mm, by S. F. McClure). Dense planar clouds were present in several of the Mozambique rubies (right, image width 3.5 mm, by S. F. McClure).
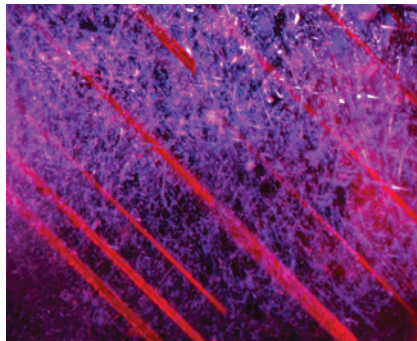
Figure 29. Rounded blue-gray to grayish blue crystals in a few of the Mozambique rubies yielded a Raman spectrum of an amphibole, close to that of pargasite. Similar inclusions are known to occur in Winza rubies. Photomicrograph by J. I. Koivula; the largest crystal is 0.17 mm long.

ownership of Mike and Laurie Roberts (Roberts Yogo Co., Great Falls, Montana). The previous owners ceased operations in late 2004 (see Fall 2005 GNI, p. 276).

Mr. Roberts and his crew of three are mining the Primary and New Downstream dikes year-round, via the access tunnel that was constructed by the former mine owners. This tunnel, a 16% decline, features compressed air and electricity, as well as ventilation fans and an escape route; it penetrates 400 feet (122 m) into the mountain.

The sapphire-bearing dikes, which vary somewhat in friability, measure 15–90 cm in width. They are mined by drilling, blasting, and mucking; pressure washing is done where possible to avoid breaking the gems. The ore is

brought to the surface in 5-tonne trucks, and the sapphire-bearing dike material is allowed to weather before processing. The mill employs gravity separation and processes 20 tonnes of ore per hour. The sapphires are then hand-picked from the jigs.

Roberts Yogo Co. has stockpiled 16,000 grams of rough and faceted nearly 10,000 carats. As with previous production, the vast majority of the sapphires are a consistent natural "cornflower" blue (e.g., figure 30), with a small percentage of well-saturated purple and a very few rare pink stones. The typically flat crystal morphology lends itself to smaller fancy cuts rather than larger rounds. Most of the stones are <1 ct, but they have produced about 100 per year above that threshold. The smaller sapphires are fashioned overseas at fair-trade cutting facilities operated by Columbia Gem House (Vancouver, Washington). The larger rough (e.g., figure 31) is cut in Montana. Full-depth brilliant-cut stones of appreciable size are uncommon, and the 2.50 ct stone in figure 31 is exceptional for Yogo sapphire.

Claire Baiz (bigskygold@imt.net)
Big Sky Gold & Diamond, Great Falls, Montana

Topaz with unstable brown color. Since early 2007, there has been an influx of orangy to reddish to pinkish brown topaz on the market in Chanthaburi, Thailand (see G. Roskin, "Topaz alert," *JCK*, Vol. 178, No. 9, 2007, p. 60). Some of the stones have been represented as coming from Myanmar, others as Brazilian goods. This material has been widely available on the Internet as well. Two of these topazes were supplied to the GIA Laboratory in Bangkok for examination by Jeffery Bergman (LGL Co., Bangkok): an orangy brown sample that had been kept in the dark, and a near-colorless topaz that had faded from orangy brown to almost colorless after being exposed to sunlight

Figure 30. Sapphires from the Vortex mine in Montana commonly show a uniform "cornflower" blue color. Photo by Amber Roberts.

Figure 31. This 2.50 ct concave-cut Yogo sapphire, fashioned by Richard Homer, is shown with a 1.5 g piece of Yogo rough. Both were produced from Montana's Vortex mine since it reopened in late 2006. Courtesy of Mike Roberts and Robert Kane/Fine Gems International; photo by Robert Weldon.
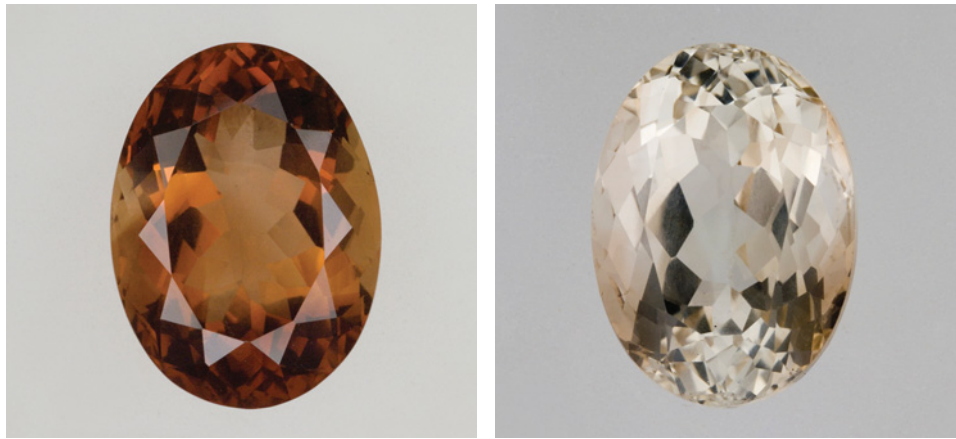
Figure 32. Some brown topaz currently on the market is not color stable. Both of these samples were the same orangy brown color when purchased. While the stone on the left (22.22 ct) was kept in the dark, the other (18.99 ct) turned near-colorless after exposure to sunlight for one day. Photo by Adirote Sripradist.

for one day (figure 32). The samples were obtained in Chanthaburi, with no disclosure of color instability.

In June 2008, some additional samples of this color-fading topaz (also purchased in Chanthaburi, in November 2007) were brought to GIA's attention by L. Allen Brown (All That Glitters, Methuen, Massachusetts). To observe the effect of light on this material first-hand, GIA purchased four faceted orangy brown topaz samples (19.18–21.29 ct) from Mr. Brown, and had three of them sawn in half; the fourth stone was retained as a reference sample. One-half of each of the three stones was kept in the dark for comparison, and the other portions were each exposed to different lighting environments: (1) placed on a windowsill in daylight for 80 hours; (2) exposed to a standard 100-watt incandescent light bulb for 80 hours at a distance of 2.5 cm; and (3) exposed to long-wave UV radiation for 40 hours, using a 6-watt bulb at a distance of 2.5 cm. As seen in figure 33, the samples exposed to daylight and incandescent light faded considerably; the fading of the latter piece was probably also enhanced by the heat of the bulb, since much brown topaz loses color above 200°C (K. Nassau, *Gemstone Enhancement*, 2nd ed., Butterworth-Heinemann, Oxford, U.K., 1994, p. 192). The

sample that was exposed to UV radiation faded even further, despite the shorter exposure time.

Some brown topaz (e.g., from the Thomas Range in Utah) may lose its color when exposed to sunlight (M. O'Donoghue, Ed., *Gems*, 6th ed., Butterworth-Heinemann, Oxford, UK, 2006, pp. 176–177). In addition, O'Donoghue (2006) noted that unstable brown color centers may develop from the laboratory irradiation of colorless topaz. To date there is no gemological test that can identify whether brown color in topaz is due to natural or laboratory irradiation, and a fade test is the only way to determine if the color is stable.

*Garry Du Toit (garry.dut@giathai.edu) and
Kamolwan Thirangoon
GIA Laboratory, Bangkok*

New tourmaline production from Keffi, Nigeria. Gem-quality tourmaline has been known from granitic pegmatites in the Keffi area of central Nigeria for about 25 years (J. Kanis and R. R. Harding, "Gemstone prospects in central Nigeria," *Journal of Gemmology*, Vol. 22, No. 4, 1990, pp. 195–202). In late 2008, there was a new find of

Figure 33. Three samples of brown topaz were sawn in half, and one piece from each pair was subjected to fade testing: in daylight for 80 hours (19.18 ct, left), in incandescent light for 80 hours (21.03 ct, center), and by exposure to long-wave UV radiation for 40 hours (21.29 ct, right). Thermal fading is probably responsible for some of the decolorization shown by the topaz exposed to the incandescent bulb. The UV-faded sample showed the most pronounced change. Composite photo by Adirote Sripradist.

Figure 34. These tourmalines are from a new find in the Keffi area of central Nigeria. The crystal at the top measures 31.6 mm long, and the cut stones range from 6.71 to 16.82 ct. Photo by Robert Weldon.

tourmaline in this region, near the village of Akwandoka (see J. C. Michelou, "New tourmaline deposit found in Nigeria," *InColor*, Fall-Winter 2008–2009, pp. 21, 24).

Eight specimens of the new Keffi tourmaline, consisting of two pieces of rough (17.5 and 6.8 g) and six faceted stones

(6.71–16.82 ct), were loaned to GIA for characterization by Dudley Blauwet (Dudley Blauwet Gems, Louisville, Colorado). The rough consisted of a well-formed crystal and a spherical nodule, both of which were mostly pink with a yellowish green zone (figure 34). The faceted stones were homogeneous pink, zoned yellow and pink, and zoned greenish yellow and pink (e.g., figure 35). Both the rough and cut samples ranged from eye-clean to very slightly included.

Standard gemological testing of the faceted stones established the following properties: RI—1.620–1.640 (both ±0.002); hydrostatic SG—3.03 (±0.02); and fluorescence—inert to long-wave, and moderate chalky blue to short-wave UV radiation; the color-zoned stones showed a zoned chalky yellow fluorescence to short-wave UV. Using a dichroscope, we observed two distinct pleochroic colors perpendicular to the c-axis: light yellow and pink in the pink tourmaline, and light green and orange in the greenish yellow tourmaline. The main internal characteristics were short needles, small particles, and "fingerprints" composed of fluid inclusions. The properties of these samples were typical of tourmaline.

Mr. Blauwet also loaned two other bicolored samples (a crystal and a nodule) of Keffi tourmaline to the University of New Orleans for chemical analysis by electron microprobe. The crystal was analyzed in 10 spots (seven pink and three yellowish green), and the nodule was analyzed in seven spots (five pink and two yellowish green). All the data showed an elbaite composition, with traces of F, Mn, Ca, K, and sometimes Fe (particularly in the yellowish green) and Ti. The elements Cr, Bi, V, Mg, Cu, Ba, Pb, and Cl were below or near the detection limits of the microprobe (i.e., 0.01–0.02 wt.% oxide). The full analyses are available in the *G&G* Data Depository.

Riccardo Befi

William B. Simmons and Alexander U. Falster
University of New Orleans, Louisiana

"Lilac"-colored Cu-bearing tourmaline from Nigeria. At the 2009 Tucson gem shows, Bill Barker (Barker & Co., Scottsdale, Arizona) had some copper-bearing tourmaline that was represented by his supplier as being from a new

Figure 35. The face-up appearance of this 12.20 ct color-zoned tourmaline changes when it is viewed at slightly different angles. Photos by Robert Weldon.

deposit in Nigeria. The stones had a consistent "lilac" pink color and reportedly were not heat treated (e.g., figure 36). He obtained the rough at the June 2008 JCK show in Las Vegas, and faceted ~400 carats into stones that ranged up to ~15 ct. The rough material consisted of broken crystals, some of which had green rims. Heat-treatment experiments performed by Mr. Barker yielded no change in color in either the pink or green material.

Mr. Barker donated several samples of the rough pink/green tourmaline to GIA, and LA-ICP-MS analyses of eight pieces by research scientist Dr. Mike Breeding showed 0.03–0.08 wt.% CuO in the pink stones and 0.05–0.10 wt.% CuO in the green material. The samples also contained trace-to-minor amounts of Fe (mainly in the green tourmaline), Mn, Ca, and Zn, and significant traces of Ti, Ga, Pb, and Sr.

The Cu content of this pink/green tourmaline is similar to that of some greenish blue samples from Nigeria that were described in a Spring 2002 GNI entry (pp. 99–100), but it is considerably less than the Cu concentrations measured in the Nigerian tourmalines reported in Fall 2001 and Winter 2007 GNI entries (pp. 239–240 and 384–385, respectively).

Brendan M. Laurs

Triphylite from Brazil. In October 2008, Brad Payne (The Gem Trader, Surprise, Arizona) informed GIA about the recent availability of some facetable triphylite (figure 37), reportedly from Galiléia in the Brazilian state of Minas Gerais. Galiléia mines are famous for producing rare col-

Figure 36. Nigeria is reportedly the source of this unheated "lilac"-colored copper-bearing tourmaline (6.35–13.92 ct). Photo by Robert Weldon.

lectible minerals, sourced from granitic pegmatites of Brasiliano age (550–500 Ma; M. L. S. C. Chaves et al., "Assembléias e paragêneses minerais singulares nos pegmatitos da região de Galiléia [Minas Gerais]," *Geociências*, Vol. 24, No. 2, 2005, pp. 143–161). Triphylite is the iron-rich variety of the triphylite-lithiophilite series $Li(Fe,Mn)PO_4$; lithiophilite is the manganese-rich variety. Gem-quality triphylite large enough to cut multi-carat stones is quite rare. Mr. Payne was aware of ~200 carats of mixed-quality faceted stones; the vast majority weighed less than 4 ct. Although the material was typically dark

Figure 37. These triphylites (0.26–9.31 ct) were recently produced from Minas Gerais, Brazil. Three of the stones show a slight color change from greenish brown in daylight (left) to brownish pink or purple in incandescent light (right). Photos by Robert Weldon.

TABLE 1. Physical properties and chemical analyses (by LA-ICP-MS) of six Brazilian triphylites.[a]						
Property	7.31 ct	9.31 ct	2.63 ct	0.56 ct	0.48 ct	0.26 ct
RI						
n_α	1.687	1.690	1.690	1.690	1.690	1.692
n_β	1.689	1.693	1.694	1.694	1.693	1.695
n_γ	1.695	1.698	1.698	1.698	1.697	1.700
SG	3.53	3.56	3.57	3.52	3.52	nd[b]
Oxide (wt.%)						
~~P_2O_5~~	~~29.02~~	~~29.64~~	~~29.41~~	~~46.90~~	~~48.12~~	~~48.13~~
~~Li_2O~~	~~12.02~~	~~12.67~~	~~13.73~~	~~10.29~~	~~10.65~~	~~10.49~~
~~FeO~~	~~30.56~~	~~38.54~~	~~38.01~~	~~28.95~~	~~27.83~~	~~28.18~~
~~MnO~~	~~27.75~~	~~17.79~~	~~17.53~~	~~12.95~~	~~12.35~~	~~12.30~~
ZnO	0.16	0.24	0.24	0.20	0.19	0.20
MgO	0.50	1.07	1.09	0.71	0.70	0.69
Total	100.01	99.95	100.01	100.00	99.84	99.99
Ion ratio						
Fe/Mn	1.10	2.17	2.17	2.24	2.25	2.29

[a] Analyses performed with a Thermo Fisher X Series II ICP-MS with a NewWave UP 213 laser ablation unit, calibrated using NIST glasses, using the following ablation parameters: 213 nm laser excitation, 7 Hz frequency, 30 μm diameter spot size, and 40 second dwell time.
[b] Abbreviation: nd = not determined (due to small sample size).

Note: The major-element data (for P, Li, Fe, and Mn) were reported incorrectly.

orangy red in both daylight-equivalent and incandescent light, some of the gems showed a slight color change.

Mr. Payne loaned GIA six faceted samples, ranging from 0.26 to 9.31 ct (again, see figure 37). Gemological testing produced the following results: color—three were dark orange red, and three exhibited a slight color change from greenish brown in daylight to brownish pink or purple in incandescent light; pleochroism—strong blue or bluish green, brownish orange, and brown; RI—n_α = 1.687–1.692, n_β = 1.689–1.695, and n_γ = 1.695–1.700; birefringence—0.007–0.008; and hydrostatic SG—3.52–3.57. All were inert to long- and short-wave UV radiation. The absorption spectrum seen with a desk-model spectroscope consisted of a strong line at 410 nm, a band at 450–460 nm, strong lines near 470 nm, and bands at 490–500 and 600 nm. These properties are consistent with those reported for triphylite (Fall 1988 Lab Notes, p. 174; M. O'Donoghue, Ed., *Gems*, 6th ed., Butterworth-Heinemann, Oxford, UK, 2006, p. 460). Microscopic observation revealed fine particles arranged in parallel bands, as well as short needles, transparent crystals, and fine-grained "fingerprints."

Infrared and Raman spectra were typical for Li-Fe-Mn-phosphates. Chemical analysis with EDXRF and LA-ICP-MS (the latter performed by research associate David Kondo; table 1) revealed traces of Mg and Zn in all the samples. The concentrations of Fe and Mn affect the optical and physical properties in the triphylite-lithiophilite series: RI and SG increase or decrease proportionally with Fe and Mn (S. L. Penfield and J. H. Pratt, "Effect of the mutual replacement of manganese and iron on the optical properties of lithiophilite and triphylite," *American Journal of Science*, Series 3, Vol. 50, No. 299, 1895, pp. 387–390). In these triphylites from Galiléia, the RI values varied according to the Fe/Mn ratio, and SG fluctuated consistently with iron content (table 1).

Pamela Cevallos (pamela.cevallos@gia.edu)
GIA Laboratory, New York

SYNTHETICS AND SIMULANTS

Colorless synthetic sapphire imitating rough diamond. Many types of near-colorless transparent crystalline materials have been fashioned to imitate rough diamond (see, e.g., Lab Notes: Fall 1996, p. 205 [cubic zirconia]; Fall 1997, pp. 217–218 [topaz]; and Fall 2007, p. 250 [phenakite]). The Dubai Gemstone Laboratory has seen cubic zirconia, topaz, phenakite, and rock crystal fashioned in this manner. Recently, we received for identification a 2.5 g near-colorless sample that resembled a water-worn, distorted octahedral diamond crystal (figure 38). Despite the client's long experience in rough diamond trading, he was unsure of its authenticity.

Standard gemological testing quickly established that the sample was not a diamond. It was doubly refractive and uniaxial, with a spot RI of approximately 1.76 and a hydrostatic SG of 4.00. These properties were consistent with corundum, which was confirmed by Raman spectroscopy. The sample was inert to long-wave UV radiation and fluoresced weak chalky blue to short-wave UV. Microscopic examination revealed no visible inclusions, nor any curved striae or Plato lines in immersion that would point to synthetic sapphire. However, the UV-Vis absorption spectrum showed transparency down to 224 nm—a strong indication that the sample was synthetic because natural corundum typically does not transmit wavelengths less than 288 nm. This identification was

Figure 38. Despite its outward appearance resembling a natural octahedral diamond crystal, this 2.5 g sample is a synthetic sapphire. Photo by N. Ahmed, © Dubai Gemstone Laboratory.

confirmed by EDXRF analysis, which showed the expected Al, and a very small amount of Fe as the only trace element (see S. Elen and E. Fritsch, "The separation of natural from synthetic colorless sapphire," Spring 1999 *G&G*, pp. 30–41).

We had never seen colorless synthetic sapphire imitating rough diamond, perhaps because its higher hardness makes it more difficult to fashion than more common simulants such as topaz and phenakite. This example shows that even experienced traders can make costly mistakes when dealing with rough diamonds from unknown sources or spot buying, and extra care should always be taken to confirm a suspect sample's identity. In this case, simple gemological testing was sufficient to detect the fraud.

Nazar Ahmed (nanezar@dm.gov.ae) and
Sutas Singbamroong
Dubai Gemstone Laboratory,
Dubai, United Arab Emirates

MISCELLANEOUS

Update on Myanmar gems. This contributor recently had the opportunity to test a bipyramidal ruby crystal with good color and luster. The sample was ~2.5 cm tall and weighed ~5 g. The faces were curved and bent, as if waterworn. Yet, the sample's luster was different from that of a natural alluvial crystal, and the horizontal striations were inclined rather than perpendicular to the vertical axis. Detailed observation with 10× magnification revealed that the pyramidal faces were not natural, but rather hand-fashioned or engraved. The presence of curved striae, also seen with the microscope, proved it was a synthetic ruby.

A colleague who recently visited the jadeite mining areas reported that the largest company mining there was Ever Winner, which was working about 100 plots, each measuring 200 × 200 ft (61 × 61 m), and employing some 800–1,000 workers. The company was operating more than 30 backhoe machines, 20 tractors, and about 40 dump trucks. Heavy rains in the jade mining area during this year's monsoon season have caused landslides and flooding along the Uru River. The floods were due to the diversion of river channels and accumulation of mine tailings, underscoring the need to enforce environmental regulations. A 30 kg piece of jadeite recovered from the Mana mining area sold at the Myanma Gems Emporium for US$25 million.

At Mong Hsu, a joint mining venture with the Myanmar Economic Corporation found some attractive rubies by following the geologic structure (fold axes) to the south-southeast in underground operations.

Gem shops in Yangon have experienced slumping sales in the downtown and Kaba Aye areas. The downturn is due to decreased tourism, economic sanctions by the U.S. government, and the global economic situation.

U Tin Hlaing
Dept. of Geology (Retired)
Panglong University, Myanmar

CONFERENCE REPORTS

3rd European Gemmological Symposium. This successful conference was held June 4–7 in Berne, Switzerland, and was hosted by the Swiss Gemmological Society, the SSEF Swiss Gemmological Institute (Basel), and the Gübelin Gem Lab (Lucerne). A number of interesting presentations—some of which are described here—were offered to the 130 participants who attended. The symposium opened with two keynote speakers: **Martin Rapaport** offered insights on the troubled diamond market, while **Gabi Tolkowsky** discussed diamonds from a different perspective, emphasizing their beauty.

Dr. Daniel Nyfeler (Gübelin Gem Lab) stressed the importance of using algorithms to handle the large quantity of data obtained with new analytical methods, especially for determining the geographic origin of gems. **This contributor** demonstrated the possibilities and limitations of LA-ICP-MS in gem testing. **Dr. Karl Schmetzer** (Petershausen, Germany) spoke on the colorimetry of color-change garnets and their vanadium, chromium, and manganese contents. **Dr. Benjamin Rondeau** (Laboratoire de Planétologie et Géodynamique, University of Nantes, France) discussed the role of organic matter in sediments as a source of vanadium in emeralds from Colombia and other localities.

Jean-Pierre Chalain (SSEF) showed a diagram illustrating the characteristic width (full width at half maximum) and position of the platelet peak of type Ia HPHT-treated diamonds. **Thomas Hainschwang** (Gemlab Gemological Laboratory, Balzers, Liechtenstein) presented the results of type Ia diamond irradiation experiments with subsequent annealing. The samples turned from near-colorless to very dark green and black upon irradiation, and then deep greenish yellow to deep orangy brown upon annealing. **George Bosshart** (Horgen, Switzerland) discussed his research on the genesis of natural green diamond colors. He postulated that the radiation-induced green color in the investigated diamonds resulted from contact with radioactive element–bearing fluids or groundwaters.

Dr. Henry Hänni (SSEF) summarized the current status of cultured pearls, explaining the three basic distinctions: beaded or beadless, mantle-grown or gonad-grown, and saltwater or freshwater. **Dr. Stefanos Karampelas** (Gübelin Gem Lab) presented Raman spectra confirming that all natural colors of freshwater cultured pearls originate from a mixture of unsubstituted polyenes and not from impurities or carotenes, as previously believed. The absence of characteristic polyenic Raman bands provides evidence of artificial color.

Further interesting topics included spessartine deposits around the world (**Dr. Claudio Milisenda**, DSEF, Idar-Oberstein, Germany); basalt-related ruby and sapphire deposits (**Dr. Dietmar Schwarz**, Gübelin Gem Lab); zircon from Ratanakiri, Cambodia (**Dr. Walter Balmer**, Chulalongkorn University, Bangkok); the detection of jewelry fakes (**Dr. Jack Ogden**, Gem-A, London); the nondestructive identification of ornamental materials (**Dr. Vera Hammer**, Natural History Museum, Vienna, Austria); the identification of treated fancy-color diamonds (**Dr. Eric Erel**,

Gübelin Gem Lab); digital photomicrography of inclusions (**Michael Hügi**, Swiss Gemmological Society); the interplay between world politics and gems in Mogok, Myanmar (**Roland Schlüssel**, Pillar & Stone International, San Francisco); historic highlights at auction and the influence of the celebrity factor ("origin") on the selling price of jewelry at auction (**Helen Molesworth**, Christie's, Geneva); the microscopic and macroscopic characteristics of ivories (**Maggie Campbell Pedersen**, *Organic Gems*); and the cultured pearl market (**Andy Muller**, Golay Buchel Japan, Kobe).

After the symposium, many participants joined an excursion to Switzerland's Grimsel region, where a visit to a protected crystal fissure—the walls of which are covered with well-formed colorless quartz crystals and pink fluorite—crowned the outing.

Michael S. Krzemnicki

ANNOUNCEMENTS

CIBJO resources for retailers. CIBJO, the World Jewellery Confederation, is releasing its *Retailers' Reference Guide: Diamonds, Gemstones, Pearls and Precious Metals*. It contains comprehensive information on various gem materials and metals, as well as handouts for sales staff. Other resources include *Believe in Me: A Jewellery Retailer's Guide to Consumer Trust*, which offers steps that can be taken to instill confidence in today's consumer, and *The Retailer's Guide to Marketing Diamond Jewellery*, which contains practical advice on analyzing your business, know-ing your customer, staff training, branding, and merchandising, plus step-by-step business tools and case studies. Visit www.cibjo.org to download these free publications.

Gem cutting notes available. The Summer 2009 GNI entry on colorless petalite and pollucite from Laghman, Afghanistan (pp. 150–151) documented three stones that were faceted by Robert C. Buchannan (Hendersonville, Tennessee). Mr. Buchannan has kindly provided information on the cutting of these gemstones, which is available in the *G&G* Data Depository (www.gia.edu/gandg). Notes on additional gems cut by Mr. Buchannan will be posted in the Depository as GNI entries on them are published.

ERRATUM

Due to a drafting error, the definition for the 3H (503.5 nm) defect in "The 'type' classification system of diamonds and its importance in gemology" on p. 100 of the Summer 2009 issue described a different lattice defect. The definition should have read:

> **3H (503.5 nm):** This defect is thought to be related to an interstitial carbon atom in the diamond lattice. It is created by radiation damage and often occurs with the GR1. On rare occasions, 3H absorbs strongly enough to enhance the green color caused by GR1 absorption.

We thank Andrea Blake for bringing this to our attention. *Gems & Gemology* regrets the error.

IN MEMORIAM
CAMPBELL R. BRIDGES (1937–2009)

The gemological community was stunned by the recent death of one of its most remarkable figures. Geologist Campbell Bridges, who is credited with the discovery of tsavorite garnet in the 1960s and led most of its mining in the decades since, was killed August 11 in southern Kenya, the victim of a mob attack over mining rights.

A native of Scotland, Mr. Bridges spent most of his life in Africa. There he became inextricably linked with tsavorite, the brilliant green grossular garnet. He encountered his first crystal in 1961 but was too involved with another newly discovered gem material, tanzanite, to pursue the find. Mr. Bridges rediscovered the green garnet six years later in Tanzania, but was forced to abandon his operation when the government nationalized the mines. Undaunted, he crossed the border into Kenya to resume the search.

His careful analysis of southern Kenya's geology and even its vegetation patterns paid dividends when he struck tsavorite on the first day of ground exploration. By 1971 he had staked numerous claims. Tiffany & Co. christened the gem, naming it after the nearby Tsavo National Park, and introduced it in September 1974. Mr. Bridges's article in the Summer 1974 issue of *Gems & Gemology* (pp. 290–295) offered a detailed study of its characteristics and geology.

Mr. Bridges was known for his rugged, adventurous spirit, and many of his mining stories featured brushes with lions, cobras, and scorpions. A popular lecturer, he spoke on East African gems at conferences around the world, including GIA's International Gemological Symposiums in 1982 and 1991.

Mr. Bridges was a director and founding member of the International Colored Gemstone Association (ICA). He was also a staunch wildlife conservationist and pioneered methods of environmentally responsible mining.

Campbell Bridges is survived by his wife, Judith, and two children, Laura and Bruce.

Robert Weldon

Challenge
WINNERS

This year, hundreds of readers participated in the 2009 GEMS & GEMOLOGY Challenge. Entries arrived from around the world, as readers tested their gemological knowledge by answering questions listed in the Spring 2009 issue. Those who earned a score of 75% or better received a GIA Letter of Completion recognizing their achievement. The participants who scored a perfect 100% are listed here.

ANSWERS

See pages 76–77 of the Spring 2009 issue for the questions.

1 (a), 2 (b), 3 (c), 4 (b), 5 (c), 6 (a), 7 (d), 8 (a), 9 (a), 10 (d), 11 (d), 12 (b), 13 (b), 14 (b), 15 (d), 16 (c), 17 (b), 18 (a), 19 (c), 20 (b), 21 (d), 22 (c), 23 (c), 24 (d), 25 (a) [Question 25 was eliminated due to an ambiguity in phrasing.]

AUSTRALIA Tasmania, *Huonville:* Joseph Bini • **BELGIUM** *Brussels:* Sheila Sylvester • **CANADA Alberta,** *Calgary:* Janusz Meier • **DENMARK** *Laesoe:* Margrethe Gram-Jensen • **FRANCE** *Les Breviaires:* Thierry Cathelineau • **GEORGIA** *Tbilisi:* I. R. Akhwlediani • **GERMANY** *Muenster:* Carolyn van der Bogert • **GREECE** *Thessaloniki:* Panagiotis Efthimiadis • **HONG KONG** *Causeway Bay:* Cristina O. Piercey-O'Brien • **INDONESIA** *Jakarta:* Warli Latumena • **ITALY** *Bergamo:* Roberto Crippa • **LITHUANIA** *Vilnius:* Saulius Fokas • **PORTUGAL** *Algarve:* Joanne Jack • **RUSSIA** *Moscow:* Vadim Prygov • **SWITZERLAND** *Geneva:* Julie Falquet. *Zurich:* Doris Gerber • **SYRIA** *Aleppo:* Hagop Topjian • **THAILAND** *Bangkok:* Cynthia Gestring-Blumberg • **UNITED KINGDOM** *Birmingham:* Anu Manchanda. *London:* Douglas Kennedy. Tenterden, *Kent:* Linda Anne Bateley • **USA Arizona,** *Oro Valley:* Luella Dykhuis. **Arkansas,** *Greenbrier:* Beverly Brannan. **California,** *Daly City:* Juliana S. Bendt. *Palo Alto:* Grace Nani Pahed. *San Diego:* Michael Jakubowski. *San Jose:* Wendy Bilodeau. **Delaware,** *Bridgeville:* Thaïs Anne Lumpp-Lamkie. **Florida,** *Deland:* Sue Angevine Guess. *Trinity:* Thomas MacKinnon. *Venice:* Robert Campbell, Geraldine Vest. **Illinois,** *Belleville:* Bruce Upperman. *Danvers:* Anne Blumer. **Indiana,** *Indianapolis:* Brian Randolph Smith, Wendy Wright Feng. **Maryland,** *Chevy Chase:* Andrea R. Blake. *Patuxent River:* Pamela Stair. *Riva:* Daniel Sullivan. **Massachusetts,** *Littleton:* Jane Millard. **Missouri,** *Saint Ann:* Bruce Hoffmann. **Nevada,** *Las Vegas:* Colleen Walsh. **New Jersey,** *Moorestown:* Rosemarie C. Hill. **New Mexico,** *Los Alamos:* Steve Pearson. **New York,** *New York:* Anna Schumate, Lois Tamir. **North Carolina,** *Kernersville:* Jean A. Bonebreak. **Ohio,** *Cuyahoga Falls:* Catherine Lee. **Pennsylvania,** *Schuylkill Haven:* Janet Steinmetz. **Puerto Rico,** *San Juan:* Berthy Nayor-Cohn. **Rhode Island,** *Rumford:* Sarah A. Horst. **South Carolina,** *Sumter:* James S. Markides. **Texas,** *Amarillo:* Daniel Novak. *Dallas:* Shawn Shannon. *Ft. Worth:* Elizabeth A. Albright. **Virginia,** *Falls Church:* Heather Widener. **Washington,** *Blaine:* John R. J. Scott.

Congratulations!

Book Reviews/Gemological Abstracts

The *Gems & Gemology* Book Reviews and Gemological Abstracts sections are available only in electronic (PDF) format. These sections are available free of charge both on the *G&G* web site (www.gia.edu/gandg) and as part of *G&G* Online (gia.metapress.com), and are paginated separately from the rest of the issue. These sections are also included in this full-issue PDF. Accordingly, the Table of Contents included in this file lists these additional sections, and thus differs from the Table of Contents in the print version. For these reasons, this PDF is *not* the official version of this issue—the "journal of record" for this issue is the combined print/online version that was released to subscribers.

BOOK Reviews

Editors

Susan B. Johnson
Jana E. Miyahira-Smith
Thomas W. Overton

Famous Diamonds, 5th Ed.

By Ian Balfour, 335 pp., illus., publ. by Antique Collectors' Club [www.antique-acc.com], Woodbridge, Suffolk, UK, 2009. $95.00

For nearly 30 years, diamond historian Ian Balfour has unmasked legends and provided factual accounts of the most exceptional diamonds. In this new edition of his now-classic reference, he makes each entry monumental through the dogged unearthing of the mythology and history of these famous treasures.

Diamonds are personal, as illustrated by Balfour's story of the Emperor Maximilian diamond. Worn by the emperor in a satchel around his neck when he was executed by a firing squad in Mexico, it was returned to his widow, Carlotta, who "as the result of these events, was to remain mentally deranged until her death near Brussels in 1927. The gem was sold in order to help pay her medical expenses" (p. 97). Balfour brings this personal touch, whether tragic or inspiring, to each diamond with a known history (regrettably, the origins of some diamonds have yet to be revealed).

The abundant details he provides on the possessors of these unequaled gems deepen our thirst for more. And because diamonds are also visual, his accounts are liberally illustrated with paintings, sketches, and photographs, each drawing us further into the story. Balfour offers images of owners as they display their proud possessions: a duke or duchess, a king or queen, or Hollywood royalty such as Audrey Hepburn or Liz Taylor. Each image complements the richness Balfour describes, causing us to pause and to celebrate.

In this fifth edition (the fourth was released in 2000), Balfour adds several new or significantly revised entries. These include the Donnersmarck, a pair of Fancy Intense yellow diamonds (a 102.54 ct cushion and 82.48 ct pear) that once belonged to La Paiva, one of the most celebrated courtesans of the mid-1800s; the Kazanjian Red (known as the Red Diamond in earlier editions, and lost until recently; a 5.05 ct squarish emerald cut once mistaken for a ruby by an American general when it was recovered from Nazi war loot; the Lesotho Promise, a 603 ct crystal discovered in 2006 and the 15th largest gem diamond ever found; and the Natasha and Victoria-Transvaal, "champagne"-colored pear-shaped diamonds (64 and 67 ct) cut from the same 280 ct crystal. The entry for the 55 ct Sancy, a storied pear-shaped double rose cut, was modified to reflect the research of Susan Ronald, whose 2005 book, the *Sancy Blood Diamond*, has rewritten the history of this stone. She traced the diamond from its first report in the late 1300s, through its ownership by Cardinal Mazarin and then the French royal family until the Revolution, when it took numerous twists and turns before being brought back to Paris for exhibition at the Louvre. There are also a number of new stones in the Notable Diamonds list at the end of the book.

Diamonds are personal. Diamonds are visual. That we cherish them and objectify the largest and rarest with appellations is no great surprise. These unique marvels possess a mystique that exerts a powerful pull on our imaginations. The gift of any talented chronographer is the ability to suffuse the reader with thoughts that not only stay with us, but somehow stir and wrest from us new inspiration. In this, Balfour succeeds.

AL GILBERTSON
*Gemological Institute of America
Carlsbad, California*

Editor's note: Additional information about this book is available in the G&G *Data Depository at www.gia.edu/gandg.*

Cameos: Old & New, 4th Ed.

By Anna M. Miller, edited by Diana Jarrett, 382 pp., illus., publ. by Gemstone Press [www.gemstonepress.com], Woodstock, VT, 2009. $19.99

Books on cameos have been written for centuries. One only needs to look in the bibliography or early chapters of *Cameos: Old & New* to see the amazing history of the "glyptic arts," which literally spans millennia. The first three editions by the late Anna Miller were filled with a tremendous amount of information and hundreds of black-and-white and color images on the subject. The fourth edition, edited by gemologist and journalist Diana Jarrett, is indeed the charm, a significant update that adds more

than 100 pages and revitalizes Ms. Miller's book for the new century. It features rewrites and improved organization of content—from the history, romance, and mythologies in the beginning of the book, to transparent gems, coral harvesting, alternate cameo materials, recent production processes, and sources and suppliers.

New finds of vintage cameos from flea markets, yard sales, and antique shops are illustrated and grouped by era. Pages of information on evaluating cameo authenticity are new, as are pointers to helpful websites. The glossary and suggested reading list are expanded as well. The historical value of cameos is addressed in depth, including the accomplished artists of more recent times. Among them are 21st century masters who are keeping the form alive in newly discovered *ateliers* in places such as Panama and Turkey, as well as in the traditional carving centers of Germany and Italy.

Overhauled for this edition are the chapters on buying and selling, with entries and tips on auction houses, the Internet, and TV shopping. The color plates in the center section give a broader representation of the full range of the art, with different types of carvings, materials, styles, and subject matter. The final chapter, new to the 4th edition, speaks to the direction in which the glyptic arts are headed, with inspirational quotes from the contemporary artists who continue this ancient skill.

Whether or not you have an earlier version of this book in your library, this edition belongs there.

CHARLES I. CARMONA
Guild Laboratories, Inc.
Los Angeles

MEDIA REVIEW

Expedition to New Ruby Mines in Winza, Tanzania

Sapphire Mining in Madagascar

Contributions to Gemology *No. 8, 46*

mins., released by GRS Gemresearch Swisslab [www.gemresearch.ch], Lucerne, Switzerland, 2009. $40.00

This DVD follows *Contributions to Gemology* No. 7 (see abstract on p. S13 of the Summer 2009 *G&G*) as a video supplement and contains two separate documentaries.

The first presents a visit to the Winza ruby mines in Tanzania by a team from GRS in August 2008. Footage from inside the mine shafts is included, as are interviews with the miners and local officials. Following their tour of the mines, the team visited buying offices in the nearby boomtown of Mpwapwa and customs offices in the capital, Dar es Salaam.

The second documentary reviews a 2007 visit to sapphire mining areas in Madagascar. The team began in Ilakaka at the Manga Tuka mine and several other open-pit mines, and then visited smaller shaft mines. Regardless of the size or depth of the workings, most mining in Madagascar is conducted entirely by hand, and aspects such as ventilation must be improvised from available materials. Mining also occurs within exposed riverbanks, though this is very dangerous because of the risk of cave-ins. Some mechanized mining also takes place, and Sri Lankan dealers support much of this activity. The video concludes with a review of gem buying and trading in Ilakaka.

This DVD is an interesting and informative video that could easily have stood on its own by virtue of the content. Thus, it is unfortunate that the producers felt it necessary to repeatedly embellish both films with distracting visual effects such as split-screens (sometimes three or four at once) and eye-straining graphics. It is also clear that the English title cards were not drafted by a native speaker, as they are frequently marred by errors in spelling and grammar.

In spite of such shortcomings, these documentaries are well worth viewing for their educational value.

TWO

OTHER BOOKS RECEIVED

Profiting by Design: A Jewelry Maker's Guide to Business Success. *By Marlene Richey, 135 pp., illus., publ. by MJSA Press [www.mjsa.org], Providence, RI, 2008, $34.95.* The author, a successful jewelry designer, discusses how to turn good designs into good business. The nuts and bolts of setting up a design shop are addressed in detail, as are the steps to surviving the all-important first year of a small business. Also included are resources for designers.

TWO

Cristalli: L'Ordine dal Caos [Crystals: Order from Chaos]. *By Adalberto Giazotto, Federico Pezzotta, and Giovanni Pratesi, 240 pp., illus., publ. by Giunti Editore [www.giunti.it], Florence, Italy, 2008 [in Italian], 48.00.* This Italian-language coffee-table book is a feast for the eyes of any mineral collector. It begins with a brief introduction to crystallography and crystal formation, recovery, and preservation. The bulk of the book, however, is a review of the first author's impressive collection of large mineral specimens, all illustrated in gorgeous full-page professional photographs.

TWO

Gill's Historical Index. *By Joseph O. Gill, 647 pp., illus., publ. by the author [www.archive.org, search for "Joseph Gill"], 2009, Free.* This online work-in-progress, a comprehensive update of the author's 1978 book, provides a searchable, annotated bibliography of gemological publications since 1652. Offered to the global gem community at no charge, this new version contains hyperlinks to many works now available on the Internet. This is a valuable resource for gemological researchers and anyone interested in the history of gemology, though it could be improved with input from a professional editor.

TWO

O9 GEMOLOGICAL Abstracts

COLORED STONES AND ORGANIC MATERIALS

Cultured freshwater pearls from the Yangtze River (China); characterisation by optical microscopy, scanning electron microscopy, cathodoluminescence, electron microprobe analysis, and Raman spectroscopy. M. Dumańska-Słowik [dumanska@uci.agh.edu.pl], W. Heflik, L. Natkaniec-Nowak, M. Sikorska, and A. Wesełucha-Birczyńska, *Australian Gemmologist*, Vol. 23, No. 4, 2008, pp. 290–299.

Unbeaded Chinese freshwater cultured pearls imitate natural pearls very closely. Their cores were found to contain polymorphic $CaCO_3$ minerals (aragonite or a mixture of aragonite, calcite, and vaterite), and their exteriors were composed of aragonite with dark to light green "oscillatory" concentric layers of mother-of-pearl. The presence of these mineral phases was confirmed by their Raman spectra. The 1526 and 1133 cm^{-1} bands characteristic of natural pearls were not recorded in the spectra of the Chinese freshwater cultured pearls, and may afford a means of distinguishing the two. *RAH*

Grüne Quarze—Farbursachen und Behandlung [Green quartz—Causes of colour and treatment]. R. Schultz-Güttler [rainersg@usp.br], U. Henn, and C. C. Milisenda, *Gemmologie: Zeitschrift der Deutschen Gemmologischen Gesellschaft*, Vol. 57, No. 1–2, 2008, pp. 61–73 [in German].

Large quantities of faceted green quartz have recently been observed in the trade. Four types are described: (1) natural green, heated in nature; (2) amethyst laboratory-heated to 400–500°C, known as *prasiolite*; (3) laboratory-irradiated quartz, the color of

which tends to fade at low temperatures (150°–200°C) or when exposed to strong sunlight; and (4) synthetic green quartz. The absorption spectrum for each is characteristic. Natural green quartz shows bands in the near-IR region at 725, 930, and 1040 nm, with a window at ~550 nm. Prasiolite has a wide absorption band with a maximum at 720 nm, while irradiated quartz has a broad absorption maximum at 592–620 nm. Synthetic green quartz shows a transmission maximum at ~510 nm and broad absorption bands with maxima at ~740 and 930 nm.

GL

Hackmanite, tugtupite and afghanite—Tenebrescence and fluorescence of some sodalite related minerals. J. Tunzi and G. Pearson [grantpearson@optusnet.com.au], *Australian Gemmologist*, Vol. 23, No. 4, 2008, pp. 349–355.

The tenebrescence of hackmanite from Afghanistan and Myanmar was compared with that of tugtupite from Greenland. The hackmanite displayed variable tenebrescence, but the tugtupite was largely inactive. Afghanite, a rare mineral from Afghanistan that is chemically related to hackmanite, was not observably tenebrescent.

RAH

Jarina, o marfim da Amazônia [Jarina, the ivory of Amazonia]. M. Lima da Costa, S. F. Santos Rodrigues, and H. Hohn, *Diamond News*, Vol. 9, No. 29, 2008, pp. 38–44 [in Portuguese].

The seed of the *Jarina* palm, known in English as ivory nut, resembles ivory. Until it was replaced by plastic in the 20th century, this seed supplied the material for nearly all shirt buttons worldwide. Recently, ivory nut has regained popularity as a material for jewelry and carvings. The authors describe the palm and its occurrence and growth conditions, the properties of the nut, color treatments, and jewelry uses. *RT*

Marble-hosted ruby deposits from Central and Southeast Asia: Towards a new genetic model. V. Garnier, G. Giuliani [giuliani@crpg.cnrs-nancy.fr], D. Ohnenstetter, A. E. Fallick, J. Dubessy, D. Banks, H. Q. Vinh, T. Lhomme, H. Maluski, A. Pêcher, K. A. Bakhsh, P. V. Long, P. T. Trinh, and D. Schwarz, *Ore Geology Reviews*, Vol. 34, 2008, pp. 169–191.

Marble-hosted ruby deposits from Afghanistan, Pakistan, Kashmir, Tajikistan, Nepal, Myanmar, northern Vietnam, and southern China share many structural, mineralogical, and radiometric features. These deposits are located in metamorphic blocks that experienced major tectonic events during the Cenozoic India-Asia collision. In many of the deposits, rubies were formed as scattered crystals along veins or certain horizons within marbles. Host marbles from all the deposits studied were rich in calcite and low in dolomite. Whole-rock chemical analyses of the marbles indicate that their Al, Cr, and V contents were

sufficient to produce rubies. The rubies are commonly associated with micas, chlorite, feldspar, graphite, pyrite, rutile, titanite, humite, and forsterite; occasionally with spinel, tourmaline, and amphibole; and rarely with sapphirine and zoisite.

Petrographic analyses show that the ruby-bearing marbles formed at a temperature of 610°–790°C and pressure of ~6 kbar. Fluid inclusions in the ruby samples were either single phase or, more commonly, two phase. They contained native sulfur, COS complexes, H_2O, CO_2, H_2S, and several solid inclusions (typically diaspore, rutile, and dolomite). Fluid inclusion studies bracket ruby formation conditions at 620–670°C and 2.6–3.3 kbar, indicating that the rubies crystallized during retrograde metamorphism of the marbles.

Stable isotope geochemical data for the (C,O,H)-isotopic compositions of minerals associated with the rubies are also presented. The (C,O)-isotopic compositions of carbonates suggest that the marbles acted as a metamorphic closed-fluid system, meaning that the fluids circulating in the marbles during metamorphism were released by the devolatilization of carbonates. Furthermore, the carbon isotopic signatures of graphite in the carbonates indicate that it had an organic source and that it exchanged C-isotopes with the carbonates during metamorphism.

The authors propose a new genetic model for the formation of these ruby deposits. First, sedimentary protoliths, including carbonates enriched with clay minerals and organic matter, were deposited on the Paleo-Tethys platform during the Precambrian to Permo-Triassic. During the India-Asia collision, these sediments were metamorphosed, transforming the carbonates into amphibolite-grade marbles. Ruby crystallized during the retrograde metamorphic path, mainly by destabilization of muscovite or spinel. The metamorphic fluids were rich in CO_2 released by carbonate devolatilization and in F, Cl, and B released by salts derived from evaporites in the protolith. These evaporites were key to the formation of the ruby deposits, as the salts mobilized typically immobile Al and transition metals in the marbles, leading to ruby crystallization.

The authors suggest taking the following guidelines into account when prospecting for new deposits: (1) the lithologic control of mineralization, and (2) the presence of indicator minerals (e.g., Na-rich phlogopite, pargasite, edenite, Mg-tourmaline, Cr-rich titanite, spinel, and anhydrite) in marbles or in alluvials. *KSM*

Morfologia di perle naturali e coltivate al microscopio elettronico a scansione (SEM) [The morphology of natural and cultured pearls under the scanning electron microscope (SEM)]. A. Maras, E. Amore, S. Mazziotti-Tagliani, M. Macrì, and A. Mancini, *Rivista Gemmologica Italiana*, Vol. 3, No. 3, 2008, pp. 201–213 [in Italian].

The nacreous surface of pearls can display surface struc-

tures that are step-like, labyrinthine (i.e., resembling fingerprints), or spiral. The aim of this investigation was to find out whether these structures are due to the pearl oysters, varying growth conditions, or both, and whether they are characteristic for certain types of pearls. The authors used visible light and scanning electron microscopy (SEM) to analyze the surface of two freshwater cultured pearls (one of them "chocolate"), a Red Sea saltwater pearl, an Akoya saltwater cultured pearl, and three additional saltwater cultured pearls (South Sea, Tahitian, and "golden"). The analysis revealed differences and similarities in samples from different sources. The results are illustrated with SEM micrographs. *RT*

Nucleated cultured pearls: What is there inside? M. Superchi [superchi@mi.camcom.it], E. Castaman, A. Donini, E. Gambini, and A. Marzola, *Gemmologie: Zeitschrift der Deutschen Gemmologischen Gesellschaft*, Vol. 57, No. 1–2, 2008, pp. 33–40.

Standards established by the Japan Pearl Promotion Society state that the nuclei of beaded cultured pearls should have a layered nacreous structure of the same material, density, and hardness as the cultured pearls themselves. However, the cost of the traditional Mississippi Basin freshwater mussel shell—and the demand for larger beads in recent years—have led to the use of other materials and the need to identify these nuclei, given the different costs and qualities they represent. Consideration has been given to mother-of-pearl from different freshwater and saltwater mollusks, shells from Tridacnidae clams, and the artificial composite "bironite." Freshwater mother-of-pearl can be separated from saltwater *Tridacnidae* and other nuclei by LA-ICP-MS analysis based on the presence (or absence) of Mn. This article illustrates how Laue diagrams may also be useful in separating the different materials, especially those in which Mn is absent, such as the saltwater beads and "bironite."

Abstractor's note: Since 2004, the *Tridacna* species have been listed as vulnerable according to the Red List of the International Union of Conservation of Nature. This gives added environmental importance to the development of a method to identify the use of nuclei made from the shells of these clams. *JEC*

The oxygen isotopic composition as an indicator of the genesis of "basaltic" corundum. S. V. Vysotsky, V. V. Yakovenko, A. V. Ignat'ev, and A. A. Karabtsov, *Russian Journal of Pacific Geology*, Vol. 3, No. 1, 2009, pp. 64–68.

Gem corundum can form in a range of geologic environments, but the material derived from alkali basalts (and similar mafic igneous rocks) are among the most important economically. Within alkali basalts, the corundum may occur as xenocrysts (foreign material) or as megacrysts (direct crystallization). For some deposits (e.g., Yogo Gulch,

Montana), the type of crystallization has been debated for years. Measuring the oxygen isotope composition of corundum is one method to help resolve these questions.

The authors of this study measured and compared oxygen isotope values for corundum and associated minerals from three sapphire deposits previously linked with basaltic rocks: (1) the Yogo lamprophyre dike; (2) the Khabok River, Tunkin Depression, Russia; and (3) alluvium derived from the Podgelbanochnyi volcano in Primorye, Russia. A total of six samples were tested. Interestingly, sapphire and phlogopite (a key constituent of the lamprophyre host rock) from Yogo shared very similar oxygen isotope values (5.6 and 6.0‰, respectively), implying that the sapphire formed directly from the lamprophyre; this contradicts previous conclusions that the sapphires are xenocrysts derived from underlying metamorphic basement rocks (see, e.g., K. A. Mychaluk, "The Yogo Sapphire Deposit," Spring 1995 *G&G*, pp. 28–41). Conversely, a plagioclase-corundum inclusion in basalt from the Tunkin Depression clearly had a xenocrystic origin. The oxygen isotope values for the corundum (9.1‰) and host basalt (6.1‰) varied by 3‰, with the value for the corundum falling outside the accepted range for "basaltic" corundum (4.5–7.0‰). Microscopic study of the same inclusion supported a xenocrystic origin (probably from a metamorphic protolith). Alluvial sapphires from Primorye showed oxygen isotopic values within the normal range for basaltic sapphire and are likely derived from alkali basalt.

This technique could evolve into a method to help determine the provenance of faceted sapphires. *KAM*

Structural, mineralogical, and biochemical diversity in the lower part of the pearl layer of cultivated seawater pearls from Polynesia. J.-P. Cuif [jean-pierre.cuif@u-psud.fr], A. D. Ball, Y. Dauphin, B. Farre, J. Nouet, A. Perez-Huerta, M. Salomé, and C. T. Williams, *Microscopy and Microanalysis*, Vol. 14, No. 5, 2008, pp. 405–417.

This study of 30 cultured pearls from *Pinctada margaritifera* mollusks of various Polynesian islands was undertaken to investigate the structural and compositional patterns of the early developmental stages of the pearl layer. The initial steps in cultured pearl formation display evidence of metabolic changes that occur during formation of the pearl sac and vary from one cultured pearl to another. In contact with the bead, the lower parts of the cultured pearl layer exhibit mineralization that differs from the regular concentric layered nacreous material produced later by the graft. An unusual association of organic and mineral materials is deposited during this early period, leading to the formation of various structures that in general have a radial orientation perpendicular to the nucleus surface. These structures are thought to result from the formation of subparallel prisms (either aragonitic or calcitic) pro-

duced simultaneously in adjacent areas of the pearl sac. Grafting and the subsequent pearl-sac formation processes appear to lead to a disturbance in the genomic activity of the grafted epithelium cells, and to unusual molecular associations in the early period of uncontrolled mineralization during pearl-sac formation. *JES*

DIAMONDS

Diamonds of Russia. G. F. Anastasenko and M. B. Leybov [m_leybov@mail.ru], *Rocks and Minerals*, Vol. 83, No. 6, 2008, pp. 508–517.

This article surveys Russia's centuries-old involvement with diamonds, from the czars' acquisitions of fine Indian and Brazilian stones to the first (noncommercial) discovery of diamonds in 1829 and the vast, state-supported geologic expeditions that discovered major commercial deposits over a century later. Several million square kilometers of dense, gnat-infested Siberian forests and swamps, with no roads and severe climate, were of intense interest. What remained unsolved, beyond a few placer deposits scattered across the Siberian craton, was the bedrock source of the diamonds. This changed in 1953–1954 when two female geologists discovered that pyrope concentrates from the Markha Basin resembled those from South African kimberlite. They traced the pyrope upriver to locate the diamondiferous kimberlite pipes in the D'yaka Valley, and in so doing developed the method of indicator mineral prospecting still in use today.

East Siberia has hundreds of kimberlite pipes, and the few diamondiferous ones were enough to position Russia among world leaders in diamond production. The giant Udachnaya pit yields about half of all Russian diamonds. The Siberian craton has produced about 200 large—50+ ct—diamonds (up to 342.5 ct). The great success in East Siberia also stimulated exploration of European Russia, especially its northern and central parts. The Arkhangelsk field, discovered in the 1980s, now accounts for 20% of Russian diamond production. About 50% of those diamonds are gem quality, and a significant number are nitrogen-free (colorless) stones used for high-tech applications. Airborne geophysical surveys have revealed about 130 "pipe-type" anomalies in the south of European Russia, an area considered promising because of its well-developed infrastructure and mild climate. *ERB*

New frosty frontiers: The challenges of mining in Canada's territories. D. Zlotnikov, *CIM Magazine*, Vol. 3, No. 7, 2008, pp. 20–24.

Extreme climate poses many problems for mining in Canada's Northwest Territories. Winter is the only time to effectively survey much of the area, since drilling can only be accomplished when all the swamps and lakes are frozen. Temperatures can reach lows of –40°C, and workers forced to stay indoors during these conditions can be struck with "cabin fever." At this temperature, steel becomes brittle, and steel containers can crack and allow noxious chemicals to escape. During the summer months, helicopters and planes are often grounded due to fog and freezing rain, delaying or preventing the delivery of equipment, food, and workers. Barges are the least expensive form of transportation, but they are not a feasible option unless the mine is located next to a body of water. The primary mode of transportation is trucking via the Tibbit to Contwoyto Winter Road. Although the road is only open from February to April, it allows delivery of most of the year's fuel and equipment. If temperatures become too mild during these months, the road closes early, increasing the probability that replacement equipment or necessary supplies will have to be delivered the following year. *JS*

Three centuries of diamonds: Preserving a tradition in Brazil. B. Farrar, *Rock & Gem*, Vol. 39, No. 3, 2009, pp. 37–40.

All significant diamond production in Brazil is from alluvial deposits or conglomerates formed from them. The *garimpeiros*, or prospectors, have an intimate knowledge of the area's formations and utilize different mining techniques at different times of the year. They work in the river during the dry season and on the sides of the valley during the rainy season. Besides their important role in world mining heritage, traditional Brazilian mining practices have less impact on the environment. When the *garimpeiros* are gone, their knowledge will go with them. One organization, Garimpo Real, seeks to preserve their methods. *MK*

What a gem! Ontario's first diamond mine. M. Scales, *Canadian Mining Journal*, Vol. 130, No. 1, January 2009, pp. 16–21.

The Victor mine is the first diamond mine in the Canadian province of Ontario. It took 37 years to research, plan, and construct, but the mine produces diamonds that are higher in per-carat value ($400/ct) than anywhere else.

Surrounding First Nation communities contributed to the project with their environmental knowledge, and they negotiated over $110 million in supporting business agreements with De Beers. The Victor mine is composed of two textural types of kimberlite, with the central part of the north pipe containing the most valuable grade of ore. This area is being mined first, and the process of separating diamonds from the ore is highly automated to promote employee safety and company profitability. *AB*

GEM LOCALITIES

Gem corundum from the St. Arnaud district, Western Victoria, Australia. W. D. Birch, *Australian Journal of Mineralogy*, Vol. 14, No. 2, 2008, pp. 73–78.

Waterworn sapphire crystals (≤7 mm) showing a wide range of colors (green, dull blue, pale yellow, pink, purple, and pale brown) are found in concentrates from an alluvial gold mine in ferruginous gravel at Carapooee, near St. Arnaud in southeastern Australia. Chemical analysis by LA-ICP-MS suggests that these sapphires were derived from mainly metamorphic and metasomatic source rocks, with a smaller magmatic component, similar to the gem corundums from basalt-related Cenozoic goldfields in eastern Australia. *RAH*

The 100-year history of the Benitoite Gem mine, San Benito County, California. W. E. Wilson [minrec@earthlink.net], *Mineralogical Record*, Vol. 39, No. 1, 2008, pp. 13–42.

This article surveys the history of the Benitoite Gem mine, the original source of California's state gemstone, beginning with a prospector's discovery of this occurrence in the New Idria district of San Benito County in 1907. Here, crystals of benitoite were found as both facetable gem material and mineral specimens (often together with black neptunite and yellow-brown joaquinite) within natrolite veins in an altered blueschist host rock. Since then, benitoite has been found at a few nearby claims in the same area, at four other places in California, and at several other world locations, but none of this material matches the quality and beauty of the original find.

This chronological report, prepared in honor of the 100th anniversary of the discovery, is based on both published information and important historical documents that include mine records from the early years of production. It highlights a number of interesting individuals, including miners, mineral and gem dealers, and professional geologists who were involved with the discovery and mining of benitoite over the past century. Following an initial period of mining activity, the operation was mostly inactive from about 1914 to 1952 except for some unauthorized mineral collecting. Since then, there has been intermittent mining of both the primary deposit and the eluvial and colluvial material that lay at the base of deposit. Most mining activity ended in 2005. Attractive mineral specimens of benitoite can today be found in a number of museums and in private collections. The largest faceted benitoite weighs 15.42 ct. *JES*

Ion microprobe zircon U-Pb age and geochemistry of the Myanmar jadeitite. G. Shi [shiguanghai@263.et.cn], W. Cui, S. Cao, N. Jiang, P. Jian, D. Liu, L. Miao and B. Chu, *Journal of the Geological Society, London*, Vol. 165, 2008, pp. 221–234.

Of the few jadeite locations worldwide, the Hpakan-Tawmaw deposit in the northern Myanmar state of Kachin is the largest and most important. This deposit is located in the western part of the Sagaing fault zone belonging to the Indo-Burman Range, which was formed by the subduction of the Indian plate beneath the Burmese

platelet. Primary jadeitites were formed as veins (1.5–5 m wide and 5–100 m long) crosscutting serpentinized peridotite. An amphibolite boundary zone 1–50 cm wide is found between jadeite veins and serpentinized peridotite bodies.

The geochemistry of eight jadeitite samples was determined using XRF (for major oxides) and ICP-MS (for trace-element abundances) to understand their petrogenesis and tectonic relationship to subduction zones. Bulk-rock trace-element compositions showed U-shaped rare-earth element (REE) patterns with positive Eu anomalies. Overall, REE abundances were low, with moderate enrichment of high-field-strength elements and some large ion lithophile elements. These observations are all consistent with a metasomatic origin for the jadeitite.

One white to pale gray jadeitite sample was crushed to extract ~200 zircon grains for electron microprobe and sensitive high-resolution ion microprobe (SHRIMP) analyses. Three groups of zircons were identified, based on their internal textures, luminescence, mineral inclusions, and chemical compositions. Group I zircons were typically zoned and contained Na-free, Mg-rich silicate mineral inclusions and also the highest U and Th contents and Th/U ratios. They were inferred to have crystallized during an igneous (e.g., formation of oceanic crust) or hydrothermal (e.g., serpentinization) event. The weighted mean age of Group I zircons from U-Pb dating was 163.2 ± 3.3 Ma, suggesting that serpentinization of the oceanic crust of the Indian plate occurred during the Middle Jurassic. Group II zircons, which occurred as rims on Group I zircon cores, did not show zoning features and had lower Th/U ratios. They contained jadeite and jadeite-rich pyroxene inclusions, suggesting Group II zircons were syngenetic with the jadeitite samples. The formation age of Group II zircons was determined to be 146.5 ± 3.4 Ma, indicating that the formation of the Myanmar jadeitites, and the subduction of the eastern Indian oceanic plate, occurred during the Late Jurassic. The low U and Th contents and Th/U ratios (lowest of the three), growth habits, and age of Group III zircons suggested that a thermal event occurred after jadeitite formation, around 122.2 ± 4.8 Ma (Early Cretaceous), resulting in localized recrystallization. The presence of Middle Jurassic Group I zircons of hydrothermal origin in jadeitite samples provides an important geochronological constraint on the evolution of the Indo-Burman Range, indicating that it may have started earlier than previous models that placed it at Late Cretaceous-Eocene age. *KSM*

Modes of occurrence and origin of precious gemstone deposits of the Mogok Stone Tract. M. Thein, *Journal of the Myanmar Geosciences Society*, Vol. 1, No. 1, 2008, pp. 75–84.

The Mogok area of Myanmar has been famous for more than a century as one of the world's most important gem sources. This article briefly reviews Mogok's regional geol-

ogy and categorizes the gem deposits into eight primary and secondary occurrences. The former include gem-bearing bands in marbles, skarns along the contact zones between marbles and nepheline syenites or syenites, segregations of gems (particularly sapphire) in the same two rock types as well as syenite pegmatites, and hydrothermal veins extending from the same pegmatites. The secondary occurrences include alluvial and eluvial placers, and what the author refers to as "fissure-filled" and "sinkhole- or cavern-filled" deposits. The marbles and the alluvial deposits are the two most economically important producers.

The author concludes by listing some special geologic conditions that may account for the abundance of gems (particularly ruby and sapphire) in Mogok: the presence of aluminous clays as bands in the original limestones, which then metamorphosed to marbles; additional alumina supplied by igneous intrusions in the region; a calcite-rich marble composition; and high-grade regional metamorphism (amphibolite to granulite facies) and contact metamorphism (pyroxene hornfels facies). *JES*

Winza, ein neues Rubinvorkommen in Tansania [Winza, a new ruby deposit in Tanzania]. K. Schmetzer, W. Radl, and D. Schwarz, *Lapis*, Vol. 34, No. 5, 2009, pp. 41–46 [in German].
This article supplements previous work by D. Schwarz et al. ("Rubies and Sapphires from Winza, Central Tanzania," Winter 2008 *G&G*, pp. 322–347). Along with a short description of the deposit and mining, it provides a detailed description of the crystal morphology. Based on their habits, the crystals could be divided into two groups: prismatic-tabular-rhombohedral and dipyramidal. In both groups, some unusual combinations of crystal faces occurred, such as pseudo-octahedral crystals (strongly resembling spinels) with negative rhombohedral faces as dominant forms. *RT*

INSTRUMENTS AND TECHNIQUES

A place for CZ masters in diamond colour grading. M. D. Cowing [michael@acagemlab.com], *Journal of Gemmology*, Vol. 31, No. 3/4, 2008, pp. 77–83.
The use of cubic zirconia master stones for diamond color grading has been controversial since their introduction more than 20 years ago. This article is a detailed discussion of how CZ master stones can be used in conjunction with diamond master stones to enhance and confirm diamond color grade calls. Traditional objections to the use of CZ master stones include the different yellow hue of CZ vs. diamond, variations in the dispersion and luster, plus concerns about the color stability of CZ. The appeal of CZ master sets is initially one of economy, but many industry professionals who trade in diamonds (and thus suffer financially if a color grade is off when buying) use CZ mas-

ter stones as a supplement to their diamond masters. The author notes, however, that it takes practice to adjust to the higher dispersion of CZ. Although nitrogen-rich type Ia diamonds may have a different shade of yellow, it is easier to grade yellow against yellow than to grade brown or gray against yellow.

The author compared two sets of CZ master stones from two different producers under five different lighting conditions (daylight fluorescent, daylight fluorescent through a Lexan plastic filter to remove UV, cool white fluorescent, a full-spectrum fluorescent, and a white LED lamp). Results from grading CZ master sets by three experienced color graders illustrated the differences in the two products, with one being decidedly superior. The differences in absorption spectra and amounts of fluorescence were not enough to materially affect the results.

JEC

Practicality of Colibri™, a diamond colour-grading product by Sarin. J. Kawano and K. Saikyo, *Gemmology*, Vol. 40, No. 476, 2009, pp. 23–27.
Color grading D-to-Z diamonds involves an element of subjective visual observation, but a completely objective method has been sought for some time. Sarin Technologies is working to fill this need through its automatic color-grading instrument, the Colibri colorimeter, which is intended for faceted type Ia diamonds with yellow (cape) color. The device is suitable for laboratory and retail use, requiring only a small desk space and weighing 1.2 kg (about 2.6 lbs.). It uses a 100-volt electric power supply or a rechargeable battery with 10 hours of continuous operation. Color grading takes about 5 seconds. According to Sarin, samples can range from 0.2 to 270 ct and can be mounted or unmounted. The machine measures the sample's color and compares it with the measurement of the empty test chamber to derive a numeric value that corresponds to standard color grades issued by GIA, AGS, and HRD.

The authors tested the Colibri at the GAAJ-Zenhokyo Laboratory by measuring some 14,000 diamonds, and they concluded that when properly used, the machine is fairly useful for objective color grading of most cape-series stones. The Colibri provided consistent measurements, especially for stones <1 ct; round brilliants with a cut grade of Good or better and fluorescence from none to medium blue; and cape diamonds. Correct color estimates for stones with brown or gray hues could be achieved by adding 1.5 to 2.0 to the numeric result; however, no correction could be made for strong blue fluorescence.

Karen G. Fenech

Visualization of the internal structures of cultured pearls by computerized X-ray microtomography. U. Wehrmeister [wehrmeis@uni-mainz.de], H. Goetz, D. E. Jacob, A. Soldati, W. Xu, H. Duschner, and W. Hofmeister, *Journal of Gemmology*, Vol. 31, No. 1/2, 2008, pp. 15–21.

While there are usually observable differences between natural pearls and beadless cultured pearls, these differences are not always sufficient for conventional X-radiography to distinguish. Through computerized X-ray microtomography, $CaCO_3$ polymorphs within a sample can be revealed at a resolution one or two orders of magnitude higher than is possible with conventional radiograms. Combined with micro-Raman spectroscopy, it is also possible to detect vaterite, a metastable polymorph associated with the remnants of graft tissue in cultured pearls. Using sample tomograms depicting two-dimensional cross-sections and three-dimensional visualizations, along with Raman intensity maps, the authors describe the structures seen in four types of cultured pearls: beadless Chinese freshwater, beadless Japanese freshwater from Lake Biwa, beaded freshwater from Lake Biwa, and beaded South Sea. The article notes that while vaterite areas are suggested by certain features in the tomograms (probably caused by higher concentrations of organic molecules), these must still be verified using micro-Raman spectroscopy. This combined technique lends itself to scientific research and the nondestructive testing of high-value pearls.

ES

SYNTHETICS AND SIMULANTS

Effects of Al and Ti/Cu on synthesis of type-IIa diamond crystals in $Ni_{70}Mn_{25}Co_5$-C system at HPHT. S.-S. Li, X.-P. Jia, C.-Y. Zang, Y. Tian, Y.-F. Zhang, H.-Y. Xiao, G.-F. Huang, L.-Q. Ma, Y. Li, X.-L. Li, and H.-A. Ma [maha@jlu.edu.cn], *Chinese Physics Letters*, Vol. 25, No. 10, 2008, pp. 3801–3804.

This study used the temperature-gradient method under high pressure and high temperature to grow low-nitrogen type IIa synthetic diamonds. They were grown in a cubic anvil high-pressure apparatus at 5.5 GPa and 1560 K using high-purity graphite as the carbon source and a $Ni_{70}Mn_{25}Co_5$ alloy as the catalyst/solvent. Al and Ti/Cu were tested as nitrogen getters to produce low nitrogen concentrations. The authors found that using Al as the nitrogen getter resulted in crystals with a yellow coloration and obvious inclusions. Using Ti/Cu as the nitrogen getter, the authors produced a colorless, inclusion-free 2 mm synthetic diamond with a nitrogen concentration <1 ppm. Decreasing the temperature gradient in the experimental assembly slowed the growth rate, which improved the clarity of the crystal.

The article explains these results in terms of reversible versus irreversible reactions. The authors describe Al reacting with N: $Al + N \Leftrightarrow AlN$. The reversibility of this reaction is given as the reason measurable amounts of N are still present in diamonds grown with Al as the nitrogen getter. Ti was found to be a more efficient nitrogen getter than Al, with the irreversible reaction $Ti + N \Rightarrow TiN$ (as long as enough Ti is added to compensate for all

the N). A similar reaction occurs between Ti and C, so Cu is added to decompose TiC by the irreversible reaction $TiC + Cu \Rightarrow Ti^- + Cu^+ + C$. The best results were achieved using a 1.8 wt.% Ti/C additive with a growth rate of 1.03 mg/hr for 20 hours. The seed crystal was 0.6 mm, and the (100) face was used as the growth surface.

JS-S

TREATMENTS

Diamants de couleur traités à haute température et à haute pression [High temperature and high pressure treated colored diamonds]. E. Erel [e.erel@gubelingemlab.ch], *Revue de Gemmologie*, No. 167, 2009, pp. 10–17 [in French].

HPHT treatment has been performed on type I, type IIa, and type IIb rough and faceted diamonds; the resulting colors depend on the chemical properties of the starting material. After treatment, type Ia diamonds with a natural weak yellow to brown color exhibit a fluorescent yellow or yellow-green intense "fancy" color, or an intense yellow or orange color without the green fluorescence. Treated pink-to-red diamonds are produced in two steps: After HPHT treatment is used to add a type Ib component to type Ia starting material, irradiation and heating at low temperature is used to obtain the desired color. Treated diamonds occasionally display characteristic visual features such as surface etching and internal graphitization. When these indicators are not present, conclusive identification requires advanced testing such as UV-Vis-NIR and infrared spectroscopy.

FP

Diamants de couleur traités par irradiation puis chauffage à "basse" temperature [Colored diamonds irradiated and heated at low temperature]. E. Erel [e.erel@gubelingemlab.ch], *Revue de Gemmologie*, No. 164, 2008, pp. 6–10 [in French].

Radiation-induced color is the result of damage caused when carbon atoms are knocked out of their normal position, creating vacancies in the atomic lattice. The result is a sharp peak at 741 nm in the diamond's spectrum, known as the GR1 (General Radiation) band. Irradiation alone produces a blue-to-green or black coloration; the GR1 color center disappears when the stone is heated to 600°C. During the heating process, radiation-induced vacancies migrate through the lattice and pair with nitrogen to create new color centers. One of the first to develop is the 595 nm absorption at 275°C; maximum absorption at 595 nm is reached at 800°C, and an associated peak is often observed at 425 nm. H3 (503 nm) and H4 (496 nm) centers appear at 500°C, as do H1b and H1c (at 5170 and 4940 cm^{-1} in the infrared spectrum). A combination of irradiation and heating at low temperature produces yellow, orange, pink, or red color, depending on the diamond type. The presence of the H1b and H1c centers is evidence that a stone has been most likely been irradiated and annealed.

GL

Pérolas tratadas [Treated pearls]. *Diamond News*, Vol. 9, No. 29, 2008, pp. 17–24 [in Portuguese].

With the exception of most Tahitian and South Sea products, cultured pearls sold in the market today are treated to improve their surface quality and color, and sometimes to produce colors not found in nature. The treatments can be classified into three groups: (1) bleaching and polishing, which removes undesired hues and improves luster; (2) irradiation, which induces greenish, bluish, and even black colors; and (3) dyeing, which produces all kinds of colors with both natural and artificial coloring agents.

RT

Study of black diamond made by nitrogen ion-implantation and irradiated green diamond. H. M. Choi, Y. C. Kim, S. K. Kim, J. W. Park, and A. Abduriyim [laboratory@gaaj-zenhokyo.co.jp], *Gemmology*, Vol. 40, No. 473, 2009, pp. 2–6 [in Japanese with English supplement].

Part one of this study discusses how deep, evenly colored black diamonds can be produced by nitrogen ion implantation and annealing. Nitrogen ion implantation typically has a shallow penetration depth and yields a weak black or green color. The facet surfaces of 10 transparent and light brown diamonds (most of them less than 0.12 ct) were subjected to three treatment conditions: (1) N^+ ion irradiation and no heating, (2) post–N^+ irradiation heat treatment at 600°C for two hours in a vacuum, and (3) triple the radiation dose and annealing time of treatment 2. N^+ ions were implanted to a depth of 40 nm, with their mass decreasing gradually from 18 to 40 nm depth. X-ray photoelectron spectroscopy indicated that diamond was converted to a 40-nm-thick layer of graphite by N^+ ion implantation; subsequent annealing led to crystallization of the graphite layer, producing a more uniform and vivid black diamond. Although the English translation is unclear on whether treatment condition 2 or 3 was responsible for these results, it appears to favor higher ion dose and longer annealing time.

In part two of the study, a 7.69 ct step-cut Fancy bluish green, type IIa diamond was examined. The color appeared uniform, but concentrations were faintly visible along facet junctions when the stone was viewed in immersion. The authors discuss the significance of the diamond's 1077.9 nm band in the near-infrared region and conclude that the green color was caused by artificial irradiation.

ERB

XPS and ToF-SIMS analysis of natural rubies and sapphires heat-treated in a reducing (5 mol% H_2/Ar) atmosphere. S. Achiwawanich, B. D. James, and J. Liesegang [j.liesegang@latrobe.edu.au], *Applied Surface Science*, Vol. 255, 2008, pp. 2388–2399.

The authors studied the effects of heat treatment in a reducing atmosphere on surface features of Mong Hsu rubies and Kanchanaburi sapphires using X-ray photoelectron spectroscopy (XPS) and time-of-flight secondary ion mass spectrometry (ToF-SIMS). Samples were heat treated in a high-temperature electric furnace with a 5 mol.% H_2/Ar atmosphere for one hour at 1000–1600°C. Visual examination and spectroscopic analyses were performed between each heating stage. The blue cores of Mong Hsu rubies were removed by heating above 1300°C, and the overall red hue was enhanced during treatment. Above 1400°C, whitish particles developed in the samples. The blue component in dark greenish gray and pale blue Kanchanaburi sapphires was diminished by heating above 1200°C. At the same time, the dark greenish gray color was intensified with increasing concentration of the associated precipitate inclusions. For both rubies and sapphires, XPS and ToF-SIMS analyses showed that surface concentrations of various trace elements (Fe, Ti, Ca, V, Mn, Cu, and Cr) had relative maxima around 1300–1400°C, indicating that bulk diffusion into the stones occurred with progressive heat-treatment stages at higher temperature. ToF-SIMS spatial images of Ti, Cr, and Fe indicated that with progressive heat treatment, Ti ions in rubies and sapphires distribute fairly uniformly on the surface, whereas Fe and Cr ions tend to cluster and then form particles on the surface.

The authors conclude that heat treatment of the corundum samples in a reducing atmosphere affected the oxidation state of Fe but not Ti. They also suggest that dissociation of Fe-Ti interaction may occur during heat treatment in a reducing atmosphere, which they attribute to differences in diffusion rates of defect clusters associated with Fe and Ti.

EVD

MISCELLANEOUS

Accessible and total lead in low-cost jewelry items. J. L. Yost and J. D. Weidenhamer [jweiden@ashland.edu], *Integrated Environmental Assessment and Management*, Vol. 4, No. 3, 2008, pp. 358–361.

Recent legislation in the U.S. has banned products intended for children that contain >0.06 wt.% lead. Previous studies by the second author have shown that much costume jewelry sold in the U.S. contains nonpermissible levels of lead; however, critics of the new rules have argued that plated lead jewelry does not contain dangerously high levels of *accessible* lead (that is, lead that could be absorbed by the human body if the object were ingested). The authors tested 64 low-cost jewelry items (all with >0.06 wt.% lead) and subjected them to the lead-accessibility test recommended by the U.S. Consumer Product Safety Commission (rinsing in dilute hydrochloric acid). Fifty of the items were found to exceed the limit for accessible lead (175 µg); 30 of these had accessible lead >1000 µg. The authors conclude that plating is generally ineffective in limiting lead exposure.

TWO

Gems. *Elements*, Vol. 5, No. 3, 2009, pp. 137–200.
This special issue contains a review of current developments in gemology. It opens with an introduction to the "developing science" of gemology by guest editors E. Fritsch and B. Rondeau. L. Groat and B. Laurs then review gem formation, production, and exploration. G. R. Rossman describes the geochemistry of gems, while B. Devouard and F. Notari review gem identification. R. E. Kane, and J. E. Shigley and S. F. McClure, describe current developments in synthetic and treated gems, respectively. The articles conclude with a review of current research on pearls and coral by J.-P. Gauthier and S. Karampelas.

TWO

Green bench practices reduce environmental impact. C. Dhein, *JCK*, Vol. 179, No. 11, 2008, pp. 68–73.
Awareness of the environmental impact of jewelry making has grown recently, and the author offers tips to help jewelers develop sustainable business practices. Jewelers are encouraged to review their supply chain and request copies of their suppliers' environmental policies. If none exist, they should encourage their suppliers to develop and abide by sustainable practices. Jewelers should buy from companies that are trying to make a difference and choose local suppliers to minimize costs and carbon footprint. Tracing the supply chain is more difficult for gems than for metals.

Other suggestions: Collect anything used in precious-metal manufacturing and turn it in for refining. Encourage customers to recycle their precious metals. Consider switching to less toxic alternatives to traditional studio practices, such as a citric pickling solution, which is greener (if slower). Reduce the size of packaging, choose recycled versions, and encourage suppliers to do the same. A list of additional reading and organizations and resources promoting responsible and ethical materials is included.

EJ

Model for responsibility. B. Moss, *Modern Jeweler*, Vol. 107, No. 8, 2008, pp. 42–47.

Because of recent consumer preferences for dealing with socially and environmentally responsible corporations, the jewelry industry is taking steps to ensure that its product, often an expression of love, is not tarnished by ethical concerns. In 2003, global diamond producer Rio Tinto established a Business Excellence Model (BEM) for Indian diamantaires and jewelry manufacturers. BEM factories and sites must comply with the Kimberley process and adhere to standards of sourcing/quality control, environmental protection, health and safety, and social responsibility. Indian diamond manufacturers, the world's principal source of diamond jewelry, are keen to adhere to global production standards. So far, manufacturers who have adopted the BEM model have given enthusiastic feedback. Positive outcomes include greater productivity and reduced product turnaround time, goodwill gained in the industry, improved worker health with lower absenteeism, and new local sponsorship of social institutions and educational systems. Ultimately, the consumer can feel confident that jewelry purchased through retailers who work with BEM suppliers has been manufactured with the highest global standards.

AB

Why China manufacturers are optimistic despite global slowdown. *Jewellery News Asia*, No. 290, October 2008, pp. 81–84.
In the wake of the global financial crisis, Chinese diamond jewelry manufacturers have turned their attention from exporting to the U.S. to creating branded jewelry lines for their domestic market. Several polished diamond wholesalers observed that Chinese consumers are broadening their preferences to include diamonds >0.50 ct and SI-clarity goods, both of which had been a difficult sell there. They are also establishing closer ties to local retailers in promoting their branded diamond jewelry pieces, noting that manufacturers must pay more attention to changing fashion trends and changes in the retail environment.

RS

For regular updates from the world of **GEMS & GEMOLOGY,** visit our website at:
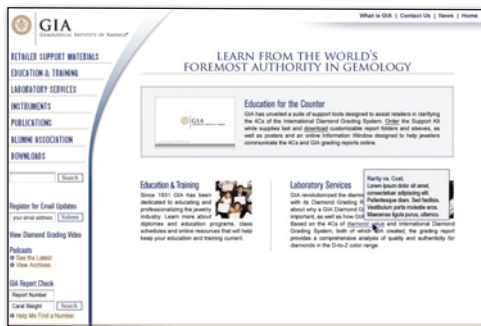
www.gia.edu/gandg

BECAUSE PUBLIC EDUCATION HAPPENS AT THE COUNTER.

GIA LAUNCHES RETAILER SUPPORT KIT AND WEBSITE

A $97.00 value, shipping and handling extra.

GIA's Retailer Support Kit has been developed to help sales associates educate the public about diamonds, the 4Cs, and thoroughly explain a GIA grading report. Take full advantage of all that GIA has to offer by visiting www.retailer.gia.edu

To order your FREE kit, log on to www.retailer.gia.edu

GIA
GEMOLOGICAL INSTITUTE OF AMERICA®

RTGG09